Circuits and Systems
Mekelweg 4,
2628 CD Delft
The Netherlands
http://ens.ewi.tudelft.nl/

CAS-2011-08

M.Sc. Thesis

Multi-Carrier Wakeup Radio Receiver

Zhenjie Huang

Abstract

In the development of wireless sensor networks, power consumption is one of the bottlenecks for wide applications. In order to improve the energy efficiency of wireless sensor networks, a wakeup radio scheme is presented. The main transceiver that is responsible for data communication is in the sleep mode most of the time. An additional device called the wakeup radio receiver is a simplified receiver with much lower power consumption and data rate than the main transceiver. It is always on to monitor the channels continuously. It detects the wakeup packet, and sends the main transceiver a wakeup trigger upon successful detection of a wakeup packet. However, the detection of a wakeup packet is a challenging task. Since the wakeup radio receiver operates in the 2.4 GHz industrial, scientific, and medical band, a wakeup packet can be greatly interfered in such a noisy channel, which may lead to detection performance degradation. Therefore, a multi-carrier wakeup radio receiver is proposed as a solution to interference mitigation by making use of frequency diversity. But in practical implementations, the impairments from the multi-carrier wakeup receiver itself cannot be neglected. The receiver detection performance may degrade due to the non-idealities at the receiver. In this thesis, the detection performance of the multi-carrier wakeup radio receiver in the presence of channel noise, fading, co-channel interference, as well as non-idealities is explored.

TU Delft

Faculty of Electrical Engineering, Mathematics and Computer Science Delft University of Technology

Multi-Carrier Wakeup Radio Receiver

Thesis

submitted in partial fulfillment of the
requirements for the degree of

Master of Science

in

Telecommunications

by

Zhenjie Huang
born in Guangdong, China

This work was performed in:

Circuits and Systems Group
Department of Telecommunications & Microelectronics
Faculty of Electrical Engineering, Mathematics and Computer Science
Delft University of Technology

Delft University of Technology

Delft University of Technology
Department of
Telecommunications & Microelectronics

The undersigned hereby certify that they have read and recommend to the Faculty of Electrical Engineering, Mathematics and Computer Science for acceptance a thesis entitled **"Multi-Carrier Wakeup Radio Receiver"** by **Zhenjie Huang** in partial fulfillment of the requirements for the degree of **Master of Science**.

Dated: August 26, 2011

Chairman:

Dr.ir. Geert Leus

Advisors:

Dr.ir. Geert Leus

Dr. Yan Zhang

Committee Members:

Dr. Ertan Onur

Abstract

In the development of wireless sensor networks, power consumption is one of the bottlenecks for wide applications. In order to improve the energy efficiency of wireless sensor networks, a wakeup radio scheme is presented. The main transceiver that is responsible for data communication is in the sleep mode most of the time. An additional device called the wakeup radio receiver is a simplified receiver with much lower power consumption and data rate than the main transceiver. It is always on to monitor the channels continuously. It detects the wakeup packet, and sends the main transceiver a wakeup trigger upon successful detection of a wakeup packet. However, the detection of a wakeup packet is a challenging task. Since the wakeup radio receiver operates in the 2.4 GHz industrial, scientific, and medical band, a wakeup packet can be greatly interfered in such a noisy channel, which may lead to detection performance degradation. Therefore, a multi-carrier wakeup radio receiver is proposed as a solution to interference mitigation by making use of frequency diversity. But in practical implementations, the impairments from the multi-carrier wakeup receiver itself cannot be neglected. The receiver detection performance may degrade due to the non-idealities at the receiver. In this thesis, the detection performance of the multi-carrier wakeup radio receiver in the presence of channel noise, fading, co-channel interference, as well as non-idealities is explored.

Acknowledgments

First of all, I would like to extend my sincere thanks to my supervisor, Dr. ir. Geert Leus. He recommended me to do the thesis work in IMEC-NL so that I could obtain some work experience in this good company. His positive attitude was really impressive for me, when I had discussions with him. He gave me valuable advice and made great efforts in the corrections of my thesis. Besides, he is a nice professor and had some pleasant talk with me about every aspect of the life, which made me feel warm in campus.

I want to thank Dr. Ertan Onur for his participation in my thesis defense committee. He is very easygoing, which makes him one of the most popular teachers in Telecommunications. Every time I met and talked with him, he always provided useful information as much as possible.

I appreciate all my supervisors in IMEC-NL for their guidance and help. I express my great gratitude to Yan Zhang, who has been involved in this project with me for the whole nine months. Her experienced supervision and rich knowledge are really useful for me. She kindly answered all my questions and provided good suggestions for the work. When I encountered difficulties in the company, she always encouraged and supported me. Even if I had left the company, she was still concerned about my progress and helped me a lot in the modification of the thesis.

I also thank Ruben de Francisco and Nauman Farooq Kiyani for their guidance in the company. Thanks for their organization of the progress meetings, where I got some valuable feedback from them. Thank Guido Dolmans for offering me the opportunity to work in the wireless communication group and helping me out of trouble.

I would like to thank all the other excellent colleagues in IMEC-NL for their support and help. They are Li Huang, Wen Qi, Yao-Hong Liu, Xiongchuan Huang, Peter Harpe, Xiaoyan Wang, Koji Imamura, Cui Zhou and Jos Huisken.

My great thanks also go to all the dear friends around me for their kindness, support and encouragement during these two years. When I was in a bad mood, they often kindly talked to me and inspired me, which made me forget all the unpleasantness. Without them, I could not have such a wonderful life here.

Finally, I would like to express my gratitude and humility to my parents, my younger sister and relatives. Without the instruction and support of my parents, I could not have the opportunity to

study at this reputable university. Even thousands of kilometers apart, they are always present through every step of my life, providing their full support and concern. They have been a constant source of inspiration, and this thesis is dedicated to them.

Zhenjie Huang

Delft, the Netherlands

August 2011

Glossary

(by order of first appearance)

Chapter 1

WSN	Wireless Sensor Network
WuRx	Wakeup Receiver
ISM	Industrial, Scientific and Medical
WLAN	Wireless Local Area Network
WPAN	Wireless Personal Area Network
MC	Multi-Carrier
PWM	Pulse Width Modulation
OOK	On-Off Keying
DBB	Digital Baseband
OFDM	Orthogonal Frequency Division Multiplexing
MIMO	Multiple-Input Multiple-Output
RSS	Received Signal Strength
SINR	Signal to Noise-plus-Interference Ratio

Chapter 2

OVSF	Orthogonal Variable Spreading Factor
PN	Pseudo-Noise
SF	Spreading Factor
SFD	Start Frame Delimiter
ASK	Amplitude Shift Keying
FSK	Frequency Shift Keying
VCO	Voltage Controlled Oscillator
WuTx	Wakeup Transmitter
AWGN	Additive White Gaussian Noise

Chapter 3

CW	Continuous Wave
PM	Phase Modulated
PSD	Power Spectral Density

ADC	Analog-to-Digital Converter
BER	Bit Error Rate
RF	Radio Frequency
SIR	Signal-to-Interference Ratio

Chapter 4

LO	Local Oscillator
PN	Phase Noise
CFO	Carrier Frequency Offset
QN	Quantization Noise
SCO	Sampling Clock Offset
PDF	Probability Density Function
RMS	Root-Mean-Square
LOS	Line-of-Sight
Tx	Transmitter
Rx	Receiver
ISI	Inter-Symbol Interference

Chapter 5

CCI	Co-Channel Interference

Contents

Abstract v

Acknowledgments vii

1. Introduction 1

1.1 Background 1

1.2 Motivation 3

1.3 Related work 5

1.4 System overview 9

1.5 Outline and contributions 10

2. Multi-Carrier Wakeup Receiver 13

2.1 MC wakeup receiver architecture 13

2.1.1 Mixer and oscillator 14

2.1.2 Integrator 14

2.1.3 Channel spacing 16

2.2 Changes at the transmitter 17

2.2.1 Address generation 17

2.2.2 Address matrix 18

2.2.3 Wakeup packet structure 18

2.2.4 OOK modulation 19

2.3 Channel selection mechanism 19

2.3.1 Architecture 19

2.3.2 Noise and interference estimation 20

2.3.3 Channel selection operations 20

2.3.4 Channel selection thresholds 23

2.4 The number of carriers 26

3. Detection Performance in AWGN Channels 29

3.1 AWGN channel model 29

3.2 BER performance with AWGN 30

3.2.1 Decision threshold 31

3.2.2 Simulink simulation 32

3.3 Address detection schemes 34

3.3.1 Hard-bit-based Hamming distance method 34

3.3.2 Soft-bit-based correlation method 39

3.3.3 Comparison of the two address detection schemes . . . 42
3.4 Effect of interference on detection performance . . . 42
3.4.1 Continuous wave interference . . . 42
3.4.2 Phase modulated interference . . . 46
4. Effects of Non-Idealities in AWGN and Fading Channels . . . 51
4.1 Individual non-idealities . . . 51
4.1.1 Phase noise . . . 51
4.1.2 Carrier frequency offset . . . 54
4.1.3 I/Q imbalance . . . 55
4.1.4 ADC quantization noise . . . 57
4.1.5 Sampling clock offset . . . 59
4.2 Simulation scenario . . . 60
4.2.1 System modeling . . . 60
4.2.2 Simulation parameters . . . 61
4.3 Effect of non-idealities in AWGN channels . . . 61
4.3.1 Impact of phase noise . . . 62
4.3.2 Impact of carrier frequency offset . . . 64
4.3.3 Impact of I/Q imbalance . . . 66
4.3.4 Impact of ADC quantization noise . . . 69
4.3.5 Impact of sampling clock offset . . . 72
4.4 Effect of non-idealities in Rayleigh fading channels . . . 74
4.4.1 Rayleigh fading channel model . . . 74
4.4.2 Impact of phase noise . . . 76
4.4.3 Impact of carrier frequency offset . . . 77
4.4.4 Impact of I/Q imbalance . . . 79
4.4.5 Impact of ADC quantization noise . . . 81
4.4.6 Impact of sampling clock offset . . . 84
4.5 Effect of non-idealities in Rician fading channels . . . 84
4.5.1 Rician fading channel model . . . 84
4.5.2 Impact of phase noise . . . 88
4.5.3 Impact of carrier frequency offset . . . 89
4.5.4 Impact of I/Q imbalance . . . 91
4.5.5 Impact of ADC quantization noise . . . 93
4.5.6 Impact of sampling clock offset . . . 93
4.6 Conclusions . . . 95
5. Further Discussions on Co-Channel Interference . . . 97
5.1 Continuous wave interference . . . 97

5.2 Phase modulated interference 99
5.3 Discussions on the number of discarded channels 101
5.3.1 Without AWGN 102
5.3.2 With AWGN 104
6. Conclusions and Future Work 107
6.1 Conclusions 107
6.2 Suggestions for future work 108
6.2.1 Digital compensation 108
6.2.2 Power consumption 108

List of Figures

1.1 Wireless sensor network 1
1.2 Duty cycle scheme 2
1.3 Wakeup radio system 2
1.4 Handshake mechanism in a wakeup radio scheme 3
1.5 Wireless standards operating in the 2.4 GHz ISM band 4
1.6 Block diagram of the AS3931 7
1.7 Block diagram of the AS3932 8

2.1 Four-carrier wakeup radio receiver architecture 14
2.2 The transfer function of an integrator with integration time *T* 15
2.3 OVSF code tree 17
2.4 Time-frequency-grid address matrix 18
2.5 Wakeup packet structure 18
2.6 Channel selection architecture 20
2.7 Channel allocations for the Wi-Fi and Zigbee nodes 21
2.8 Simulation scenario for the channel selection mechanism 22
2.9 Probabilities of miss detection for the three different wakeup radio schemes 22
2.10 Probabilities of false alarm for the three different wakeup radio schemes 23
2.11 Probabilities of miss detection for the MC wakeup radio with different channel selection thresholds 24
2.12 Probabilities of false alarm for the MC wakeup radio with different channel selection thresholds 25
2.13 Probabilities of the all-delete problem with different channel selection thresholds 25
2.14 Probabilities of miss detection with different number of carriers 26
2.15 Probabilities of false alarm with different number of carriers 27

3.1 AWGN channel model 29
3.2 PSD of white Gaussian noise in channels 30
3.3 Wakeup receiver single-carrier chain 30
3.4 BER of a single-carrier wakeup receiver with optimum thresholds 32
3.5 Co-simulation through MATLAB and Simulink 33
3.6 Simulink model of a single-carrier wakeup receiver 33
3.7 BER performance of a single-carrier wakeup receiver with Simulink simulation 34

3.8 Relationship between Hamming distance threshold and error probabilities in the case of different SNR levels 35
3.9 Relationship between correlation thresholds with hard decision and error probabilities (SNR = 5 dB) 36
3.10 The theoretical values and simulation results for the error probabilities at different SNRs with a Hamming distance threshold of 4 38
3.11 4-bit ADC 39
3.12 Relationship between correlation thresholds with soft decision and error probabilities in the case of different SNR levels 41
3.13 Relationship between SNR and the error probabilities with a correlation threshold of 0.4 . 41
3.14 Comparison of the error probabilities with the hard-bit-based Hamming distance method and soft-bit-based correlation method (SNR = 5 dB) 42
3.15 Co-channel CW interference 43
3.16 BER performance with CW interference (initial phase $\phi_o = \pi$, SNR = 8 dB). 45
3.17 Error probabilities with CW interference (initial phase $\phi_o = \pi$, SNR = 8 dB). 46
3.18 Constellation diagram for BPSK 47
3.19 Constellation diagram for QPSK 47
3.20 BER performance with PM interference (SNR = 8 dB) 48
3.21 Error probabilities with PM interference (SNR = 8 dB) 49

4.1 The spread of a LO output signal in frequency domain due to phase noise 52
4.2 Phase noise model 52
4.3 Contour of the relative I/Q imbalance interference I (in dB) with amplitude error and phase error 56
4.4 8-bit ADC 57
4.5 ADC quantization illustration 58
4.6 PDF of the ADC quantization error 58
4.7 Sampling clock offset illustration 59
4.8 System modeling in Simulink 60
4.9 BER performance with phase noise in AWGN channels (SNR = 6 dB) 62
4.10 Error probabilities with phase noise in AWGN channels (SNR = 6 dB) 63
4.11 BER performance with different amounts of phase noise at different SNRs. 63
4.12 Error probabilities with different amounts of phase noise at different SNRs. 64
4.13 BER performance with carrier frequency offset in AWGN channels (SNR = 6 dB) . . . 64
4.14 Error probabilities with carrier frequency offset in AWGN channels (SNR = d dB). . . 65
4.15 BER performance with different carrier frequency offsets at different SNRs 66

4.16 Error probabilities with different carrier frequency offsets at different SNRs 67
4.17 BER performance with I/Q mismatch in AWGN channels (SNR = 0, 6, 10 dB) 67
4.18 Error probabilities with I/Q mismatch in AWGN channels (SNR = 6 dB) 68
4.19 BER performance with different amounts of relative I/Q mismatch interference at different SNRs 68
4.20 Error probabilities with different amounts of relative I/Q mismatch interference at different SNRs 69
4.21 BER performance with ADC quantization noise in AWGN channels 70
4.22 Error probabilities with ADC quantization noise in AWGN channels 70
4.23 BER performance with different ADC word lengths at different SNRs 71
4.24 Error probabilities with different ADC word lengths at different SNRs 71
4.25 BER performance with sampling clock offset in AWGN channels (SNR = 6 dB) 72
4.26 Error probabilities with sampling clock offset in AWGN channels (SNR = 6 dB) 73
4.27 BER performance with different sampling clock offsets at different SNRs 73
4.28 Error probabilities with different sampling clock offsets at different SNRs 74
4.29 Rayleigh fading channel model 75
4.30 BER performance with different amounts of phase noise at different SNRs. 76
4.31 Error probabilities with different amounts of phase noise at different SNRs. 77
4.32 BER performance with frequency offset in Rayleigh fading channels (SNR = 6 dB) . . . 77
4.33 Error probabilities with frequency offset in Rayleigh fading channels (SNR = 6 dB) . . . 78
4.34 BER performance with different carrier frequency offsets at different SNRs 78
4.35 Error probabilities with different carrier frequency offsets at different SNRs 79
4.36 BER performance with different amounts of relative I/Q mismatch interference at different SNRs 80
4.37 Error probabilities with different amounts of relative I/Q mismatch interference at different SNRs 80
4.38 BER performance with ADC quantization noise in Rayleigh fading channels. 81
4.39 Error probabilities with ADC quantization noise in Rayleigh fading channels. 82
4.40 BER performance with different ADC word lengths at different SNRs. 82
4.41 Error probabilities with different ADC word lengths at different SNRs 83
4.42 BER performance with different sampling clock offsets at different SNRs 83
4.43 Error probabilities with different sampling clock offsets at different SNRs 84
4.44 Rician fading channel scenario 84
4.45 Rician fading channel model in MATLAB. 86
4.46 PDF of Rayleigh fading and Rician fading for $\sigma_o^2 = 1$. 87
4.47 BER performance without any impairment for 3 different channel models 87
4.48 BER performance with different amounts of phase noise at different SNRs 88

4.49 Error probabilities with different amounts of phase noise at different SNRs. 89
4.50 BER performance with carrier frequency offset in Rician fading channels (SNR = 6 dB) . 89
4.51 Error probabilities with carrier frequency offset in Rician fading channels (SNR = 6 dB) . 90
4.52 BER performance with different carrier frequency offsets at different SNRs 90
4.53 Error probabilities with different carrier frequency offsets at different SNRs 91
4.54 BER performance with different amounts of relative I/Q mismatch interference. 92
4.55 Error probabilities with different amounts of relative I/Q mismatch interference. 92
4.56 BER performance with different ADC word lengths at different SNRs 93
4.57 Error probabilities with different ADC word lengths at different SNRs 94
4.58 BER performance with different sampling clock offsets at different SNRs 94
4.59 Error probabilities with different sampling clock offsets at different SNRs. 95

5.1 Worst case: all four carriers with co-channel CW interference 97
5.2 BER performance without any impairment in different CW interference cases (SNR = 6 dB). 98
5.3 Error probabilities without any impairment in different CW interference cases (SNR = 6 dB) 99
5.4 BER performance without any impairment in different PM interference cases (SNR = 6 dB). 100
5.5 Error probabilities without any impairment in different PM interference cases (SNR = 6 dB). 100

List of Tables

3.1 Hamming distances and normalized correlation results 36

4.1 Phase noise variance σ^2 vs. power spectral density $L(\Delta f)$ 54

4.2 Simulation parameters 61

5.1 Distribution of the different bits between any two OVSF codes 101

5.2 Error probabilities with channel selection mechanism (without AWGN) 104

5.3 Error probabilities with channel selection mechanism (with AWGN) 106

Introduction 1

1.1 Background

Wireless Sensor Networks (WSNs) are a multi-disciplinary technology, which has developed rapidly in the recent years. It involves the most advanced technologies in the field of electronics and telecommunication, including analog and digital circuit design, wireless communications, signal processing, and so on. WSNs are typically composed of a large number of sensors which are distributed in the environment of interest, as shown in Figure 1.1. The sensors can monitor the environment, collect the data, process the data and wirelessly communicate with other sensors. Because of its autonomy and smartness, it has been widely used in many applications, such as environment monitoring, traffic control, health monitoring, etc. Particularly, WSNs can be deployed in some occasions where wired communication is difficult or impossible to achieve.

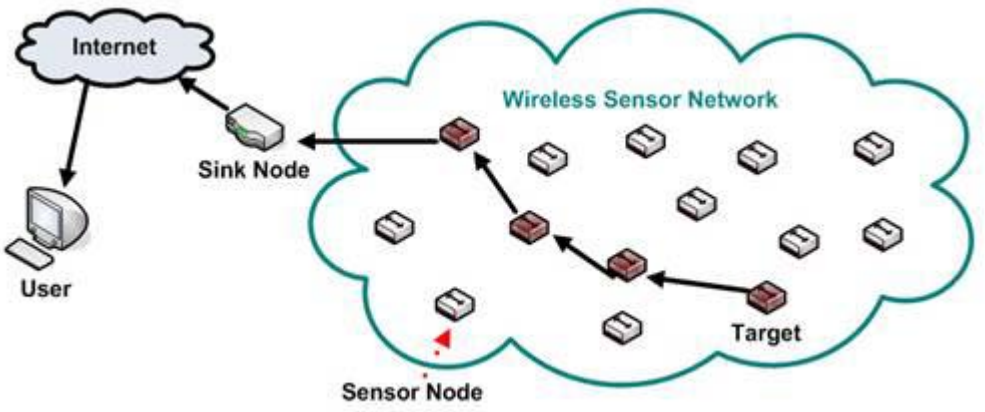

Figure 1.1: Wireless Sensor Network

Although WSNs bring lots of benefits in many areas, power consumption is one of the bottlenecks for wide applications. The reason is that the sensor nodes in the network are supplied by batteries, which are usually not or never rechargeable. Hence, improving the energy efficiency of WSNs becomes a hot topic in both research and industry. In general, the data communication and sensing activities of the sensor nodes are dominant in the power consumption [1]. In order to reduce the power consumption, many schemes are presented. Duty cycling control and a wakeup radio assisted scheme are the two most discussed solutions among them. In a duty cycle scheme, the transceivers of the sensor nodes are kept in the sleep mode but they wake up regularly to listen to the radio channel and to check if others want to communicate with them [2]. The power

consumption can be decreased significantly when the sensor nodes are in the sleep mode most of the time, though it is at the cost of packet latency. Moreover, power is also wasted when the transceivers wake up on a regular basis and find there is no communication request for them. This can be particularly severe in networks with sporadic traffic but demanding low latency, where the sensor nodes have to wake up and listen frequently (see Figure 1.2).

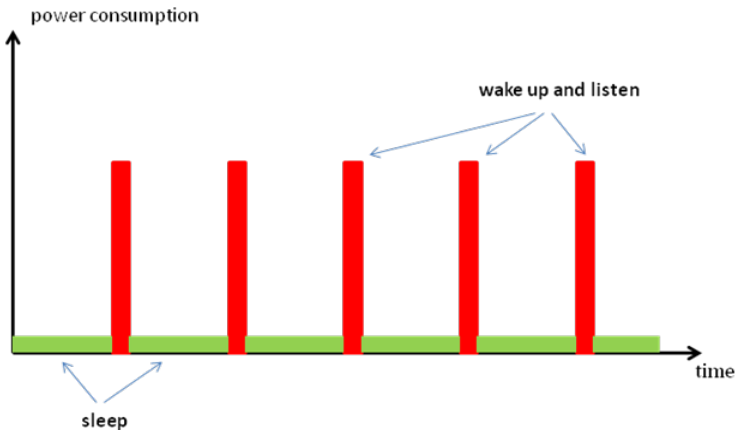

Figure 1.2: Duty cycle scheme

The other scheme is the wakeup radio which can lead to a much lower power consumption than the duty cycle scheme. Compared to the duty cycle scheme, the main transceiver that is responsible for data communication does not have to wake up periodically. Instead, it is in the sleep mode most of the time. An additional device called the wakeup radio receiver (WuRx) is a simplified receiver with much lower power consumption and data rate than the main transceiver. It is always on to monitor the channels continuously. It detects the wakeup packet, and sends the main transceiver a wakeup trigger upon successful detection of a wakeup packet. Then the main transceiver will wake up and start the data communication with the sensor node transmitting the wakeup packet. The wakeup radio system is shown in Figure 1.3 [3].

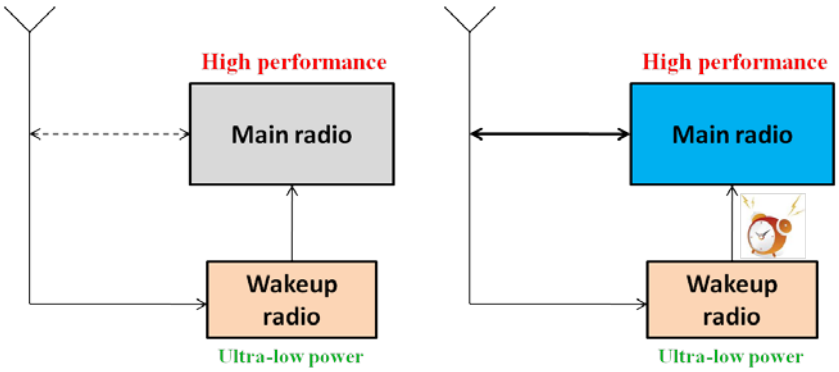

Figure 1.3: Wakeup radio system (left is the main radio in sleep mode and right is the main radio woken up)

In addition, we can benefit from the wakeup radio scheme because of the simplified protocol as well. The communication between WSN nodes is guaranteed by the handshake mechanism described in Figure 1.4, which is also widely used in other communication systems nowadays.

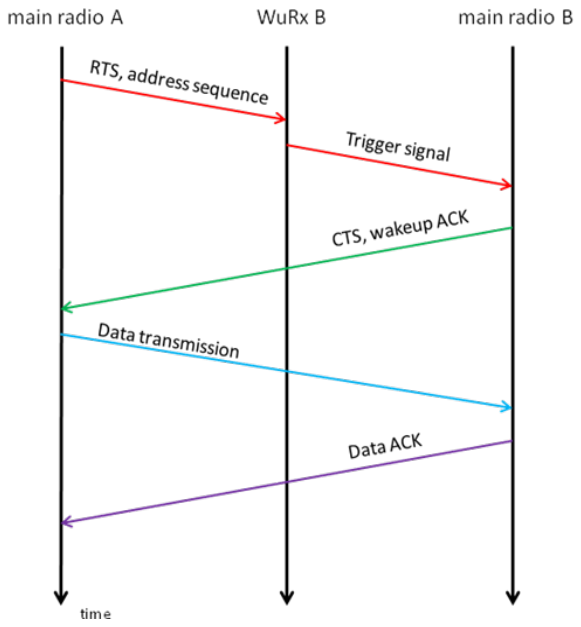

Figure 1.4: Handshake mechanism in a wakeup radio scheme

The wakeup radio scheme results in a significant reduction in power consumption, because the main transceiver is only awake when there is a real event. It requires the wakeup radio receiver to detect the wakeup packet accurately. If so, the wakeup radio helps to prolong the lifetime of a sensor node, and also that of the whole wireless sensor network.

1.2 Motivation

Due to its low power property, the wakeup radio is nowadays of increasing interest in research and commercial market. The low-power wakeup radio has been studied and improved by many universities and companies since its definition was presented. Lots of papers and documents are published to boost its evolution. Most of them are focused on the architecture and circuit design of a low-power wakeup radio receiver, especially the front-end of the wakeup radio receiver. These previous designs aim at decreasing the power consumption of the wakeup radio receiver as much as possible.

The accurate detection of a wakeup packet is of crucial importance for the wakeup radio receiver. The detection performance is typically characterized by two error probabilities, i.e., the miss detection probability P_{md} and false alarm probability P_{fa}. Miss detection means the receiver

ignores the wakeup packet which is destined for it, while a false alarm indicates that the receiver accepts the wakeup signal that is meant actually for another receiver, and then sends a wakeup trigger to the main radio. If the wakeup packet is wrongly detected and the main transceiver is falsely alarmed, extra power will be consumed. In order for the sensor nodes to achieve a low-power consumption, an accurate wakeup signal detection should be obtained at the wakeup radio receiver.

But it is really a challenging task. As we know, the spectrum is very precious nowadays and has been shared by many wireless technologies, especially in the industrial, scientific, and medical (ISM) band. Most of the wireless local area network (WLAN) and wireless personal area network (WPAN) systems, such as Bluetooth, Zigbee, and Wi-Fi, work in the 2.4 GHz ISM band where neither resource planning nor bandwidth allocation can be guaranteed [4]. Additionally, a microwave oven also works in the 2.4 GHz ISM band. The most common wireless standards operating in the ISM band can be seen in Figure 1.5.

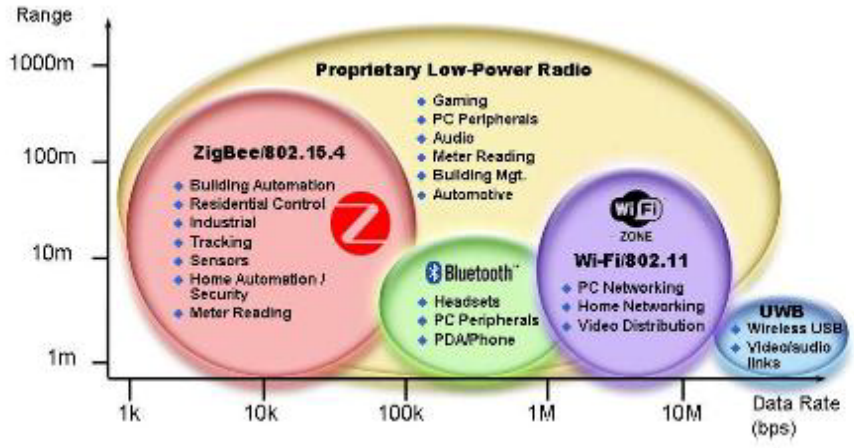

Figure 1.5: Wireless standards operating in the 2.4 GHz ISM band

The channels in the ISM band are typically very busy and much interference from other ISM equipments may exist in some specific channels for a long time. Since the wakeup radio receiver also operates in the 2.4 GHz ISM band, a wakeup signal can be greatly interfered in such a noisy channel, which may lead to a false alarm or miss detection at the receiver. If the destined receiver cannot correctly detect the wakeup packet, it remains in the sleep mode. Then the wakeup packet has to be transmitted again, which also increases the power consumption of sensor nodes.

In short, interference robustness is absolutely another concern in the design of a wakeup radio receiver besides low-power consumption. Therefore, a multi-carrier (MC) wakeup radio receiver is proposed in IMEC-NL/Holst Centre as a solution to interference mitigation.

1.3 Related work

In the literature, we can find the development of the wakeup radio in the past few years. As discussed in the previous sections, many works focus on the architecture design of wakeup radio receivers so that a low-power consumption can be achieved. So far, a wakeup radio receiver has already achieved ultra-low power consumption. Most of the designs are based on an envelope detector. An envelope detector can be used to demodulate an AM-modulated signal by removing all the high frequency components of the signal. The capacitor and resistor form a low-pass filter to filter out the carrier frequency. It can extract the envelope of the modulated signal which is equivalent to the baseband signal. Envelope detection techniques used at the receiver can get rid of the frequency conversion circuits like the mixer and PLL, which improves integration and reduces power consumption [5]. So low-power consumption is one of the biggest advantages of the envelope detector, which explains why the envelope detector becomes the most selected element in the design of low-power wakeup radio receivers.

In the past few years, the power consumption of wakeup radio receivers has decreased significantly. The work presented by the Berkeley wireless research group in [6] demonstrates that the power consumed by the analog front-end is 65uW with a single supply of 0.5V. Later on, the paper [7] presents a promising architecture for the realization of a complete ultra-low power wakeup radio. Single-channel transmission and reception is deployed in the design, and the antenna can be shared by the main transceiver and the wakeup radio device. In [7], binary pulse width modulation (PWM) is chosen to transmit the address code instead of on-off keying (OOK). The reason given is that PWM contains clocking information which can be used to synchronize the decoder to the incoming message. The total power consumption is kept below a threshold of 50uW. In the most recent research [8], the power consumption of the analog front-end can be even reduced to 7.5uW with a supply of 1.5V. However, the additional power needed in the digital baseband is not estimated at all in the above works. The paper [9] describes the design and implementation of an ultra-low power digital baseband (DBB) circuit for a wakeup receiver. In the design, the baseband circuit only consumes 3.72uW with a standard supply of 1.2V and achieves excellent packet detection performance. It also discusses the wakeup packet structure that can be a reference for our proposal.

The literature discussed above mainly aims at reducing the power consumption of envelope-detector-based wakeup radio receivers. However, envelope detectors are more susceptible to noise and interference than other detectors such as the product detector [5]. Before the envelope detector, there is typically a bandpass filter which is also a wideband filter. Then interference will be mixed to the modulated signal. Moreover, the 2.4 GHz ISM band where the wakeup radio receiver is operating in is a really noisy spectrum as we discussed in Section 1.2. In the ISM band, multiple technologies coexist, such as microwave ovens, Bluetooth, Zigbee and

Wi-Fi, which can act as interferers for the desired signal. Unfortunately, not much prior research refers to the issue of interference robustness in the design of envelope-detector-based wakeup radio receivers. Only a few papers mention that resistance to interference is also a design goal for wakeup radio, but they do not detailedly explain the implementations of interference resistance. [7] demonstrates that a tradeoff has to be made between power consumption and the ability to withstand interferers. A longer address code reduces the probability of false alarms but implies longer transmit time leading to larger power consumption. It also discusses the modulation used for a wakeup radio and presents that the probability of these devices interfering is greater if the modulation used is similar to the ones used by other devices in the same band. On the other hand, if a simple modulation like PWM and OOK is used, the more sophisticated modulations will be perceived more as background noise than interferers, and more importantly, the receiver structure will be much simpler. In [10], the concept of interference removal is discussed for low-power radio design. But still no further details are given for the realization of interference mitigation.

From the previous works [11], we can see that the diversity scheme is a popular method to impair the interference in communication systems. Diversity can play an important role in combating fading or interference. It is based on the fact that individual channels encounter different levels of interference and fading. Diversity can be conducted at the transmitter and the signals are combined at the receiver. It is usually classified into time diversity, frequency diversity, space diversity, and polarization diversity. Time diversity means that the desired signal is transmitted at different time instants and different copies undergo independent fading or interference. Frequency diversity requires that the desired signal is modulated through different carriers. In different channels, the signal experiences different levels of interference. Orthogonal frequency division multiplexing (OFDM) and spread spectrum are the classical examples of frequency diversity. In space diversity schemes, the signal is transmitted over multiple propagation paths, which can be achieved by antenna diversity using multiple transmitter antennas and multiple receiver antennas such as multiple-input multiple-output (MIMO).

In the patent [12], a new wakeup receiver for detecting wakeup packets and processing multiple frequency channels in parallel is presented. It brings up channel removal, and only those channels that are not identified as ‘restricted’ are processed. It can help to reduce receiver power consumption by processing only the channels where unwanted signals are not present. Although a multi-channel approach is presented, it only exists at the receiver. The receiver scans several channels in parallel, but just to look for a single wakeup signal which is transmitted over a single frequency channel.

In the current commercial market, AUSTRIAMICROSYSTEMS has recently produced AS3931, an ultra-low power and three-channel wakeup radio receiver. It repeatedly transmits and receives the same wakeup packet in multiple channels. It detects a low-frequency AM-modulated signal by

looking for a digital wakeup pattern and generates a WAKE signal after successful pattern detection [13]. Compared to previous wakeup radio receivers, it features the multi-channel property. It means the wakeup packet can be transmitted in multiple channels. The channel with the highest received signal strength (RSS) will be selected and the wakeup pattern in the received signal will be correlated with the local pattern. The device also incorporates an intelligent pattern detection algorithm that provides reliable operation in the presence of strong interference. It can solve the problem resulting from a single channel where the interference may be quite large and exist for a long time by measuring RSS and selecting the best channel. But only one channel is selected finally. High sensitivity and high dynamic range can also be obtained. Figure 1.6 shows the block diagram of the AS3931. In this three-channel wakeup receiver, three envelope amplifiers, detectors and correlators are required in the receiver to achieve the desired functionality. But they are not really necessary if only the best channel with the highest RSS is chosen finally for wakeup packet detection.

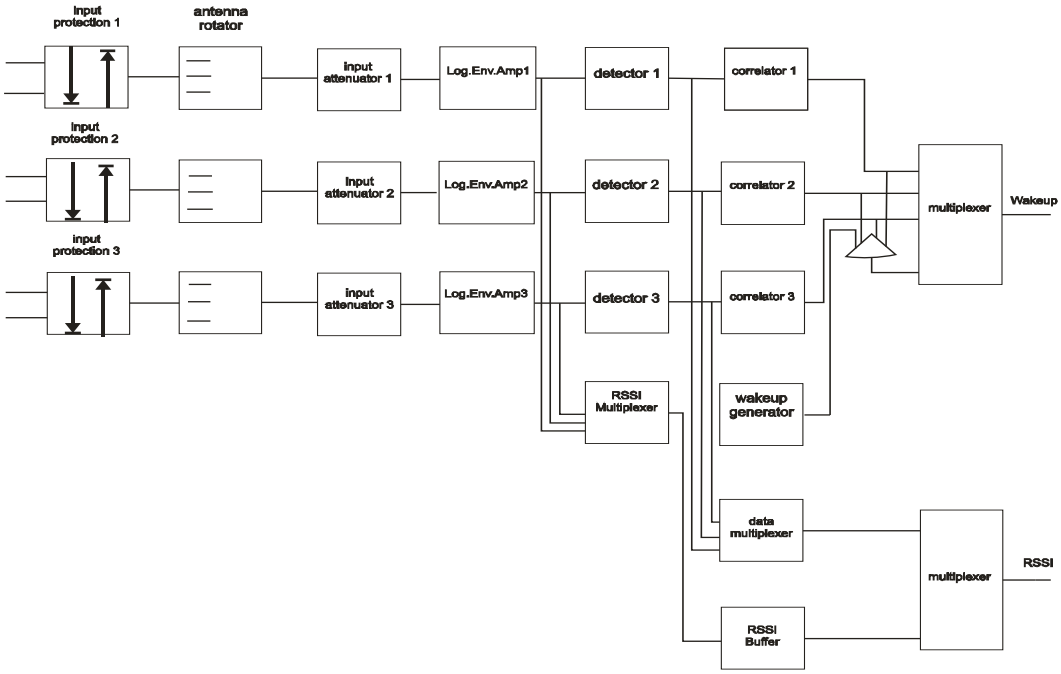

Figure 1.6: Block diagram of the AS3931

The AS3932 is a revision of the AS3931. In comparison with the AS3931, there is only one envelope detector and one data correlator in the AS3932, leading to a simpler architecture and lower power consumption. The channel selector combines the output of the three channel amplifiers and then decides which channel to connect to the envelope detector according to the RSSI. The modified circuit and architecture can be observed in Figure 1.7. The AS3932 supports a programmable data rate and Manchester decoding with clock recovery [14]. The integrated correlator can be used for detection of a programmable 16-bit wakeup pattern. The programmable features of the AS3932 enable to optimize its setting for achieving a longer distance while

retaining a reliable wakeup generation. The sensitivity level of the AS3932 can be adjusted in the presence of a strong field or noisy environment.

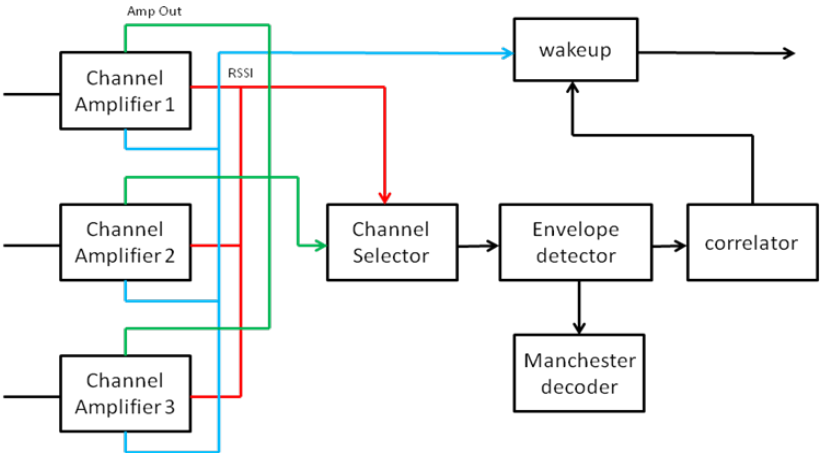

Figure 1.7: Block diagram of the AS3932

It is the most recent product in the area of multi-channel wakeup radio receivers. It is similar to our design but there are still some differences, which will be discussed below. It supports multi-channel transmission and reception so that the impact of interference in channels can be restricted. The receiver listens to these channels in parallel. Channel selection is also presented in the design of the AS3931. Based on the measure of RSS, the channel with the highest RSS is selected. The correlator is used for the detection of the wakeup packet. It can judge whether the received address matches the local address or not. If they do match, a wakeup trigger is generated and sent to the main transceiver. On the other hand, the same wakeup packet is simply and repeatedly transmitted in multiple channels in the AS3931. In other words, the design of the AS3932 does not consider a time-frequency grid transmission which is a portion of our design. In the AS3931, the received signal measured for RSS includes the desired signal, noise and interference. It means the noise and interference also have an impact on the RSS. Furthermore, only one channel with the highest RSS is finally selected in the AS3932. But in our selection of good channels, we differentiate and estimate the desired signal and the noise-plus-interference. According to the signal to noise-plus-interference ratio (SINR) calculated from the channels employed in the transmission, we remove the bad channels. In the AS3931, the complete wakeup pattern can be found in the selected channel. After channel selection, the packet is sent to the envelope detector where the bandpass signal is transformed into a baseband signal and then the analog signal is converted to digital bits through a comparator. We may select more than one channel as long as the SINR of each channel in use meets the requirement. In terms of system performance, the wakeup sensitivity level, dynamic range and data rate of the wakeup receiver are tested and mentioned in the datasheets of the AS3931, AS3932 and AS3933. In comparison, we are more concerned about the probability of false alarm, the probability of miss detection and

power consumption in the wakeup receiver. Unfortunately, none of them is considered in the design of the AS39 series by AUSTRIAMICROSYSTEMS.

1.4 System overview

As can be observed from the related work above, low-power consumption is always the first goal in the design of a wakeup radio receiver. There has been a great progress in the reduction of the power consumption of wakeup radio receivers. All the architectures in the prior researches are envelope-detector-based, since the envelope detector consumes less power and also has a simpler architecture. But as discussed in the related work, envelope detector is more susceptible to interference or noise than others. In practice, the co-channel interference is really high in the license-free ISM band. The interference added to the desired signal will affect the wakeup packet detection performance of the receiver. In the previous researches on interference avoidance in communication systems, frequency diversity and space diversity are attractive, which can be seen from the increasing interest in the study of OFDM and MIMO.

In our proposal, frequency diversity is used where only one antenna is needed at the transmitter and receiver. Instead of transmitting an address code in a single carrier as in [12] [13] [14] [15], we propose a system in which an address matrix is constructed and transmitted over a time-frequency grid, using a predefined number of time slots and frequency channels. At the transmitter, the long address vector of a wakeup packet is reconstructed into an address matrix with N rows and M columns. The sub-addresses in columns are modulated to different carriers and then transmitted in multiple channels. During the transmission, the sub-addresses from different columns experience different levels of interference and fading in space. At the front-end of the receiver, selection combining is chosen among all possible diversity combining technologies. After the SINR estimation for all the channels in use, only the channels with SINRs above a certain threshold are selected and further processed, leading to power saving and interference robustness. So the interference is combated with the use of frequency diversity and the channel selection mechanism. In the simulations, the probability of false alarm and the probability of miss detection are used to reflect the detection performance of a wakeup radio receiver. The requirement of the system is to make these two probabilities as low as possible and simultaneously achieve a low-power consumption. However, in practical implementations, the impairments from the wakeup receiver itself cannot be neglected, such as RF impairments, ADC quantization noise and sampling clock offset. The detection performance may degrade due to RF impairments and ADC quantization noise at the MC wakeup receiver. The influence of these impairments on the receiver detection performance has to be explored as well.

1.5 Outline and contributions

Here we would like to provide an overview of the work described in this thesis. The first contribution is the analysis on the MC wakeup receiver architecture and the research on the receiver detection performance in the presence of channel noise and different kinds of interference. The second contribution is the proposal of different address correlation detection schemes. The third contribution is the performance analysis with RF impairments, ADC quantization noise and sampling clock offset in different channel models. The main content of each chapter in the thesis is outlined as follows.

Chapter 1: Introduction

In this section, an introduction is given to describe the technical background of a wakeup radio receiver. The motivation for the research of a multi-carrier wakeup radio receiver is presented. A literature overview is also provided to demonstrate the development of wakeup radio receivers in the last few years. Then the multi-carrier wakeup receiver is briefly described and the problem existing in practical implementations is also raised.

Chapter 2: Multi-Carrier Wakeup Receiver

A multi-carrier wakeup receiver architecture is proposed by IMEC-NL as a solution to the interference robustness in channels. The address transmission over a time-frequency grid is considered for the MC wakeup radio. In the MC wakeup radio receiver, not all the sub-addresses in channels are further processed for the wakeup packet detection. Based on the SINR in each channel, bad channels are discovered and removed to improve the interference robustness. The advantages of multi-carrier wakeup radios over single-carrier ones are explored.

Chapter 3: Detection Performance in AWGN Channels

Typically noise and interference exist in the channels and they always deteriorate the desired wakeup signals, which leads to a decrease of the receiver detection performance. Moreover, different kinds of interference result in different effects on the detection performance. The relationship between interference strength and receiver performance is explored. In this chapter, two address correlation detection schemes, hard-decision Hamming distance and soft-decision correlation, are proposed for the wakeup packet detection.

Chapter 4: Effects of Non-Idealities in AWGN and Fading Channels

In practical system designs and implementations, RF impairments are a crucial problem that must be taken into consideration, such as phase noise, frequency offset, I/Q mismatch, etc. The ADC quantization noise also has a negative effect on the detection performance. The detection

performance degradation as a function of various impairment parameters is investigated to identify the performance bottleneck for the multi-carrier wakeup receiver.

Chapter 5: Further Discussions on Co-Channel Interference

In this chapter, the effects of co-channel interference on the detection performance of the MC wakeup receiver are further studied. Continues wave interference and phase modulated interference are taken into consideration. The worst detection performance in practice is explored, when all the frequency channels in use experience interference. In the last part of this chapter, we discuss the effect of the number of discarded channels when the channel selection mechanism is used to mitigate the interference.

Chapter 6: Conclusions and Future Work

This chapter summarizes the work described in the thesis and provides some suggestions for further research and development on this topic.

Multi-Carrier Wakeup Receiver 2

In this chapter, the multi-carrier wakeup radio receiver proposed by IMEC-NL is introduced first. For a better understanding of the new MC wakeup receiver architecture, the functionality of each element is explained. In practical implementations, the channel spacing is a factor that may affect the receiver detection performance. Thus theoretical analysis is conducted to derive the optimal channel spacing. For this MC wakeup receiver architecture, a time-frequency-grid address reconstruction scheme is proposed. The codes used for address generation, the wakeup packet structure, as well as the modulation are discussed to explore the introduced changes at the transmitter. In the multi-carrier wakeup radio receiver, not all the channels in use will be selected for the address detection. A channel selection mechanism is introduced to estimate the noise and interference power level in channels and then to select the channels which meet the requirements. In the channel selection mechanism, different selection thresholds lead to different detection performances of the MC wakeup receiver. Moreover, the number of carriers to be used is viewed as a tradeoff between detection performance and system complexity.

2.1 MC wakeup receiver architecture

At the receiver, the first task is the demodulation of the desired signals. An example with four-carrier wakeup receiver is demonstrated in Figure 2.1. The signals are demodulated in parallel. In the four-carrier case, the received signal in the absence of noise and interference can be expressed as:

$$r(t) = A_1 \cdot \cos(w_1 t) + A_2 \cdot \cos(w_2 t) + A_3 \cdot \cos(w_3 t) + A_4 \cdot \cos(w_4 t) \qquad (2.1)$$

Each chain in the wakeup radio receiver corresponds to one carrier, and is used to demodulate the signal from that carrier and to recover the sub-address for address correlation detection. For each chain, only the signals of interest are detected, and the signals on other carriers are suppressed as interference. The output of each chain with mixers, integrators and squaring devices will be derived and discussed in Section 2.1.3.

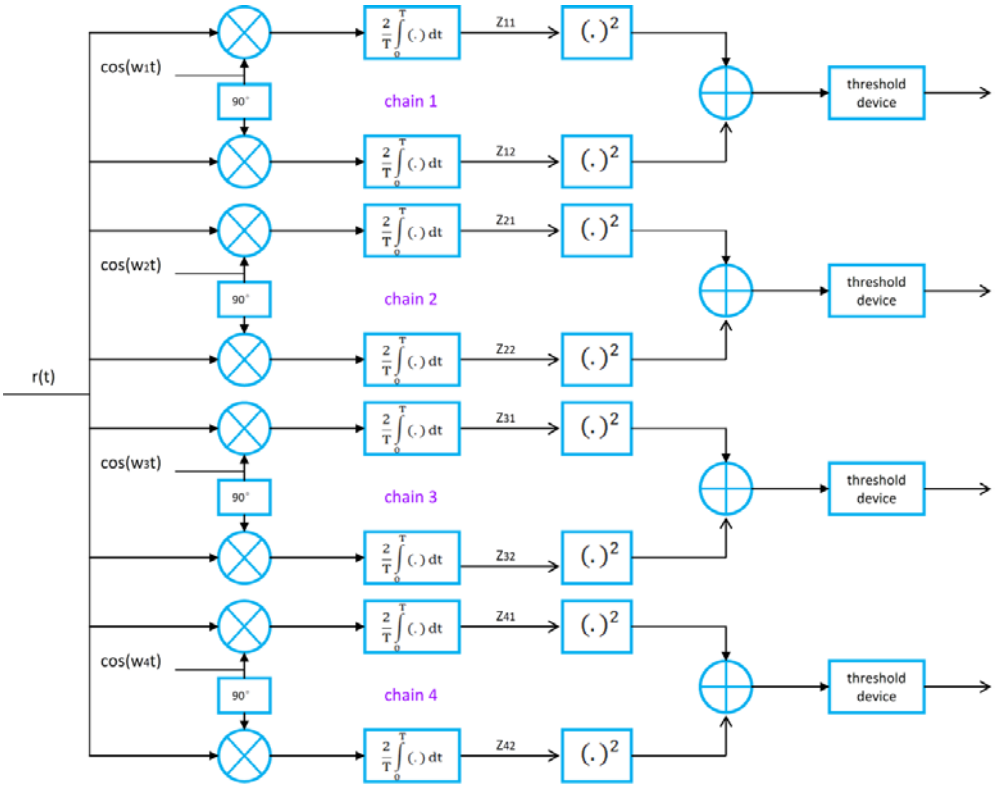

Figure 2.1: Four-carrier wakeup radio receiver architecture

2.1.1 Mixer and oscillator

The functionality of the product mixer at the front-end of the wakeup receiver is to down-convert the modulated desired signal from the bandpass frequency to baseband. The frequency shift is typically done by multiplying the received signal with a carrier signal from an oscillator. Several kinds of oscillators exist nowadays, such as RC oscillators, LC oscillators and voltage controlled oscillators (VCOs). A VCO usually has a sufficient linear relationship between the input voltage and output frequency, and consumes very little current.

An ideal oscillator is expected to generate a pure sine wave of the carrier frequency. Unfortunately, the oscillators are non-ideal in practice. Phase noise and frequency offset are the most common impairments in the oscillators. Due to these impairments in oscillators, the receiver detection performance may degrade significantly. The performance of the MC wakeup radio receiver with these impairments will be discussed and analyzed in detail in Chapter 4.

2.1.2 Integrator

An integrator is a device that performs the mathematical operation known as integration. An integrator can be viewed as a low-pass filter though the operations of these two devices are

different. An integrator is defined by the formula (2.2), where $x(t)$ and $y(t)$ are the input and output of the integrator individually:

$$y(t) = \frac{1}{T} \int_{t-\frac{T}{2}}^{t+\frac{T}{2}} x(\tau) d\tau \qquad (2.2)$$

where T is the integration time.

It is also expressed as (2.3) by a convolution with $\frac{p_T(t)}{T}$ representing a rectangular function:

$$y(t) = x(t) \otimes \frac{p_T(t)}{T} \qquad (2.3)$$

With the Fourier transform, it is transferred to:

$$Y(w) = X(w) \cdot \frac{\sin(wT/2)}{wT/2} \qquad (2.4)$$

So the transfer function of an integrator can be defined as:

$$H(w) = \frac{\sin(wT/2)}{wT/2} \qquad (2.5)$$

The transfer function $H(w)$ is sketched in Figure 2.2. It is seen that an ideal integrator can be viewed as a low-pass filter. The cut-off frequency equals $\frac{1}{T}$. But the integrator output is typically a triangle wave, which means that the envelope of the original signal cannot be retrieved with an integrator functioning as a low-pass filter.

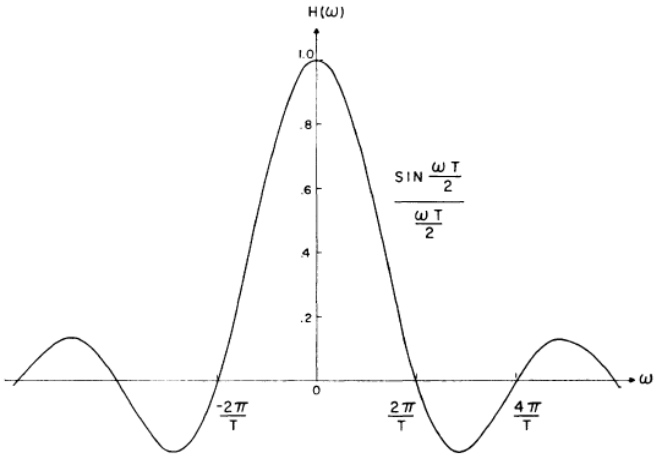

Figure 2.2: The transfer function of an integrator with integration time T

2.1.3 Channel spacing

In order to simplify and better explain the derivation of the output of each chain with mixers, integrators and squaring devices, it is reduced to a two-carrier case. Then the received signal is:

$$r(t) = A_1 \cdot \cos(w_1 t) + A_2 \cdot \cos(w_2 t) \tag{2.6}$$

After the front-ends and integrators, the signals in the two branches of the first chain are individually marked as Z_{11} and Z_{12}:

$$\begin{aligned} Z_{11} &= \frac{2}{T}\int_0^T [A_1 \cdot \cos(w_1 t) + A_2 \cdot \cos(w_2 t)] \cdot \cos(w_1 t) dt \\ &= A_1 + \frac{A_1}{2w_1 T} \cdot \sin(2w_1 T) + \frac{A_2}{(w_1 + w_2)T} \cdot \sin(w_1 + w_2)T + \frac{A_2}{\Delta w T} \cdot \sin(\Delta w T) \end{aligned} \tag{2.7}$$

$$\begin{aligned} Z_{12} &= \frac{2}{T}\int_0^T [A_1 \cdot \cos(w_1 t) + A_2 \cdot \cos(w_2 t)] \cdot \sin(w_1 t) dt \\ &= \frac{A_1}{w_1 T} \cdot \sin^2(w_1 T) + \frac{2A_2}{(w_1 + w_2)T} \cdot \sin^2(\frac{(w_1 + w_2)T}{2}) - \frac{2A_2}{\Delta w T} \cdot \sin^2(\frac{\Delta w T}{2}) \end{aligned} \tag{2.8}$$

where Δw is called the channel spacing and it is defined by $\Delta w = w_2 - w_1 = 2\pi(f_2 - f_1)$. After the squaring devices and sum, the output of the first chain is:

$$Z_{11}^2 + Z_{12}^2 \approx A_1^2 + [\frac{2A_2}{\Delta w T} \cdot \sin(\frac{\Delta w T}{2})]^2 + \frac{2A_1 A_2}{\Delta w T} \cdot \sin(\Delta w T) \tag{2.9}$$

If $\Delta w T$ equals $2k\pi$, the second and third terms in the formula (2.9) become zero, and $Z_{11}^2 + Z_{12}^2$ reduces to A_1^2. Therefore, the desired signal in each channel is recovered with the interference from the other carriers removed at the receiver. It can be concluded that $2k\pi / T$ is the optimal channel spacing for the receiver detection performance. But in case Δw equals $k\pi / T$, the detection performance would be greatly deteriorated.

2.2 Changes at the transmitter

2.2.1 Address generation

In order to distinguish the different wakeup receivers, each wakeup receiver is assigned a unique address sequence. Typically the wakeup receiver addresses are generated with two kinds of codes, orthogonal variable spreading factor **(**OVSF) codes and pseudo-noise **(**PN) codes.

OVSF codes are a set of spreading codes derived from a tree-structured set of orthogonal codes. The OVSF codes are characterized by the spreading factor (SF) and the orthogonality between any two codes with the same length. The OVSF codes can be created with the use of a code tree, as depicted in Figure 2.3.

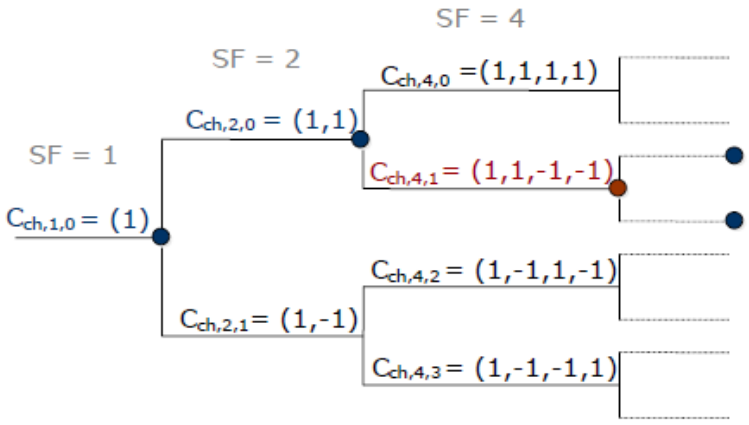

Figure 2.3: OVSF code tree [16]

Each node in the tree has two branches, each representing a code of double length. The spreading factor equals the number of available OVSF codes in the vertical level as well as the length of the OVSF codes. Consequently, a set of 2^k OVSF codes with a length of 2^k bits is available at the k^{th} level. A code is basically created through the multiplication of a code of the next lower level. The code being multiplied is called the mother code. Two double-length codes are generated from a mother code through the chaining of two copies of the mother code or the chaining of the mother code with a copy multiplied by -1 [17]. Therefore, the distance between any two OVSF codes with the same length is always a half of the code length. The biggest advantage of OVSF codes is the orthogonal property, but a bottleneck also exists in OVSF codes. The number of available OVSF codes at a certain level is limited. For example, with a SF of 16 (i.e., a length of 16 bits), the number of OVSF codes is only 16. With OVSF codes, the address assigned to a wakeup radio receiver is one of the predefined set.

In comparison, the bits in a PN sequence are random-like, which means that a code can be generated by mathematically precise rules, but statistically it satisfies the requirements of a truly random sequence in the limiting sense [18]. PN codes are usually generated by shift registers and XOR gates. The length of a PN code is determined by the number of registers. For *m* registers, the length of a PN code is $2^m - 1$. PN codes have an important property, i.e., the time-shifted version of the same PN code has very little correlation with itself. The code distance between any two PN sequences can be as small as 1.

2.2.2 Address matrix

In a single-carrier wakeup radio, the address is sent as a vector on a single carrier to find the intended wakeup receiver. But in order to align with the multi-carrier structure of the wakeup receiver, the address vector is reshaped into a matrix of dimension $N \times M$, in which the M columns represent all the frequency channels to be used. Note that the correlation property changes with the conversion from an address vector to an address matrix. A time-frequency-grid address matrix of size 4×8 is shown in Figure 2.4. In an address matrix, the sequence in each column, called a sub-address, consists of N bits and it is transmitted over an individual frequency channel.

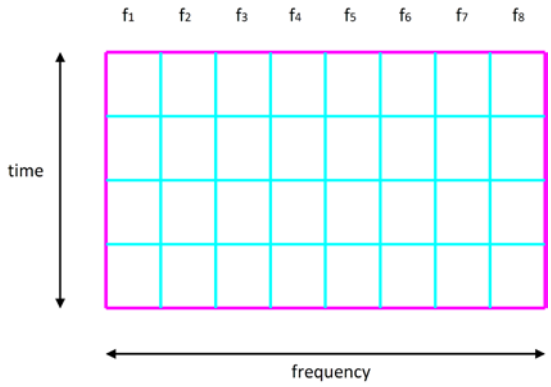

Figure 2.4: Time-frequency-grid address matrix

2.2.3 Wakeup packet structure

After the address reshaping from a vector into a matrix, the sub-addresses are encapsulated into wakeup packets. Some redundant bits are added for synchronization and noise estimation. The structure of a wakeup packet is described in Figure 2.5.

Figure 2.5: Wakeup packet structure

Before the address code are the preamble and start frame delimiter (SFD), used for amplitude estimation and packet synchronization respectively [9]. The address sequence is created with an OVSF code as explained in Section 2.2.1 and employed to identify the intended wakeup receiver. In order to increase the robustness, the address can be Manchester-encoded. In Manchester encoding, a 0 is expressed by a low-to-high transition while a 1 is represented by a high-to-low transition. In other words, all the 1s and 0s are encoded as 10 and 01 individually, giving rise to an equal number of 1s and 0s in the Manchester-encoded address. The address code in the wakeup packet is followed by a one-bit flag, which is used to indicate if there is a payload part in the packet or not. For wakeup receiver identity detection, the address part is of crucial importance, as it will be compared with the local receiver address for the discovery of the intended one. If it is greatly ruined during the packet transmission, the correct wakeup receiver cannot be found.

2.2.4 OOK modulation

For a minimum complexity of the wakeup receiver, simple modulation and demodulation schemes are preferred. OOK is the simplest form of amplitude-shift keying (ASK) modulation. The binary digital information of a wakeup packet is carried in the amplitude of a carrier signal. The binary data can be represented by the presence and absence of a carrier signal during a symbol period. In practice, the stabilized oscillator in the transmitter is simply turned on and off in synchronization with the data to be transmitted. One advantage of using this type of modulation is at least a 50% reduction in battery current drain, compared to that consumed by a frequency-shift keying (FSK) transmitter [19]. The FSK transmitter must be on 100% of the time when the data is being transferred. Additionally, the OOK signal can be used to estimate the noise power in the channels because no carrier signal is transmitted for the digital information 0.

2.3 Channel selection mechanism

In the MC wakeup receiver, not all the channels in use will be selected for the address correlation detection. A channel selection mechanism is proposed to discover and remove the poor channels for an improvement in the detection performance.

2.3.1 Architecture

In the channel selection mechanism, the channels with high noise-plus-interference power levels are regarded as bad channels. The sub-addresses from these bad channels are spoilt. In case they are still used for address correlation detection, they will cause a diminution in the detection performance. By removing these bad channels in the calculation of address correlation, the detection performance can be improved. Therefore, it is necessary that the noise and interference

power level in each channel is estimated individually and then channel selection is conducted before the address correlation detection. The channel selection architecture is shown in Figure 2.6.

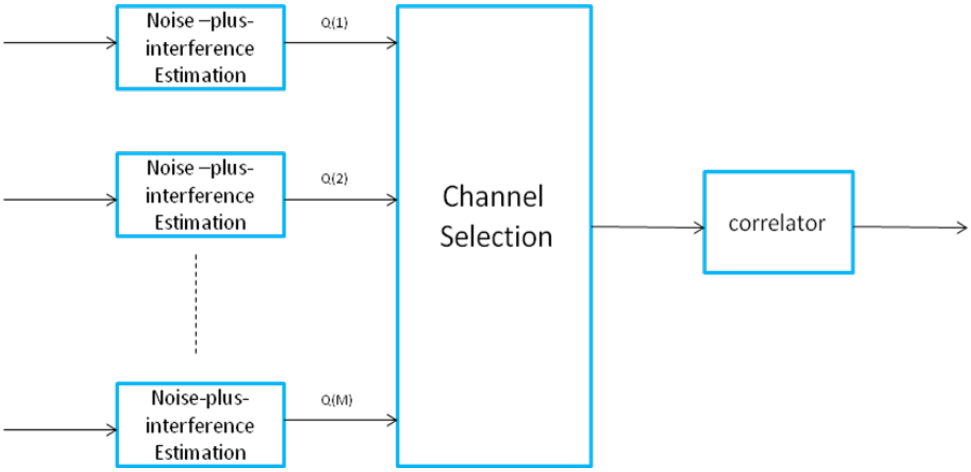

Figure 2.6: Channel selection architecture

2.3.2 Noise and interference estimation

The noise-plus-interference power can be estimated for each carrier frequency, which in practice can be done by monitoring the energy level in the channels when there is no signal coming in. For OOK signaling, this can even be done during signal transmission. The noise-plus-interference power estimated in the m^{th} channel is denoted as $P_n(m)+P_i(m)$. The average received signal power in the same channel is marked as $P_d(m)$. Then the quality of the m^{th} channel $Q(m)$ can be characterized by a noise-plus-interference power to desired signal power ratio, as defined below:

$$Q(m)=\frac{P_n(m)+P_i(m)}{P_d(m)} \qquad (2.10)$$

2.3.3 Channel selection operations

The channel quality factor is very substantial in the channel selection operation, as it decides whether the m^{th} channel will be selected or removed. $Q(m)$ is compared with a channel selection threshold defined as C_s. If $Q(m)$ is smaller than or equal to C_s, the corresponding channel is kept for the address correlation calculation. Otherwise, the m^{th} channel is viewed as a bad channel and then deleted. With the channel selection mechanism, the detection performance

of a MC wakeup receiver is improved because of the removal of poor channels. The advantages of a MC wakeup receiver with the channel selection mechanism over a single-carrier wakeup receiver and a MC wakeup receiver without channel selection will be exploited through the simulations below.

The simulations in this section have already been done by IMEC-NL and the results have been published in [20]. The simulations are based on the channel allocation depicted in Figure 2.7. The 2.400–2.4835 GHz Wi-Fi band is divided into 13 channels, each with a width of 22 MHz, but the center frequencies are only 5 MHz apart. Availability of these channels for Wi-Fi is regulated by every country individually. The Wi-Fi channel allocation in the simulations is based on the North America standards, in which the channels for Wi-Fi communication are 1-11. In the 2.4 GHz ISM band, there are also 16 channels for Zigbee with channel indexes from 11 to 26. As the Wi-Fi channels, each center frequency of the 16 Zigbee channels are separated by a frequency distance of 5 MHz as well. The first Zigbee channel in the 2.4 GHz ISM band is centered at 2405 MHz. The width of each Zigbee channel is only 2 MHz and thus there is no possibility of any overlap between the Zigbee channels. In the simulations, it is assumed that the Wi-Fi and Zigbee nodes are working in non-overlapping frequency channels. The wakeup signals are located between 2402 MHz and 2480 MHz. The bandwidth of each wakeup signal is 1 MHz and 4 carriers are used for signal transmission. The wakeup receiver is assigned an address of 32 bits.

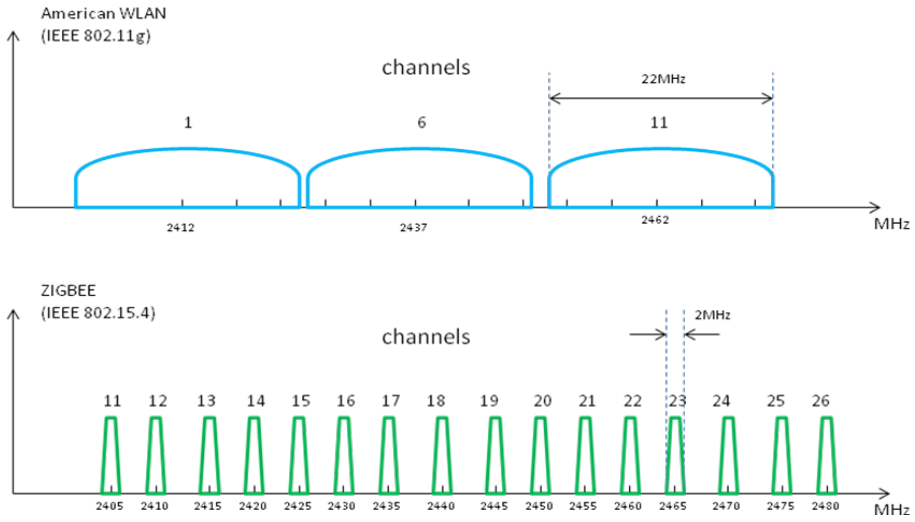

Figure 2.7: Channel allocations for the Wi-Fi and Zigbee nodes

In the simulation scenario shown in Figure 2.8, the wakeup transmitter (WuTx) and the wakeup receiver (WuRx) are separated by a random distance, and the distance varies from 1 meter to 20 meters. All the Wi-Fi and Zigbee interferers are randomly distributed within a radius of 20 meters

around the wakeup receiver. Due to the random positions of the interferers, the noise-plus-interference power in each channel is also random and it can only be estimated at the wakeup receiver. The considered channel model is path loss and additive white Gaussian noise (AWGN) channel. After the channel quality factor $Q(m)$ is compared with a selection threshold of 2, bad channels are discovered and then deleted to improve the detection performance of the wakeup receiver. The advantages of the MC wakeup receiver over the two other schemes can be observed in terms of the miss detection probability and false alarm probability in Figures 2.9 and 2.10.

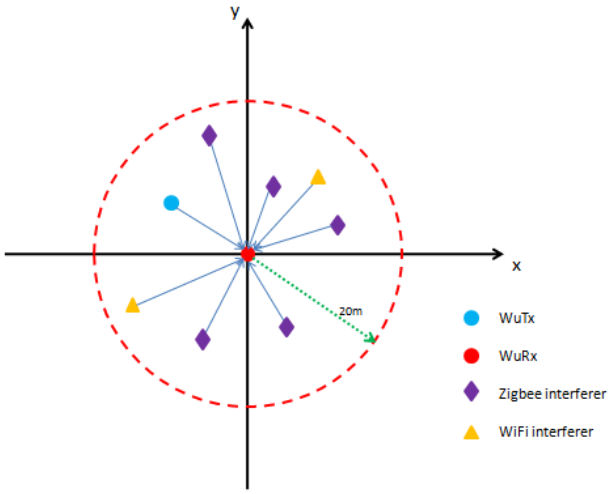

Figure 2.8: Simulation scenario for the channel selection mechanism [20]

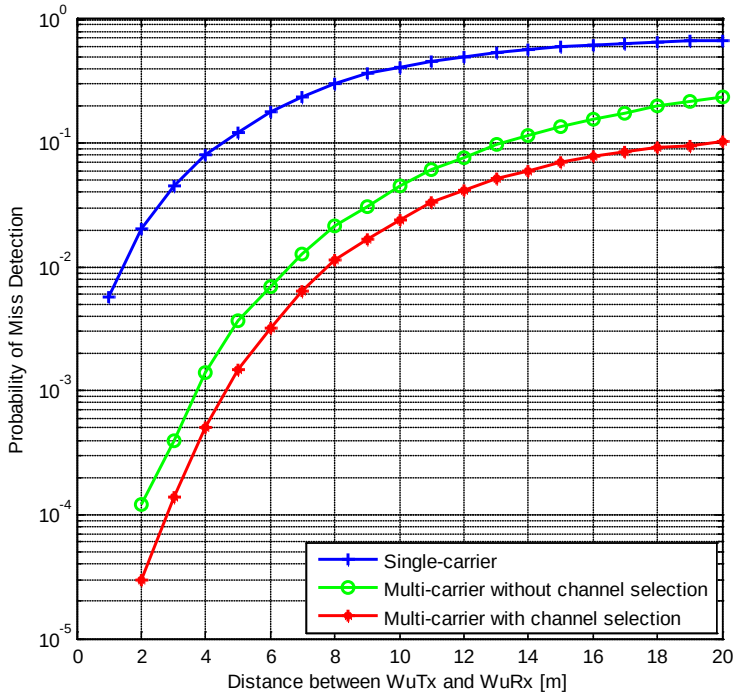

Figure 2.9: Probabilities of miss detection for the three different wakeup radio schemes

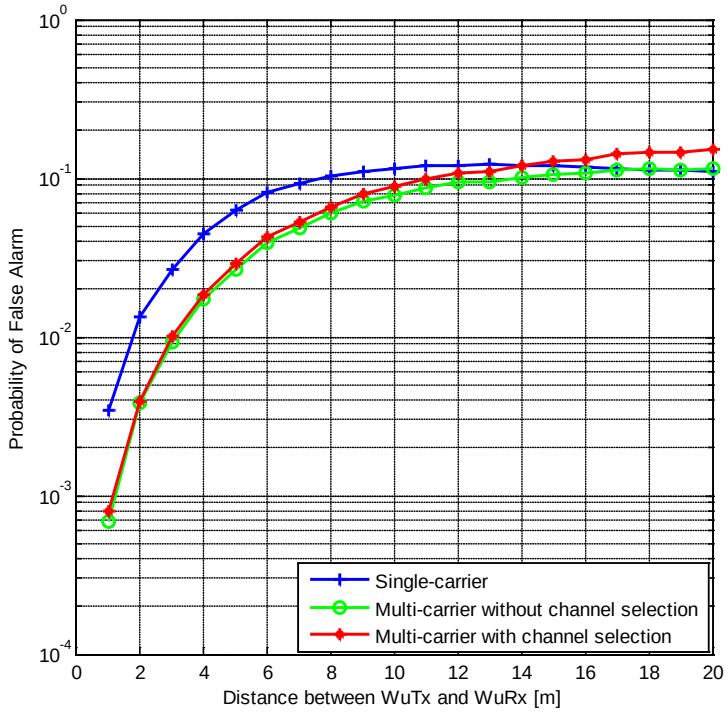

Figure 2.10: Probabilities of false alarm for the three different wakeup radio schemes

With an increase in the transmission distance between the WuTx and WuRx, the unwanted Wi-Fi and Zigbee interference swells so that the receiver detection performance goes down. A significant improvement with a multi-carrier wakeup radio over a single-carrier case is obtained, as indicated in Figure 2.9. The performance gain with a multi-carrier scheme is even higher, when the distance between the WuTx and WuRx is small. It can be clearly seen that with a channel selection mechanism, the receiver detection performance can be further improved, compared to the case without channel selection.

2.3.4 Channel selection thresholds

As mentioned in Section 2.3.3, the channel selection threshold decides the removal of poor channels, so it can significantly affect the detection performance of a MC wakeup receiver. In practical implementations, the channel selection threshold should be carefully designed for a good detection performance. A smaller selection threshold means a higher requirement for the channel quality and it gives rise to less noise-plus-interference in the selected channels, but more channels may not meet the requirement and will be removed. It is possible that all the channels in use are regarded as poor channels and then deleted at the receiver, which is defined as the all-delete problem. Therefore, in the case of a lower selection threshold, the probability of the all-delete problem becomes higher. If the all-delete problem occurs, the multi-carrier wakeup receiver loses

its functionality and has no final output. Then the transmitter has to send the wakeup packets again, leading to an increase in power consumption.

To explore the effect of different channel selection thresholds on the detection performance of a MC wakeup receiver, the 32-bit address is transmitted over four channels in the simulation. The miss detection and false alarm probabilities with different selection thresholds are revealed in Figures 2.11 and 2.12. For the calculation of the all-delete probability, the distance between the WuTx and WuRx is fixed at 20m.

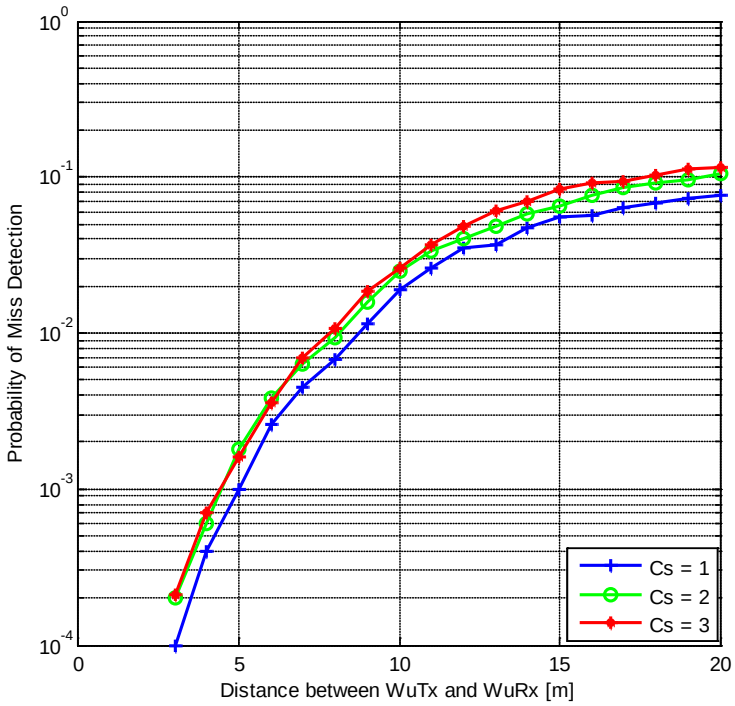

Figure 2.11: Probabilities of miss detection for the MC wakeup radio with different channel selection thresholds

It is seen that there is a tradeoff between the probability of miss detection and the probability of the all-delete problem, after a comparison of Figures 2.11 and 2.13. A channel selection threshold of 1 can bring about a small gain in the detection performance over that of 2. However, the probability of the all-delete problem with a selection threshold of 1 is almost twice that with a threshold of 2. As interpreted above, the removal of all the channels in use will cause a complete loss of the address correlation calculation for the wakeup packet detection and the retransmission of the wakeup packets.

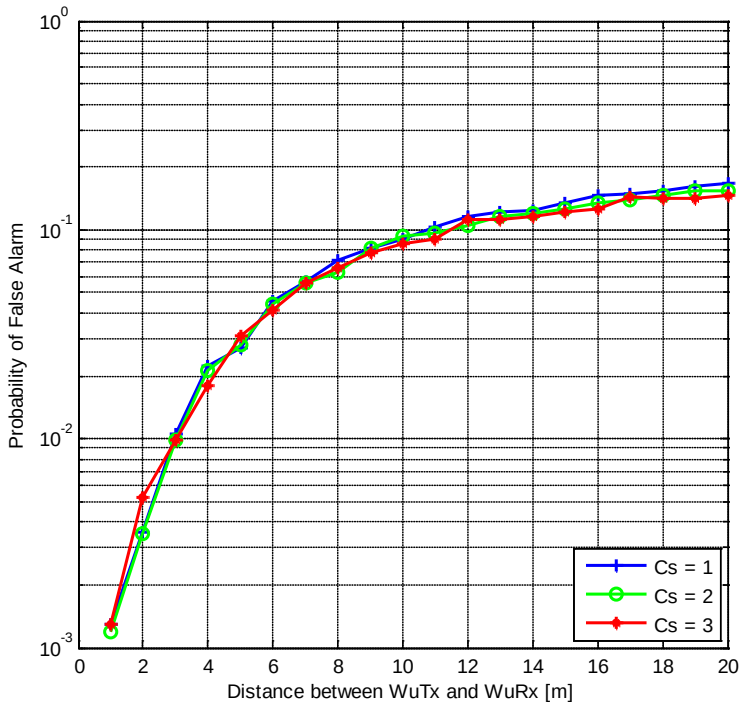

Figure 2.12: Probabilities of false alarm for the MC wakeup radio with different channel selection thresholds

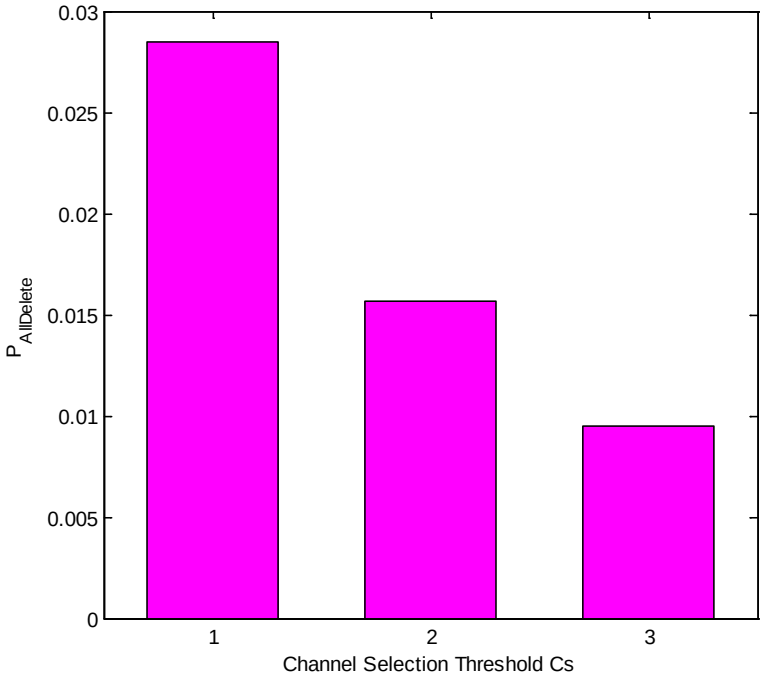

Figure 2.13: Probabilities of the all-delete problem with different channel selection thresholds

2.4 The number of carriers

As sketched in Figures 2.9 and 2.10, the detection performance is improved with the use of a multi-carrier wakeup radio, compared to a single-carrier wakeup radio. But the number of channels to be used to obtain a decent detection performance becomes another consideration in the design of a multi-carrier wakeup receiver. With more channels in use, the MC wakeup receiver architecture would be more complicated, causing an increase in the power consumption as well. The detection performance with a 32-bit address and a 4-carrier transmission is compared with the 2-carrier and 8-carrier cases, as revealed in Figures 2.14 and 2.15. In the simulation, the channel selection mechanism with a selection threshold of 2 is employed.

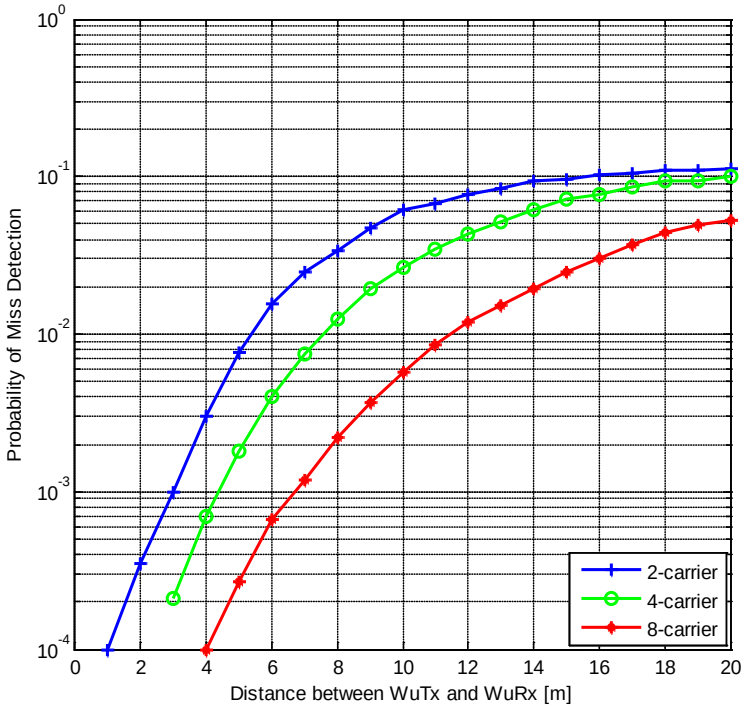

Figure 2.14: Probabilities of miss detection with different number of carriers

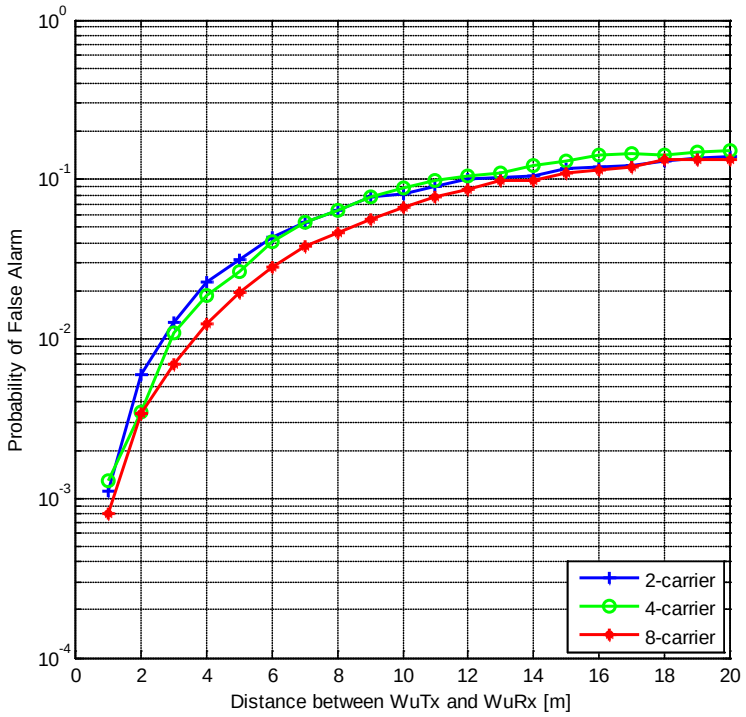

Figure 2.15: Probabilities of false alarm with different number of carriers

As presented in Figure 2.14, the probability of miss detection greatly decreases with more channels used to transmit the address. The performance improvement is more significant when the distance between the WuTx and WuRx is moderate. But in terms of false alarm probability, there is no big difference between the 2-carrier case and 4-carrier case. As the number of carriers to be used is under consideration, the issue of power consumption cannot be neglected either. The usage of more channels can lead to a lower miss detection probability, but it will raise the power consumption of a MC wakeup radio receiver due to the increase in the number of chains at the receiver. So a good tradeoff between the detection performance and receiver power consumption is always expected in practical implementations.

Detection Performance in AWGN Channels 3

This chapter analyses the impact of the white Gaussian noise and interference on the receiver detection performance. Due to the noise in channels, the wakeup packets for the target receiver may be wrongly detected in the digital baseband subsystem and thus either a miss detection or false alarm occurs. For the address detection, two schemes are proposed and some expressions are invented to describe the probabilities of miss detection and false alarm in the presence of channel noise. Besides the white noise, different kinds of interference exist in channels, which can deteriorate the detection performance as well. In this section, continuous wave (CW) interference and phase modulated (PM) interference are taken into consideration.

3.1 AWGN channel model

The AWGN channel model is a channel whose sole effect is the addition of a white Gaussian noise process $n(t)$ to the transmitted desired signal $s(t)$. The AWGN channel model can be mathematically described by the relation:

$$r(t) = s(t) + n(t) \tag{3.1}$$

where $r(t)$ is the received waveform. OOK modulation is used for the desired signals at the transmitter side. To send a 0, no signal is transmitted in the time interval of T whereas to send a 1, a signal waveform is transmitted.

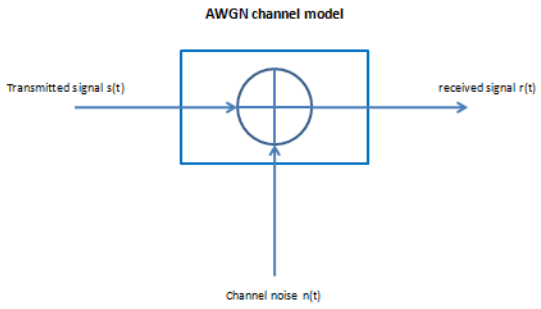

Figure 3.1: AWGN channel model

The function $n(t)$ is a waveform of zero-mean white Gaussian noise process with a constant power spectral density (PSD). The one-sided PSD is denoted by N_o while $N_o/2$ indicates the two-sided PSD. $N_o B$ is the noise power in the transmitted bandwidth.

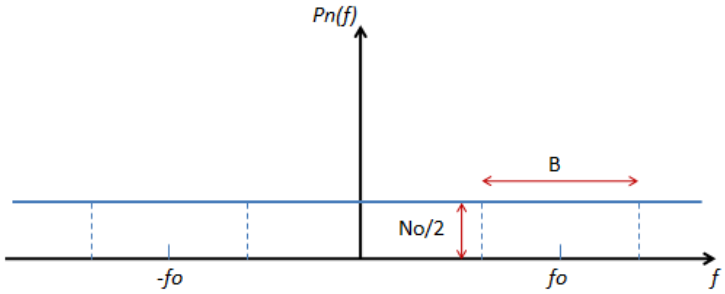

Figure 3.2: PSD of white Gaussian noise in channels

The mathematical AWGN model for the random process $n(t)$ can be characterized by a zero-mean Gaussian process with autocorrelation function:

$$E[n(t_1)n(t_2)] = \frac{N_o}{2}\delta(t_1 - t_2) \tag{3.2}$$

3.2 BER performance with AWGN

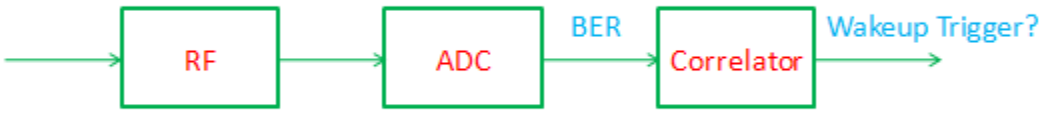

Figure 3.3: Wakeup receiver single-carrier chain

In the analog-to-digital converter (ADC), the analog signal is sampled and then compared to a threshold. If the sample is bigger than or equal to the decisison threshold, the output is 1. Otherwise, the output is 0. After the ADC part, the bit error rate (BER) can be calculated by comparing the received data and the transmitted data. The BER is one of the indicators of the receiver detection performance.

3.2.1 Decision threshold

In [21] and [22], the error rate behavior is studied for non-coherent OOK detection in AWGN channels. The optimum threshold in AWGN channels is dependent on SNR. In [21], the probability of Mark error P_m and the probability of Space error P_s are given. Mark is defined as a value larger than or equal to a certain threshold, while Space denotes a value below the threshold level. Mark error means that the received data is decided as Space when a Mark is actually transmitted. Inversely, Space error indicates that a Space is wrongly received as a Mark. Then an equation is derived to obtain the optimum thresholds for non-coherent OOK detection with different SNRs in AWGN channels.

The probability of Mark error:

$$P_m = 1 - Q\left(\sqrt{\frac{2K\gamma}{1+K+\gamma}}, \beta_n \sqrt{\frac{1+K}{1+K+\gamma}}\right) \tag{3.3}$$

The probability of Space error:

$$P_s = \exp(-\beta_n^2/2) \tag{3.4}$$

where β_n is the normalized threshold level and γ is defined as the average SNR per bit: $\gamma = (A_s^2/2)/\sigma_n^2 = E_b/(N_o/2) = 2E_b/N_o$. With the threshold β for non-coherent OOK detection, we obtain $\beta = \beta_n \cdot \sigma_n$, where σ_n^2 is the variance of the AWGN.

The average error probability is given by:

$$P_e = \frac{1}{2}(P_m + P_s) \tag{3.5}$$

In order to minimize the error rate P_e, it is required that $\frac{\partial P_e}{\partial \beta_n} = 0$.

Finally, the relationship between β_n and γ is found with $K \to \infty$ in AWGN channels:

$$e^{-\gamma} \cdot I_o(\beta_n \sqrt{2\gamma}) = 1 \tag{3.6}$$

where $I_o(\cdot)$ is the modified Bessel function of the 1st kind of zero order. With different values for γ in AWGN channels, the optimum normalized threshold β_n can be calculated. Based on the expressions of P_m and P_s, the theoretical BER for non-coherent OOK detectors are obtained and then the relation curve of γ and P_e is plotted in Figure 3.4.

With the optimum thresholds derived from the formula (3.6), the BER for a single-carrier wakeup receiver simulated in MATLAB is compared with the theoretical values. In Figure 3.4, the two curves completely match.

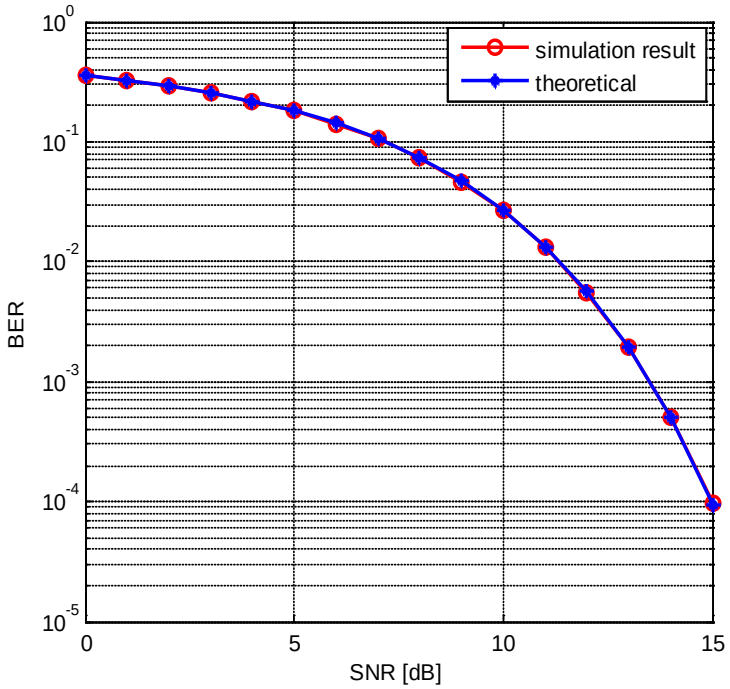

Figure 3.4: BER of a single-carrier wakeup receiver with optimum thresholds

3.2.2 Simulink simulation

The radio frequency (RF) part of a wakeup receiver can be built in Simulink. Simulink, developed by MathWorks, is an enviroment for multi-domain simulation and model-based design for dynamic systems. It provides an interactive graphical enviroment and a customizable set of block libraries, with which we can model, simulate and test a great variety of systems, including communications, controls, signal processing and image processing.

Simulink is suitable for analog design while MATLAB is always employed for algorithm development. Co-simulation is desirable when both the digital part and analog part are considered in the modeling. The cooperation of MATLAB and Simulink is depicted in Figure 3.5.

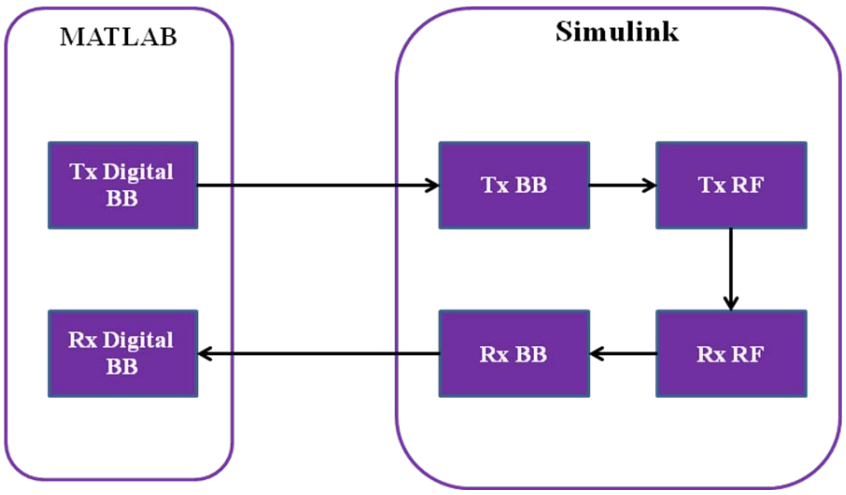

Figure 3.5: Co-simulation through MATLAB and Simulink

For the receiver detection performance analysis, the co-simulation through MATLAB and Simulink is adopted. The Simulink model for a single-carrier wakeup receiver is displayed in Figure 3.6. The BER performance with co-simulation in Figure 3.7 is compared with the results from pure MATLAB simulation and the theoretical analysis shown in Figure 3.4. The same performance as the theoretical case verifies the correctness of the Simulink model.

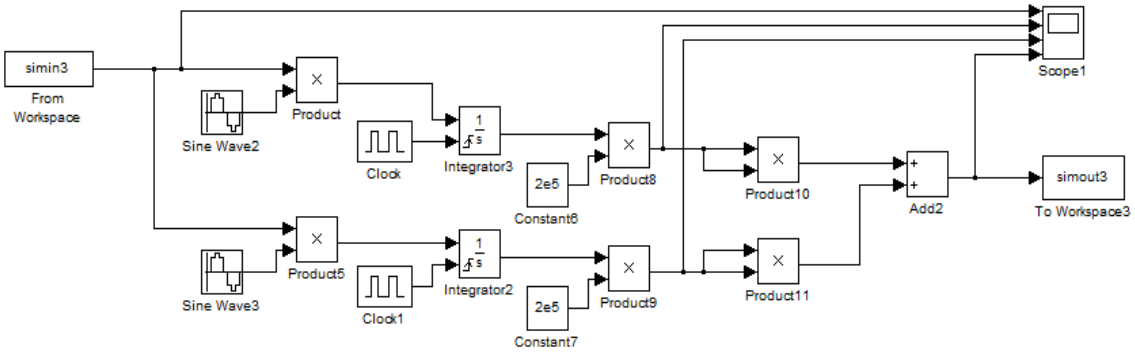

Figure 3.6: Simulink model of a single-carrier wakeup receiver

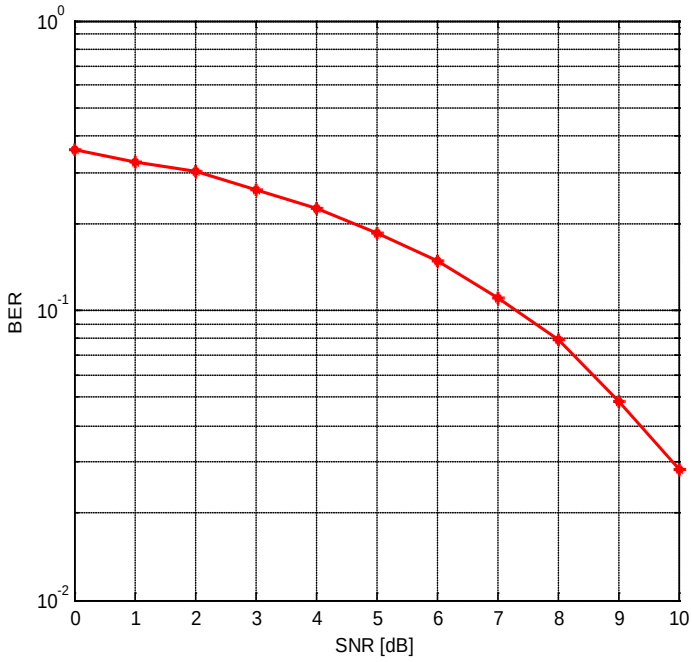

Figure 3.7: BER performance of a single-carrier wakeup receiver with Simulink simulation

3.3 Address detection schemes

The probabilities of miss detection and false alarm are the main parameters that reflect the detection performance of a wakeup receiver. The detection of a wakeup packet is executed by the correlation calculation of the received address and the local address. The address identification at the digital baseband subsystem of a wakeup receiver can be conducted by two schemes. One is the hard-bit-based Hamming distance method and the other one is the soft-bit-based address correlation.

3.3.1 Hard-bit-based Hamming distance scheme

In the hard decision method, the received signal strength is compared to an optimum threshold and then decided as 1 or 0. If the received signal strength is larger than or equal to the threshold, the result is 1. Otherwise, the output is 0. Then the received address of N bits is compared with the local address and the Hamming distance is calculated to find the similarity between the two addresses. The Hamming distance denotes the number of symbols where the two addresses disagree. Typically, there is a Hamming distance threshold on the judgment of the similarity. Different Hamming distance thresholds d can lead to different sets of the miss detection probability and false alarm probability. With a Hamming distance smaller than or equal to the threshold d, the received address is identified

with the local address and then a wakeup trigger signal is sent to the main radio. If the Hamming distance is larger than the threshold d, it is assumed that the local address is not the target address. Firstly, a decent Hamming distance threshold d has to been found for the wakeup signal detection. The relationship between the Hamming distance thresholds d and the two error probabilities P_{md} and P_{fa} with different SNRs is shown in Figure 3.8 .

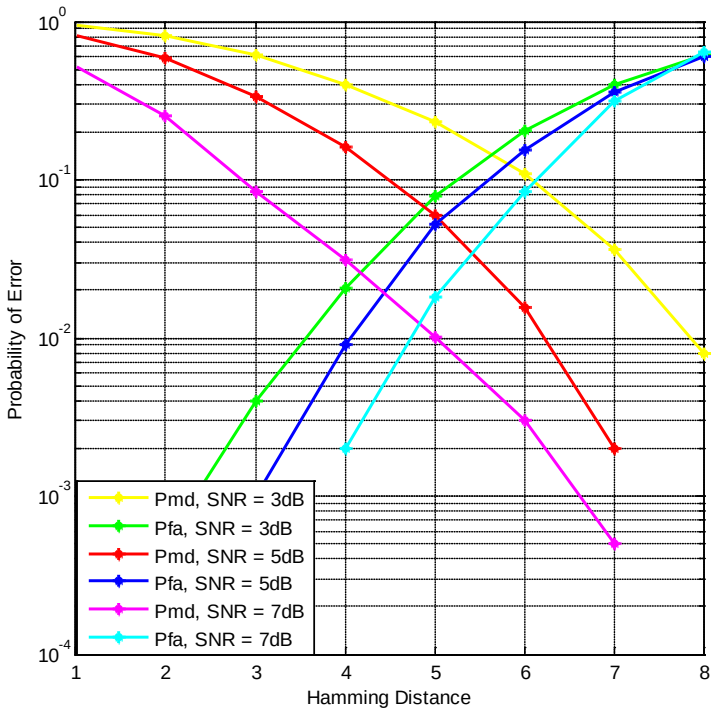

Figure 3.8: Relationship between Hamming distance threshold and error probabilities in the case of different SNR levels

With an increase in the Hamming distance threshold, a smaller miss detection probability can be acquired, while the false alarm probability rises. Because of the large unnecessary power consumption caused by false alarm, the probability of false alarm should be constrained below a low level (e.g. 10^{-2}). As shown in the Figure 3.8, the Hamming distances smaller than or equal to 4 can meet the SNR constraint of $5\,dB$. In the tradeoff between the false alarm probability and miss detection probability, the Hamming distance threshold is set to 4 for the 16-bit address detection in the simulation.

With a hard decision, the Hamming distance method can also be expressed in terms of the correlation. To calculate the address correlation, the exclusive NOR Gate $\odot$ is used. The Exclusive-NOR Gate

function or Ex-NOR for short, is a digital logic gate that is the reverse form of the Exclusive-OR function. It is a combination of the Exclusive-OR gate and the NOT gate. The output of an Exclusive-NOR gate is only 1 when the two inputs have the same value which can be either 1 or 0.

$$C = \sum_{i=0}^{15} C_i = \sum_{i=0}^{15} a_i \odot b_i \qquad (3.7)$$

If the received address a of 16 bits is totally matched with the local address b, the correlation result is 16. In case they are completely different, the correlation result becomes 0. The range of the correlation result is [0, 16]. In the simulation, the correlation result is normalized and then adjusted to [-1, 1]. The relation between the different Hamming distances and the normalized correlation results is presented in Table 3.1.

Table 3.1: Hamming distances and normalized correlation results

Hamming distance	1	2	3	4	5	6	7	8
Normalized correlation result	0.875	0.75	0.625	0.5	0.375	0.25	0.125	0

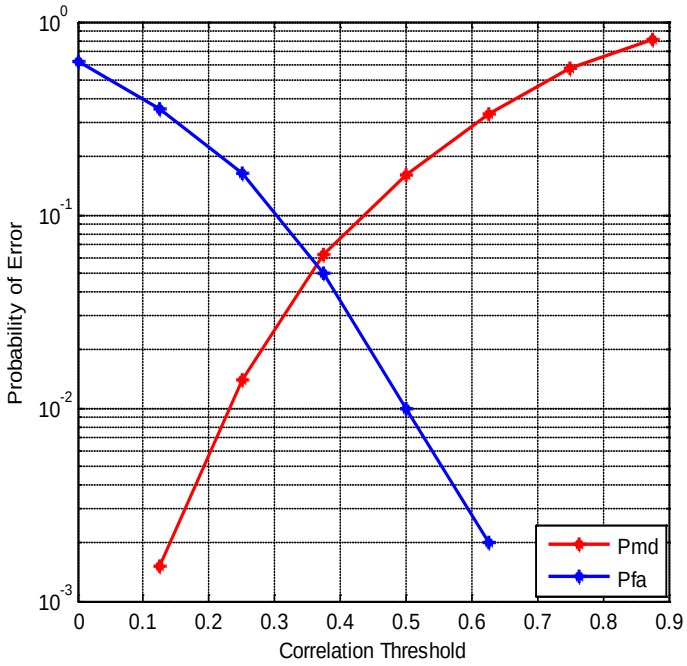

Figure 3.9: Relationship between correlation thresholds with hard decision and error probabilities (SNR = 5 dB)

As explained before, the false alarm probability is constrained below a level of 10^{-2} and a Hamming distance threshold of 4 is selected for the wakeup signal detection. The variations of the two error probabilities with different SNRs in the simulation can be observed in Figure 3.10. With a Hamming distance threshold of 4, the theoretical analysis for the miss detection probability P_{md} and false alarm probability P_{fa} are as follows:

The probability of miss detection:

$$P_{md} = 1 - \sum_{k=12}^{16} \binom{16}{k} (1-P_e)^k P_e^{16-k} \tag{3.8}$$

The probability of false alarm:

$$\begin{aligned} P_{fa} = & \binom{8}{8} (1-P_e)^8 P_e^0 \sum_{k=4}^{8} \binom{8}{k} P_e^k (1-P_e)^{8-k} \\ & + \binom{8}{7} (1-P_e)^7 P_e^1 \sum_{k=5}^{8} \binom{8}{k} P_e^k (1-P_e)^{8-k} \\ & + \binom{8}{6} (1-P_e)^6 P_e^2 \sum_{k=6}^{8} \binom{8}{k} P_e^k (1-P_e)^{8-k} \\ & + \binom{8}{5} (1-P_e)^5 P_e^3 \sum_{k=7}^{8} \binom{8}{k} P_e^k (1-P_e)^{8-k} \\ & + \binom{8}{4} (1-P_e)^4 P_e^4 \sum_{k=8}^{8} \binom{8}{k} P_e^k (1-P_e)^{8-k} \end{aligned} \tag{3.9}$$

In the formulas (3.8) and (3.9), P_e is the BER value shown in Figure 3.4. Based on the BER values in Figure 3.4, the theoretical miss detection and false alarm probabilities with different SNRs can be calculated. The simulation results P_{md} / P_{fa} , and the theoretical results are compared in Figure 3.10. It can be seen that the simulation results match the mathematical values from the formulas (3.8) and (3.9), indicating the accuracy of the invented expressions for the two error probabilities P_{md} / P_{fa} .

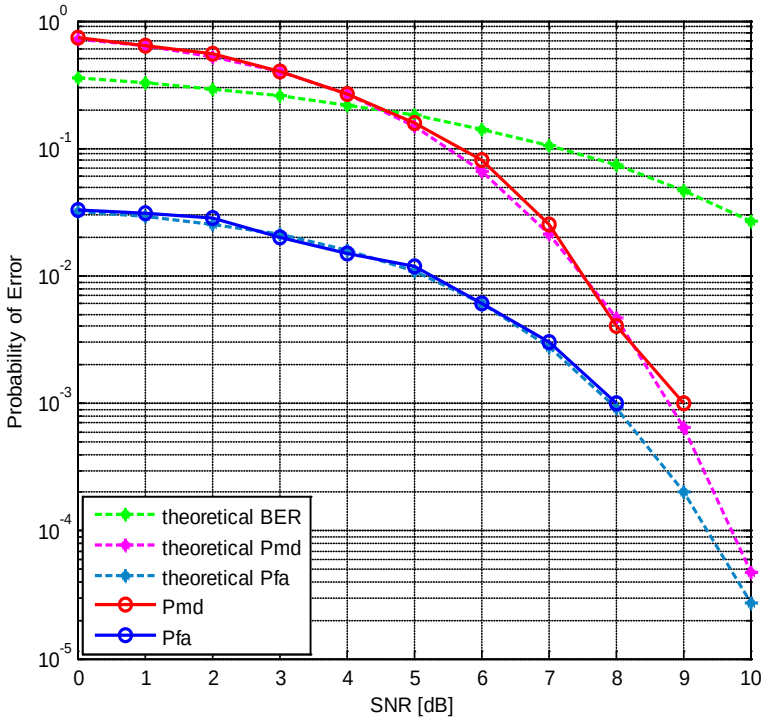

Figure 3.10: The theoretical values and simulation results for the error probabilities at different SNRs with a Hamming distance threshold of 4

If the address length is N bits and the Hamming distance threshold for the wakeup signal detection is d, the general formulas for the miss detection probability and false alarm probability are as follows:

The probability of miss detection:

$$P_{md}(N,d) = 1 - \sum_{k=N-d}^{N} \binom{N}{k} (1-P_e)^k P_e^{N-k} \qquad (3.10)$$

The probability of false alarm:

$$
\begin{aligned}
P_{fa}(N,d) = & \binom{N/2}{N/2}(1-P_e)^{\frac{N}{2}} P_e^0 \sum_{k=\frac{N}{2}-d}^{\frac{N}{2}} \binom{N/2}{k} P_e^k (1-P_e)^{\frac{N}{2}-k} \\
& + \binom{N/2}{N/2-1}(1-P_e)^{\frac{N}{2}-1} P_e^1 \sum_{k=\frac{N}{2}-d+1}^{\frac{N}{2}} \binom{N/2}{k} P_e^k (1-P_e)^{\frac{N}{2}-k} \\
& + \binom{N/2}{N/2-2}(1-P_e)^{\frac{N}{2}-2} P_e^2 \sum_{k=\frac{N}{2}-d+2}^{\frac{N}{2}} \binom{N/2}{k} P_e^k (1-P_e)^{\frac{N}{2}-k} \\
& + \ldots + \binom{N/2}{N/2-d}(1-P_e)^{\frac{N}{2}-d} P_e^d \sum_{k=\frac{N}{2}}^{\frac{N}{2}} \binom{N/2}{k} P_e^k (1-P_e)^{\frac{N}{2}-k} \\
= & \sum_{x=0}^{d} \left[\binom{N/2}{N/2-x}(1-P_e)^{\frac{N}{2}-x} P_e^x \sum_{k=\frac{N}{2}-d+x}^{\frac{N}{2}} \binom{N/2}{k} P_e^k (1-P_e)^{\frac{N}{2}-k} \right]
\end{aligned}
\qquad (3.11)
$$

3.3.2 Soft-bit-based correlation scheme

In the soft decision method, the received data is not simply decided as 1 or 0 any more after it is sampled. Instead, it is transferred to one of 16 levels and expressed in 4 bits.

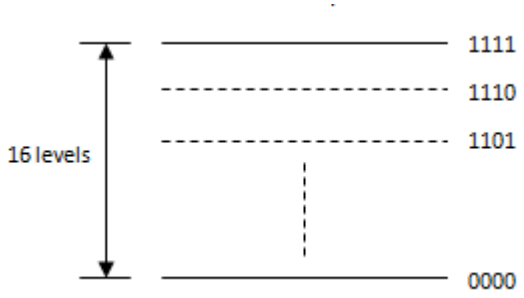

Figure 3.11: 4-bit ADC

Correspondingly, each bit in the local address is also converted to one of the 16 levels. Then the address correlation is computed by multiplying the received address vector a with the local address vector b, as shown below:

$$C = a' \cdot b = \begin{bmatrix} a_1 & a_2 & a_3 & a_4 \end{bmatrix} \cdot \begin{bmatrix} b_1 \\ b_2 \\ b_3 \\ b_4 \end{bmatrix} = \sum_{n=1}^{4} a_n \cdot b_n \qquad (3.12)$$

In case the two addresses a and b are represented on a time-frequency-grid (i.e., address matrix), the correlation result C can be obtained using the matrix trace:

$$C = tr(a' \cdot b) = tr\left(\begin{bmatrix} a_{11} & a_{21} & a_{31} & a_{41} \\ a_{12} & a_{22} & a_{32} & a_{42} \\ a_{13} & a_{23} & a_{33} & a_{43} \\ a_{14} & a_{24} & a_{34} & a_{44} \end{bmatrix} \cdot \begin{bmatrix} b_{11} & b_{12} & b_{13} & b_{14} \\ b_{21} & b_{22} & b_{23} & b_{24} \\ b_{31} & b_{32} & b_{33} & b_{34} \\ b_{41} & b_{42} & b_{43} & b_{44} \end{bmatrix} \right) = \sum_{n,m=1}^{4} a_{nm} \cdot b_{nm} \qquad (3.13)$$

A large correlation result indicates a good similarity between the local address and the received address. The correlation result C is compared with a correlation threshold. If C is bigger than the threshold, the local receiver is regarded as the intended receiver and then a wakeup trigger signal is sent to the main radio. As the hard-bit-based Hamming distance scheme, the correlation threshold is also a consideration for a decent receiver detection performance.

It is obviously seen in Figure 3.12 that both the error probabilities are sensitive to the decision threshold. The miss detection probability varies directly with the correlation threshold, while the false alarm probability goes inversely. The tradeoff between these two probabilities has to be taken into consideration for the selection of a correlation threshold as well. With a correlation threshold larger than 0.375, the false alarm probability remains below 10^{-2} for an SNR of $5\,dB$. In the simulation, the correlation threshold is set to 0.4. The relationship between the SNR and the error probabilities is depicted in Figure 3.13.

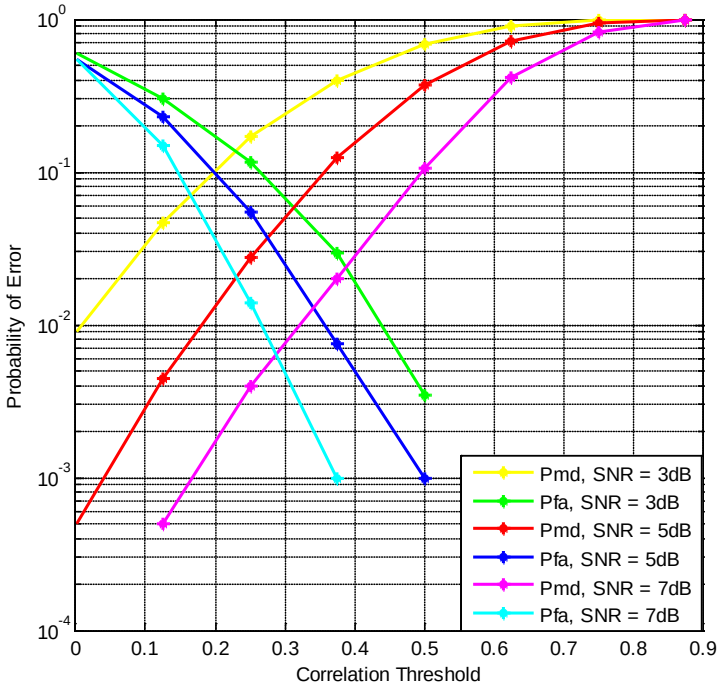

Figure 3.12: Relationship between correlation thresholds with soft decision and error probabilities in the case of different SNR levels

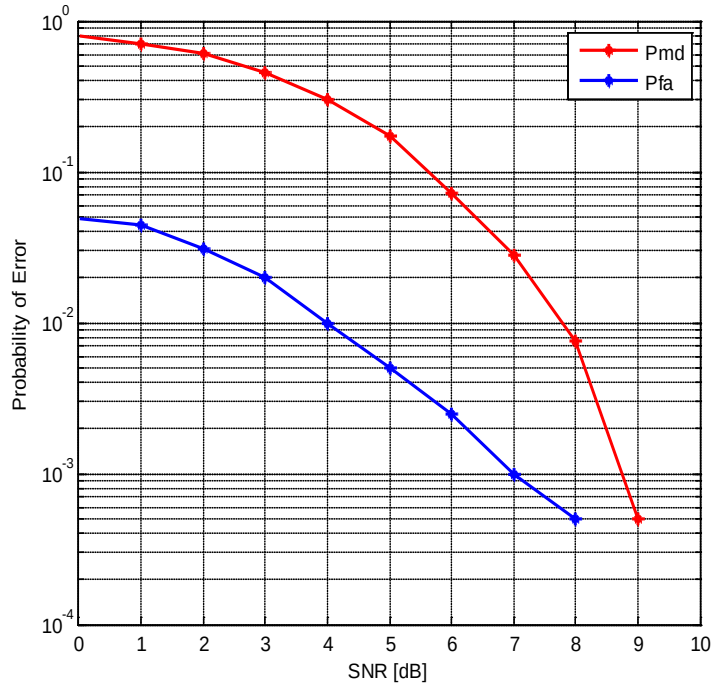

Figure 3.13: Relationship between SNR and the error probabilities with a correlation threshold of 0.4

3.3.3 Comparison of the two address detection schemes

Assuming a same false alarm probability in both schemes, the miss detection performance with the soft-bit-based correlation dominates that with the hard-bit-based Hamming distance method for a fixed SNR of 5dB. But the performance difference is not significant. In practical implementations, the hamming distance scheme is simpler, leading to less power consumption. So it cannot be concluded which method is absolutely better than the other one, as a tradeoff exists in the system complexity and receiver detection performance. Either one of them can be selected for the wakeup packet detection according to the practical situations.

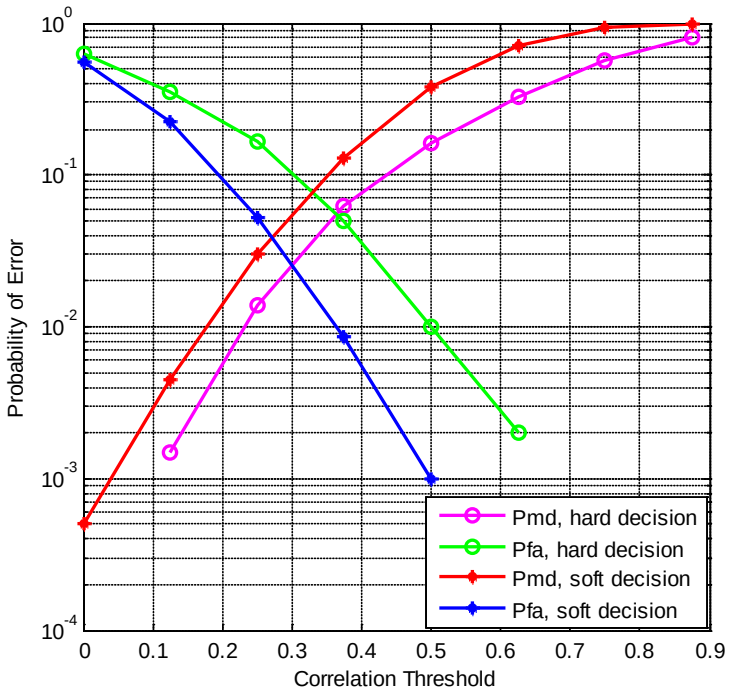

Figure 3.14: Comparison of the error probabilities with the hard-bit-based Hamming distance method and soft-bit-based correlation method (SNR = 5 dB)

3.4 Effect of interference on detection performance

3.4.1 Continuous wave interference

If a jammer is around the wakeup receiver, the single-tone signal $s_i(t)$ which it always generates, acts as an interferer to the wakeup receiver [23]. Single-tone interference can also be expressed as CW interference. The mathematical expression for CW interference is:

$$s_i(t) = A_i \cdot \cos(w_o t + \phi_o) = \sqrt{2P_i} \cdot \cos(2\pi f_o t + \phi_o) \tag{3.14}$$

where P_i, f_o, and ϕ_o are the average interference power, carrier frequency and initial phase of the interference signal, respectively. If the CW interference is co-channel interference, f_o equals the frequency of the desired signal. ϕ_o is a random variable that is uniformly distributed in $[0, 2\pi]$. Then at the receiver, the desired signal $s(t)$ is corrupted by both CW interference $s_i(t)$ and additive white Gaussian noise $n(t)$:

$$r(t) = s(t) + n(t) + s_i(t) \tag{3.15}$$

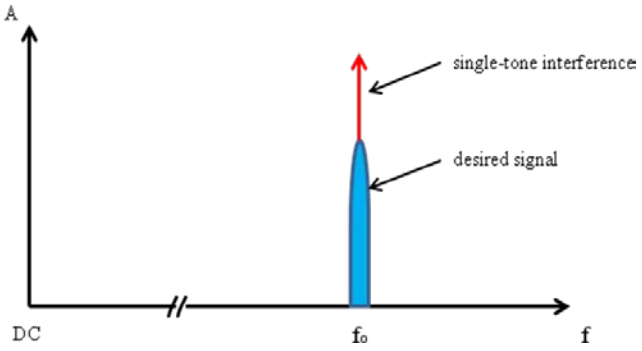

Figure 3.15: Co-channel CW interference

Subsequently, the impact of CW interference on the wakeup receiver detection performance is analyzed by means of a mathematical derivation. It will be done for two kinds of wakeup receivers in the absence of AWGN. One is the traditional envelope-detector-based receiver and the other is the new wakeup receiver architecture of Figure 2.1.

In an envelope-detector-based receiver, the received signal $r(t)$ has to go through a squaring device and then a low-pass filter. After the squaring device, the signal is as follows:

$$\begin{aligned} R(t) = r^2(t) &= \left(A_d \cdot \cos(w_o t) + A_i \cdot \cos(w_o t + \phi_o)\right)^2 \\ &= \frac{1}{2}A_d^2 + \frac{1}{2}A_i^2 + A_d A_i \cos\phi_o + \frac{1}{2}A_d^2 \cos(2w_o t) + \frac{1}{2}A_i^2 \cos(2\phi_o)\cos(2w_o t) \\ &\quad - \frac{1}{2}A_i^2 \sin(2\phi_o)\sin(2w_o t) + A_d A_i \cos\phi_o \cos(2w_o t) - A_d A_i \sin\phi_o \sin(2w_o t) \end{aligned} \tag{3.16}$$

The spectrum of the signal $R(t)$ can be described with the Fourier Transform:

$$R(f)=\frac{1}{2}\Big[A_d^2\delta(f)+A_i^2\delta(f)+2A_dA_i\cos\phi_o\delta(f)+\frac{1}{2}A_d^2\delta(f-2f_o)+\frac{1}{2}A_d^2\delta(f+2f_o)$$
$$+A_dA_ie^{j\phi_o}\delta(f-2f_o)+A_dA_ie^{-j\phi_o}\delta(f+2f_o)+\frac{1}{2}A_i^2e^{j2\phi_o}\delta(f-2f_o)+\frac{1}{2}A_i^2e^{-j2\phi_o}\delta(f+2f_o)\Big] \tag{3.17}$$

When the signal $R(t)$ passes through a low-pass filter, all the high-frequency components will be filtered out and then the output becomes:

$$R(f)=\frac{1}{2}\Big[A_d^2\delta(f)+A_i^2\delta(f)+2A_dA_i\cos\phi_o\delta(f)\Big] \tag{3.18}$$

For the influence of the CW interference on the wakeup receiver of Figure 2.1, the analysis can be done in the time domain. Z_{11} and Z_{12} are the outputs of the integrators in the first chain.

$$\begin{aligned}Z_{11}&=\frac{2}{T}\int_0^T r(t)\cdot\cos(w_1t)\,dt\\&=\frac{2}{T}\int_0^T\big(A_1\cdot\cos(w_1t)+A_i\cdot\cos(w_1t+\phi_o)\big)\cdot\cos(w_1t)\,dt\\&=A_1+A_i\cos\phi_o+\frac{A_1+A_i\cos\phi_o}{2w_1T}\cdot\sin(2w_1T)+\frac{A_i\sin\phi_o}{2w_1T}\big(\cos(2w_1t)-1\big)\end{aligned} \tag{3.19}$$

$$\begin{aligned}Z_{12}&=\frac{2}{T}\int_0^T r(t)\cdot\sin(w_1t)\,dt\\&=\frac{2}{T}\int_0^T\big(A_1\cdot\cos(w_1t)+A_i\cdot\cos(w_1t+\phi_o)\big)\cdot\sin(w_1t)\,dt\\&=-A_i\sin\phi_o+\frac{A_1+A_i\cos\phi_o}{2w_1T}\big(1-\cos(2w_1T)\big)+\frac{A_i\sin\phi_o}{2w_1T}\cdot\sin(2w_1T)\end{aligned} \tag{3.20}$$

In case $2w_1T$ equals an integer multiple of 2π, Z_{11} and Z_{12} will reduce to $A_1+A_i\cos\phi_o$ and $-A_i\sin\phi_o$, respectively.

$$\begin{aligned}Z=Z_{11}^2+Z_{12}^2&=\big(A_1+A_i\cos\phi_o\big)^2+\big(-A_i\sin\phi_o\big)^2\\&=A_1^2+A_i^2+2A_1A_i\cos\phi_o\end{aligned} \tag{3.21}$$

From the results derived above, it can be observed that the CW interference has the same influence on the envelope-detector-based receiver and the wakeup receiver of Figure 2.1. In the formula (3.21), the

final result is related to the initial phase ϕ_o of the CW interference signal. In a real system, the initial phase ϕ_o is unknown and randomly distributed within the range of $[0, 2\pi]$ and thus $\cos\phi_o$ can be any value within [-1, 1]. For $\phi_o = \pi$, the signal is the most attenuated.

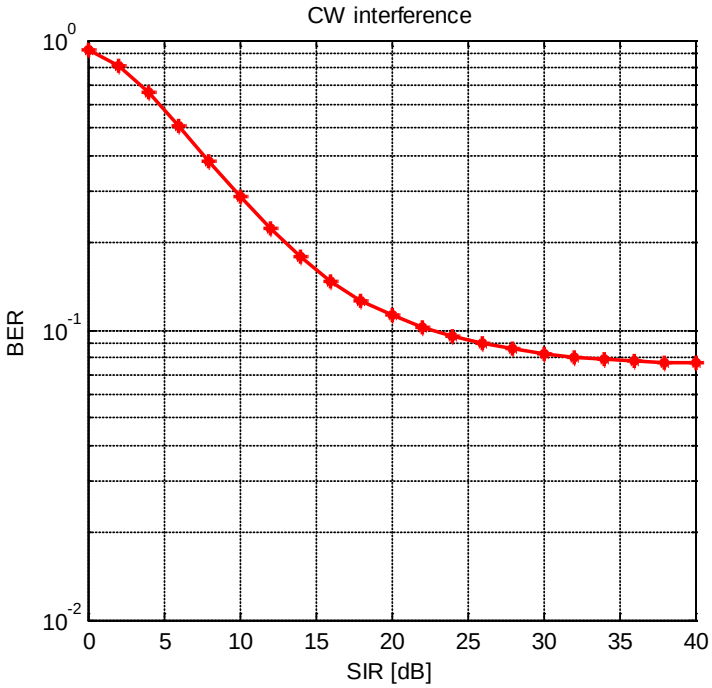

Figure 3.16: BER performance with CW interference (initial phase $\phi_o = \pi$, SNR = 8 dB)

In Figures 3.16 and 3.17, the SNR is fixed at 8 dB but the performance goes down with the decrease in the signal-to-interference power ratio (SIR). At the high region of SIR, the interference signal becomes weak and the BER gradually approaches the corresponding value (≈ 0.08) in Figure 3.10. Below an SIR of 6 dB, the miss detection performance is very poor, with a miss detection probability of almost 100%. In the region of 6 dB to 25 dB, the miss detection probability varies inversely and linearly with SIR. But the probability of false alarm rises directly with SIR when SIR is below 6 dB. After the peak, the false alarm probability descends and returns to the case without CW interference when the SIR is 30 dB or higher.

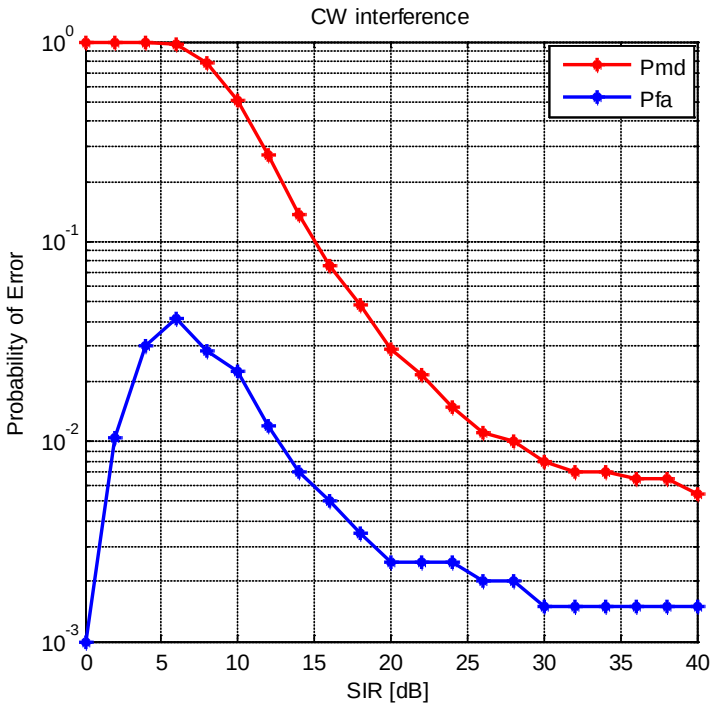

Figure 3.17: Error probabilities with CW interference (initial phase $\phi_o = \pi$, SNR = 8 dB)

3.4.2 Phase modulated interference

Phase modulated interference is very common in channels. The interference signal can be mathematically expressed as:

$$s_i(t) = A_i \cdot \cos(w_o t + \phi_o + \phi') \qquad (3.22)$$

where A_i is the amplitude of the PM interference signal, and ϕ_o is the initial phase. The difference from CW interference exists in ϕ', which is a constant in CW interference. Unlike CW interference, the phase ϕ' is variable in PM interference. ϕ' is used to carry the desired bit information. The modulated signal changes its phase ϕ' by π radians to send a bit 0 and keeps the same phase to send a bit 1.

Information	Phase ϕ′
1	0
0	π

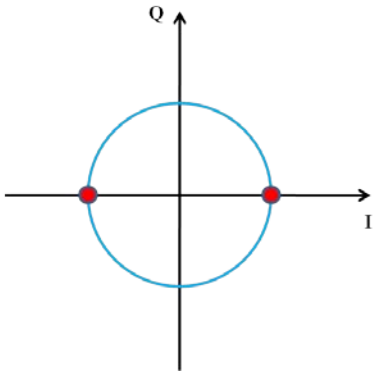

Figure 3.18: Constellation diagram for BPSK

For quadrature phase modulated interference, four different phases are introduced in the carrier to represent the four information states, which means QPSK can encode two bits per symbol with four phases. QPSK involves four points on the constellation diagram, equally spaced around a circle as shown in Figure 3.19.

Information	Phase ϕ′
00	1π/4
01	3π/4
10	5π/4
11	7π/4

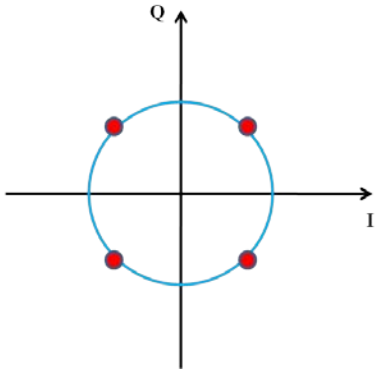

Figure 3.19: Constellation diagram for QPSK

For an envelope-detector-based wakeup receiver, the signal $R(t)$ after passing through a squaring device is given as:

$$\begin{aligned} R(t) = r^2(t) &= \left(A_d \cdot \cos(w_o t) + A_i \cdot \cos(w_o t + \phi_o + \phi')\right)^2 \\ &= \frac{1}{2}A_d^2 + \frac{1}{2}A_i^2 + A_d A_i \cos\left(\phi_o + \phi'\right) + \frac{1}{2}A_d^2 \cos(2w_o t) + \frac{1}{2}A_i^2 \cos\left(2\left(\phi_o + \phi'\right)\right)\cos(2w_o t) \\ &\quad - \frac{1}{2}A_i^2 \sin\left(2\left(\phi_o + \phi'\right)\right)\sin(2w_o t) + A_d A_i \cos\left(\phi_o + \phi'\right)\cos(2w_o t) - A_d A_i \sin\left(\phi_o + \phi'\right)\sin(2w_o t) \end{aligned} \quad (3.23)$$

The spectrum of the signal $R(t)$ can be obtained with the Fourier Transform:

$$R(f)=\frac{1}{2}\Big[A_d^2\delta(f)+A_i^2\delta(f)+2A_dA_i\cos(\phi_o+\phi')\delta(f)+\frac{1}{2}A_d^2\delta(f-2f_o)+\frac{1}{2}A_d^2\delta(f+2f_o)$$
$$+A_dA_ie^{j(\phi_o+\phi')}\delta(f-2f_o)+A_dA_ie^{-j(\phi_o+\phi')}\delta(f+2f_o)+\frac{1}{2}A_i^2e^{j2(\phi_o+\phi')}\delta(f-2f_o)+\frac{1}{2}A_i^2e^{-j2(\phi_o+\phi')}\delta(f+2f_o)\Big] \quad (3.24)$$

After a low-pass filter, all the high-frequency components will be removed and the output becomes:

$$R(f)=\frac{1}{2}\Big[A_d^2\delta(f)+A_i^2\delta(f)+2A_dA_i\cos(\phi_o+\phi')\delta(f)\Big] \quad (3.25)$$

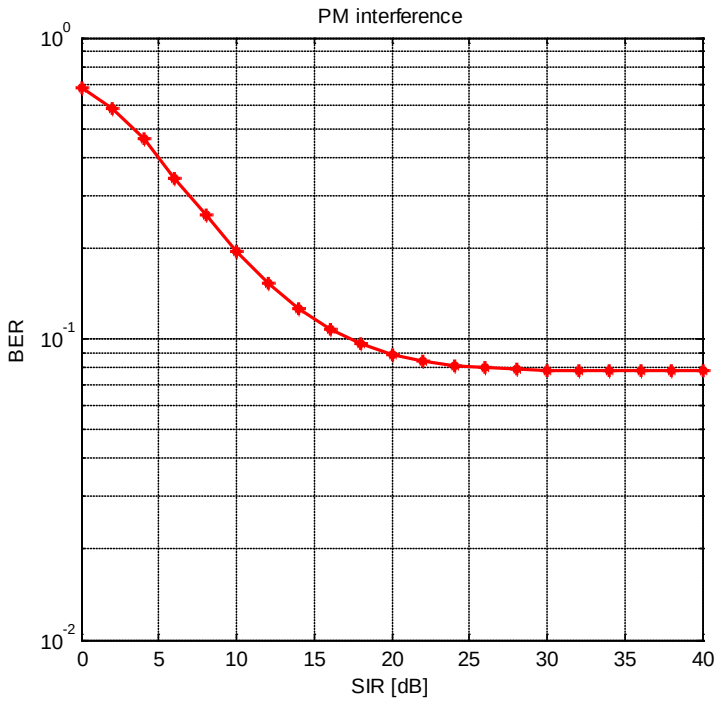

Figure 3.20: BER performance with PM interference (SNR = 8 dB)

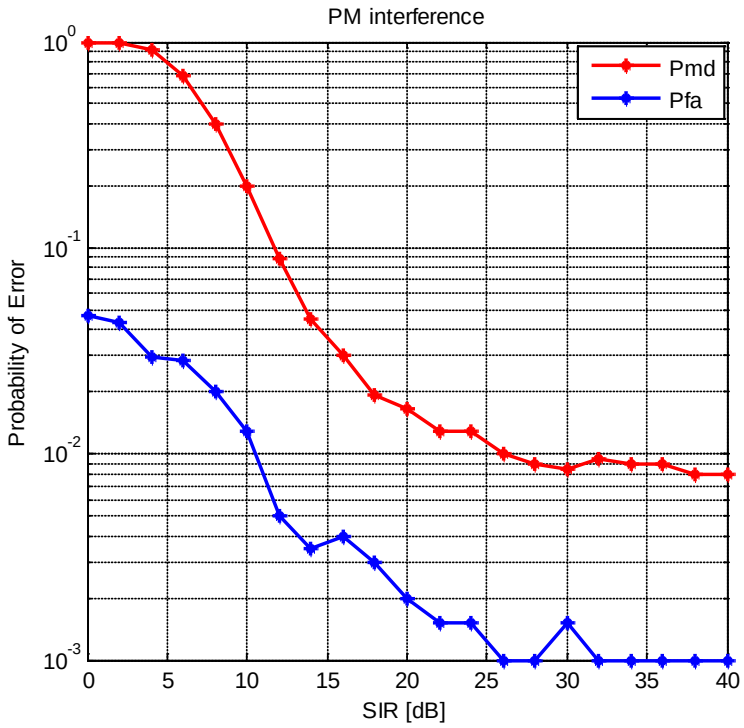

Figure 3.21: Error probabilities with PM interference (SNR = 8 dB)

Below an SIR of 2 dB, the miss detection probability is up to 100%, indicating that the wakeup packet will never be detected by the wakeup receiver. But compared to the effect of CW interference on the receiver performance, the ideal BER value (≈ 0.08) for an SNR of 8 dB can be retrieved with an SIR of 25 dB, which has a benefit of 5 dB over CW interference. It can be concluded that for the MC wakeup receiver architecture of Figure 2.1, the impact of CW interference is more severe on the detection performance than PM interference.

Effects of Non-Idealities in AWGN and Fading Channels

4

The physical layer implementation of a MC wakeup receiver consists of an analog part and a digital part. The analog part is often referred to as the front-end. A mixer in the front-end can be used for the down-conversion of the desired signal from radio frequency to baseband. It is usually performed by multiplying the desired signal with a carrier signal from a local oscillator (LO). Unfortunately, the local oscillator is typically not ideal, and the RF imperfections always lead to system performance degradation. The main impairments at the analog front-end introduced by the mixing process are phase noise (PN), carrier frequency offset (CFO), and I/Q imbalance. After the analog part, the desired signal is converted to a digital signal via the ADC which is actually the interface between the analog and the digital sections. However, in the quantization process, non-idealities exist as well, such as ADC quantization noise (QN), and sampling clock offset (SCO). In this chapter, our contributions are the analysis of the effects of all the possible impairments on the MC wakeup receiver architecture shown in Figure 2.1. Then the performance boundary of the new wakeup receiver architecture is discovered in AWGN and fading channels. Finally, we draw the conclusion on how severely the receiver detection performance is influenced by the individual impairment.

4.1 Individual non-idealities

4.1.1 Phase noise

Ideally, the output of a local oscillator is a pure single-frequency sine wave. The expression of an ideal LO output signal is:

$$c(t) = A_c \cdot \cos(2\pi f_o t) \tag{4.1}$$

But due to the process by which the LO is generated in the synthesizer, the output is not a pure single-frequency sine wave. Phase noise is the frequency-domain representation of rapid, short-term, random fluctuations in the phase of a waveform. It can also be described as a frequency-domain view of the noise spectrum around the oscillator carrier frequency. With a phase fluctuation $\Delta\phi(t)$ in the time domain, the LO output signal is:

$$c(t) = A_c \cdot \cos\left(2\pi f_o t + \Delta\phi(t)\right) \tag{4.2}$$

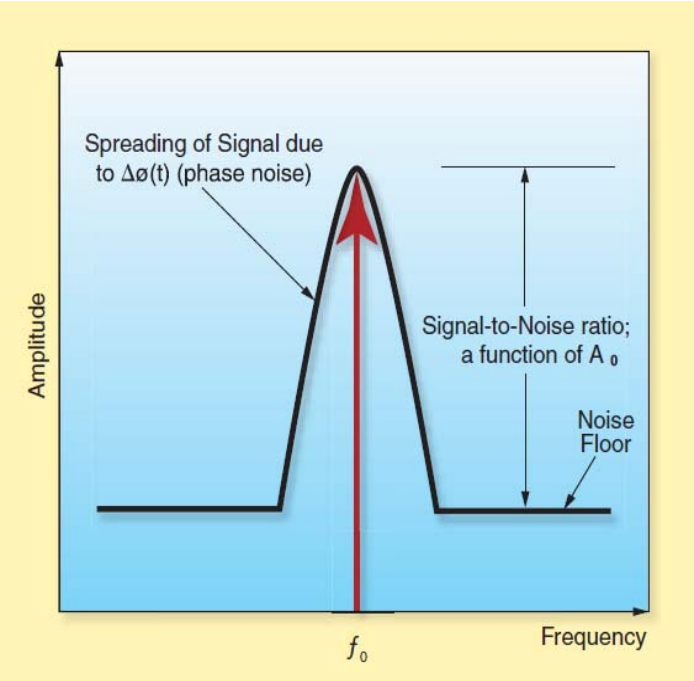

Figure 4.1: The spread of a LO output signal in frequency domain due to phase noise [25]

The power spectral density of the phase noise is usually defined as a piece-wise linear model, as shown in Figure 4.2.

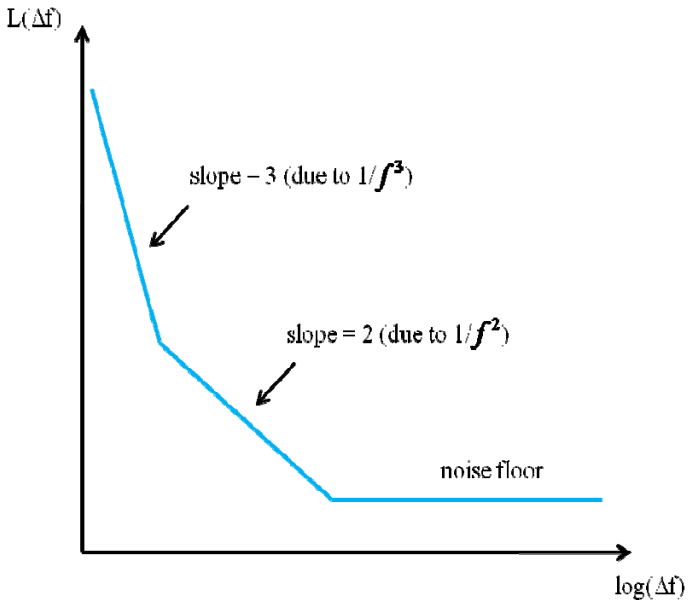

Figure 4.2: Phase noise model

Phase noise can be modeled either in the time domain or in the frequency domain. In the time domain approach, the PSD is employed to define the impulse response of a filter and then the samples of the phase noise are obtained by filtering Gaussian noise with a filter.

Phase noise is modeled by means of a random continuous time shift $a(t)$, leading to an oscillator output:

$$c(t) = A_c \cdot \cos\left(2\pi f_o \left(t + a(t)\right)\right) \tag{4.3}$$

Then the phase noise itself is $\Delta\phi(t) = 2\pi f_o a(t)$, and f_o is the desired carrier frequency. So the phase noise variance σ^2 can be expressed as:

$$\sigma^2 = \left(2\pi f_o\right)^2 \sigma_a^2 \tag{4.4}$$

where σ_a^2 is the variance of $a(t)$. The most common phase noise model is based on a free running VCO. In this oscillator, phase noise is considered as a Wiener process [26] and given by:

$$a(t) = \frac{\Delta\phi(t)}{2\pi f_o} = \sqrt{c}\int_0^t \xi(t')\, dt' \tag{4.5}$$

where c is defined by the carrier frequency offset Δf in the power spectral density $L(\Delta f)$ and it can be approximated as:

$$c = 10^{\frac{L(\Delta f)}{10\,dBc/Hz}} \cdot \frac{\Delta f^2}{f_o^2} \tag{4.6}$$

dBc/Hz is the unit for $L(\Delta f)$. *dBc* is a decibel, which is used to describe how far spurious signals and noise are relative to a desired signal. The relationship between σ_a^2 and c is given in [26]:

$$\sigma_a^2 = c \cdot T \tag{4.7}$$

Then the relationship between the phase noise variance σ^2 and the power spectral density $L(\Delta f)$ can be exploited as:

$$\sigma^2 = (2\pi\Delta f)^2 T \cdot 10^{\frac{L(\Delta f)}{10dBc/Hz}} \tag{4.8}$$

Table 4.1: Phase noise variance σ^2 vs. power spectral density $L(\Delta f)$

Δf = 1kHz		Δf = 10kHz	
σ^2	L(Δf)	σ^2	L(Δf)
0	- ∞ dBc/Hz	0	- ∞ dBc/Hz
0.01	- 46 dBc/Hz	0.01	- 66 dBc/Hz
0.02	- 43 dBc/Hz	0.02	- 63 dBc/Hz
0.04	- 40 dBc/Hz	0.04	- 60 dBc/Hz

4.1.2 Carrier frequency offset

At the receiver front-end, the RF signal needs to be down-converted to baseband (typically 0 Hz). Hence, the output signal frequency of a LO is required to be exactly the same as the carrier frequency of the desired signal. But the difference between the LO frequency and the required carrier frequency exists due to the frequency shift in LO. The output signal $c(t)$ of a LO with a carrier frequency offset Δf is given as:

$$c(t) = A_c \cdot \cos(2\pi(f_o - \Delta f)t) \tag{4.9}$$

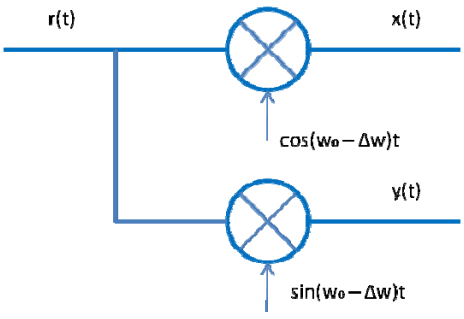

Suppose the received RF signal is given by:

$$r(t) = A_1 \cdot \cos(w_1 t) + A_2 \cdot \cos(w_2 t) + A_3 \cdot \cos(w_3 t) + A_4 \cdot \cos(w_4 t) \qquad (4.10)$$

After the integrators which function as low-pass filters, we obtain in the first chain:

$$Z_{11} = \frac{2}{T}\int_0^T r(t) \cdot \cos(w_1 - \Delta w)t \, dt = \frac{\sin(\Delta wT)}{\Delta wT} \cdot A_1 \qquad (4.11)$$

$$Z_{12} = \frac{2}{T}\int_0^T r(t) \cdot \sin(w_1 - \Delta w)t \, dt = \frac{\cos(\Delta wT) - 1}{\Delta wT} \cdot A_1 \qquad (4.12)$$

Without a carrier frequency offset (i.e., $\Delta w = 0$):

$$Z_{11}^2 + Z_{12}^2 = A_1^2 \qquad (4.13)$$

In the presence of a carrier frequency offset Δw :

$$Z_{11}^2 + Z_{12}^2 = \frac{2(1 - \cos(\Delta wT))}{(\Delta wT)^2} \cdot A_1^2 \qquad (4.14)$$

From the equation (4.14), it is revealed that the desired signal is attenuated by a factor $\frac{2(1-\cos(\Delta wT))}{(\Delta wT)^2}$ due to the carrier frequency offset Δw in the LO.

4.1.3 I/Q imbalance

In each chain of the receiver, there are I and Q branches. System performance may be weakened due to I/Q mismatch, which typically consists of an amplitude error ε and a phase error θ as modeled below. I/Q imbalance can exist at the transmitter, receiver or both. But it is only considered at the receiver here, as the study aims at the impact of the imperfections on the receiver performance. The receiver I/Q mismatch equivalent model is shown below.

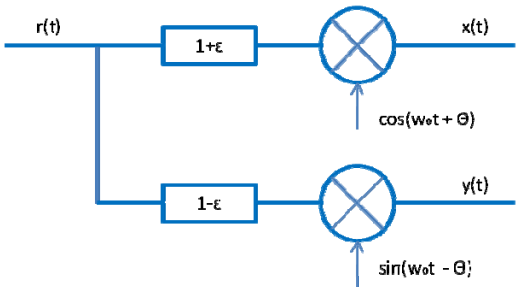

Then the baseband signal $x_{LP}(t)$ after the frequency down-conversion is:

$$\begin{aligned} x_{LP}(t) &= r(t)\cdot x_{LO}(t) \\ &= \left(x_I(t)\cdot\cos(w_o t) - x_Q(t)\sin(w_o t)\right)\cdot\left[(1+\varepsilon)\cos(w_o t+\theta) - j(1-\varepsilon)\sin(w_o t-\theta)\right] \\ &= (\cos\theta - j\varepsilon\sin\theta)\cdot\left(x_I(t) + jx_Q(t)\right) + (\varepsilon\cos\theta + j\sin\theta)\cdot\left(x_I(t) - jx_Q(t)\right) \\ &= \alpha\cdot x_L(t) + \beta\cdot x_L^*(t) \end{aligned} \tag{4.15}$$

where $\alpha = \cos\theta - j\varepsilon\sin\theta$ and $\beta = \varepsilon\cos\theta + j\sin\theta$.

It demonstrates that the desired baseband signal $x_L(t)$ is impaired with a coefficient α and a complex conjugate $x_L^*(t)$ is introduced by I/Q imbalance. Then the relative I/Q imbalance interference I (in dB) is defined as a function of the amplitude error ε and the phase error θ in [27].

$$I = 10\cdot\log_{10}\left(\frac{|\beta|^2}{|\alpha|^2}\right) = 10\cdot\log_{10}\left(\frac{\varepsilon^2 + \tan^2\theta}{1+\varepsilon^2\tan^2\theta}\right) \tag{4.16}$$

The relationship between the three parameters I, ε, and θ is discovered in Figure 4.3.

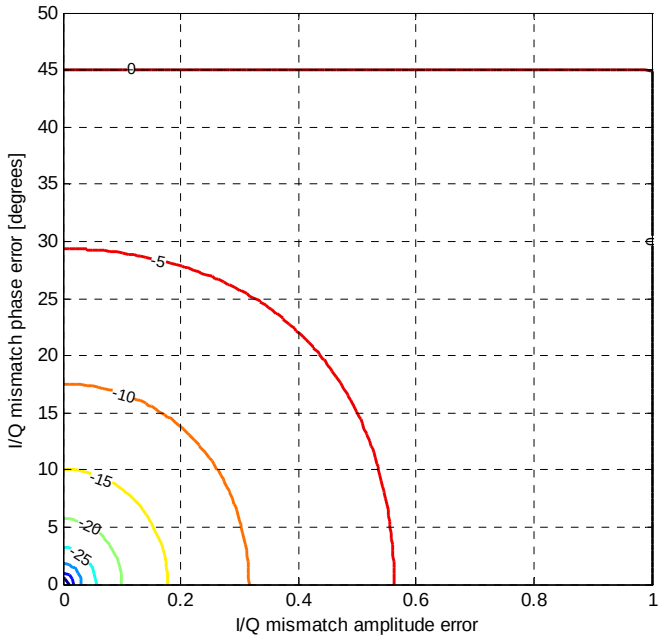

Figure 4.3: Contour of the relative I/Q imbalance interference I (in dB) with amplitude error and phase error

4.1.4 ADC quantization noise

The ADC does the conversion from an analog signal to a digital representation of that signal. Most ADCs convert an input voltage to a digital word (i.e. 1 or 0). Digital words have a fixed number of different values, whereas analog quantities have an infinite number of different values. The example of an 8-bit ADC is shown in Figure 4.4.

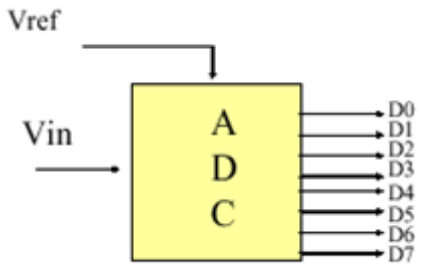

Figure 4.4: 8-bit ADC

The decimal value of the ADC output D can be obtained with the following equation:

$$D = 2^n \cdot \frac{V_{in}}{V_{ref}} \qquad (4.17)$$

where n is the number of bits in a digital output code. V_{in} and V_{ref} represent the input analog signal and reference voltage level individually.

The number of ADC quantization levels is given by $L = 2^n$. With more bits to represent an analog value, the quantized value is closer to the real value and thus a smaller quantization error can be achieved. As shown in Figure 4.5, the accuracy of ADC quantization can be characterized by a quantization error and quantization noise. More bits indicate a smaller amount of quantization noise on the digital outputs.

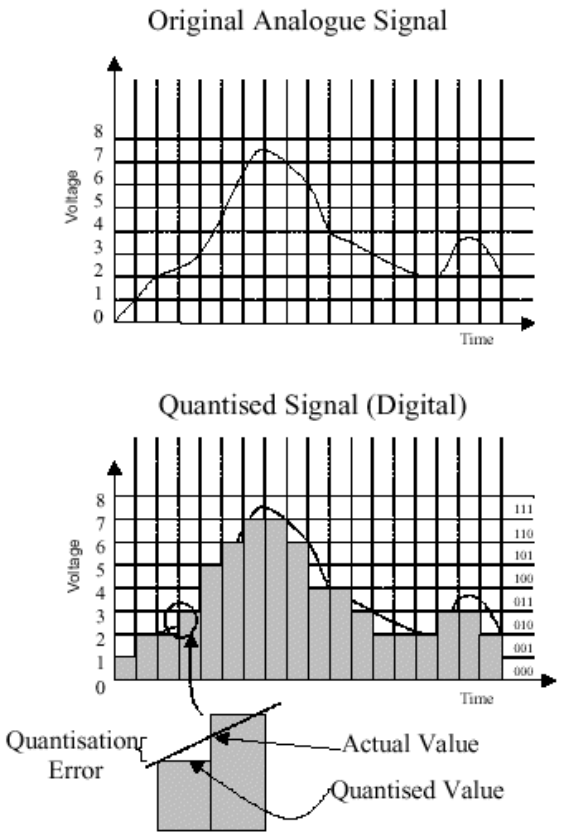

Figure 4.5: ADC quantization illustration

But an increase in the number of bits in a digital output code gives rise to larger system complexity and power consumption. In order to achieve a low power consumption at the receiver, the number of bits in the ADC section should be kept as low as possible, however leading to a large amount of quantization noise. Assuming an ADC with word length n and clipping level A_c, the quantization step size Δ is defined as $A_c/2^{n-1}$. The quantization error e is uniformly distributed over $[-\Delta/2, \Delta/2]$. The probability density function (PDF) of the ADC quantization error e is sketched in Figure 4.6.

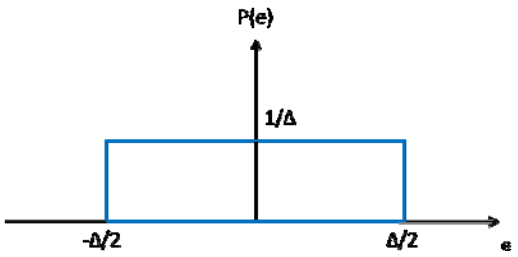

Figure 4.6: PDF of the ADC quantization error

The ADC quantization noise power can be obtained by calculating the variance σ^2 of the quantization error e :

$$\sigma^2 = E\left(e^2\right) = \int_{-\Delta/2}^{\Delta/2} \frac{1}{\Delta} \cdot e^2 \, de = \frac{\Delta^2}{12} = \frac{A_c^2}{3 \cdot 2^{2n}} \tag{4.18}$$

It indicates that the ADC quantization noise is in direct proportion to the quantization step Δ , but in inverse proportion to the number of quantization levels 2^n .

4.1.5 Sampling clock offset

The sampling clock offset (SCO) occurs at the receiver due to a mismatch between the transmitter and receiver oscillators, or due to a Doppler frequency shift. A sampling clock offset is another source of system performance degradation. Figure 4.7 illustrates that the sampling frequency is deviated by a factor δ with respect to the ideal sampling frequency f_s , which causes the phase offset in the clock to vary with time [28]. The sampling points in time are $(1+\delta)\cdot(1, 2, \ldots, N)\cdot T_s$ instead of $(1, 2, \ldots, N)\cdot T_s$. In other words, an accumulative sampling time shift of $n\delta T_s$ exists at the n^{th} sample. Due to the sampling time shift, the received signal is no longer sampled at the optimal points. Furthermore, a complete sample will be shifted by a time of T_s/δ . Therefore, SCO often causes a decrease in the system performance.

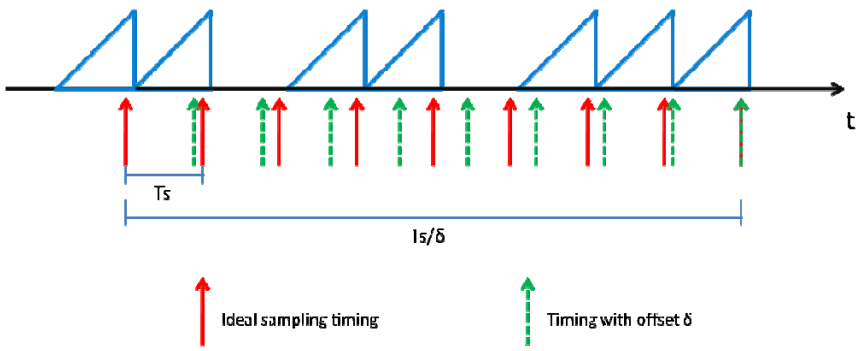

Figure 4.7: Sampling clock offset illustration

In a single-carrier wakeup receiver, the received address length is 16-bit and thus the accumulative sampling time shift at the n^{th} symbol is larger than that in a multi-carrier wakeup radio, where the sub-addresses from the four carriers are sampled in each chain separately and the number of bits in

a sampling process is divided by the number of carriers. Then the multi-carrier wakeup radio scheme can resist the effect of a sampling clock offset on the receiver performance, as the address length is shortened in each sampling process, avoiding a big accumulation of sampling clock offsets.

4.2 Simulation scenario

4.2.1 System modeling

As discussed in Section 3.2.2, the co-simulation through MATLAB and Simulink is desirable, in case the analog and digital parts are both considered in the system simulation. In the analysis of the effects of non-idealities on the MC wakeup receiver, an example of 4-carrier wakeup receiver is used. The address generation and detection are conducted in MATLAB, while the MC wakeup receiver is modeled in Simulink. The Simulink model is shown in Figure 4.8.

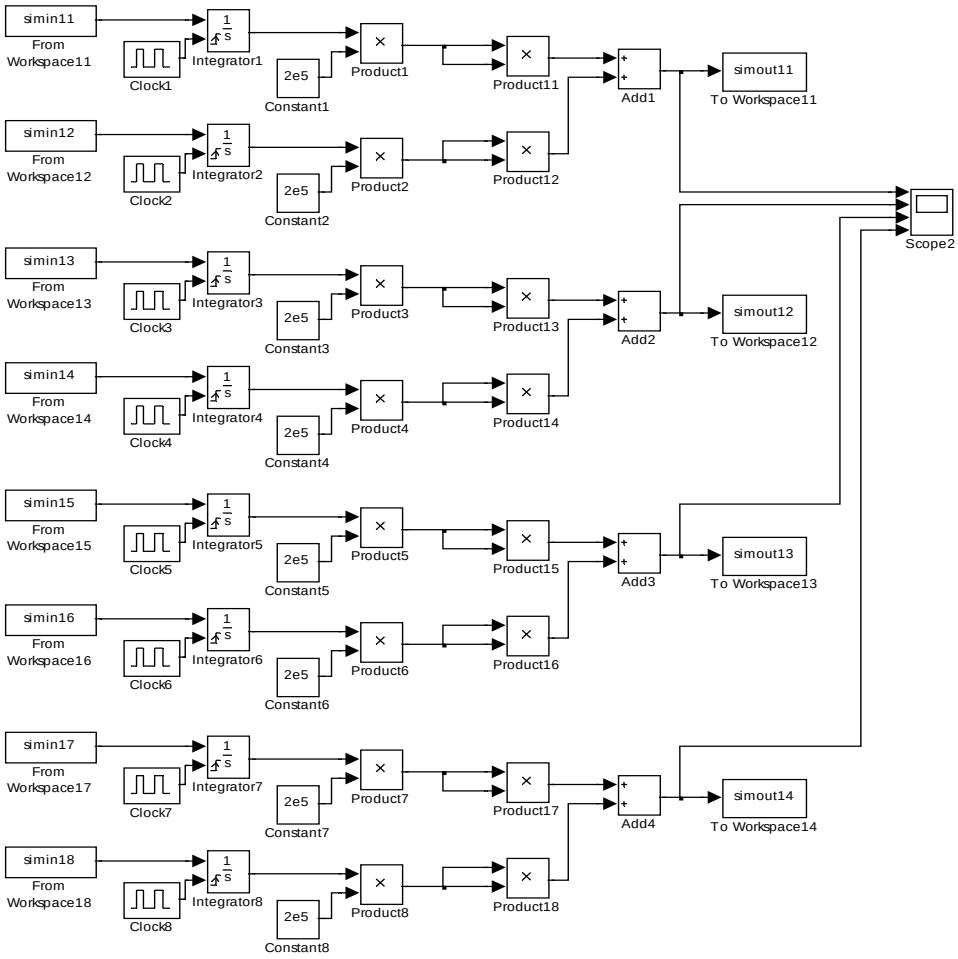

Figure 4.8: System modeling in Simulink

4.2.2 Simulation parameters

The simulation details and parameters are indicated in Table 4.2.

Table 4.2: Simulation parameters

the number of carriers	4
channel spacing	5 MHz
the length of address code	16 bits
address code generation	OVSF codes
the number of available address codes	15
data rate	100 kbps
the bandwidth of each frequency channel	100 kHz
modulation	OOK
address correlation detection scheme	hard-bit Hamming distance method

The same simulation model and parameters in Table 4.2 are applied to the cases of AWGN and fading channels. The simulation results in different channel models are shown and analyzed in the following sections. As defined in Chapters 2 and 3, the BER, P_{md}, and P_{fa} are used to reflect the detection performance of the MC wakeup receiver in the presence of non-idealities.

4.3 Effect of non-idealities in AWGN channels

The most frequently employed and simplest channel model is the AWGN channel (see Section 3.1). The AWGN channel is of importance in communication theory and practice, particularly for deep space and satellite communications. In the AWGN channel model, Gaussian noise is linearly added to the desired signal. The discrete-time values n_i added by the AWGN channel can be considered as a Gaussian distributed random variable with zero mean, which can be any real value and is independent of the channel input. A real-value Gaussian distributed random variable X with mean value μ and variance σ^2 can be characterized by its probability density function $f_X(x)$.

$$f_X(x) = \frac{1}{\sqrt{2\pi}\sigma} \exp\left[-\frac{(x-\mu)^2}{2\sigma^2} \right] \tag{4.19}$$

The limitation of the AWGN channel model exists in that it does not account for channel fading, interference, nonlinearity or dispersion. Nevertheless, it provides a mathematical model which is useful for getting insight into the underlying behavior of a MC wakeup receiver before other phenomena are analyzed.

4.3.1 Impact of phase noise

In the ideal case (i.e., no phase noise), the BER at an SNR of 6 dB is around 0.15 (see Figure 3.4). With a phase noise variance of 0.01, the bit error rate doubles, up to almost 0.3. The phase noise variance can be transferred to PSD values through Table 4.1. It can be seen that the BER performance and the two error probabilities are sensitive to phase noise. As described in Figure 4.11, to achieve a BER of 0.2, the required SNR with a phase noise variance of 0.01 increases to 9 dB, while it is only 4.5 dB in the case without phase noise. A degradation of 4.5 dB in SNR for a BER of 0.2 is significant, and furthermore, the performance degradation is more severe when a lower BER is required. In Figure 4.12, for a false alarm probability of 0.01, an extra SNR of 5 dB is demanded with a phase noise variance of 0.01.

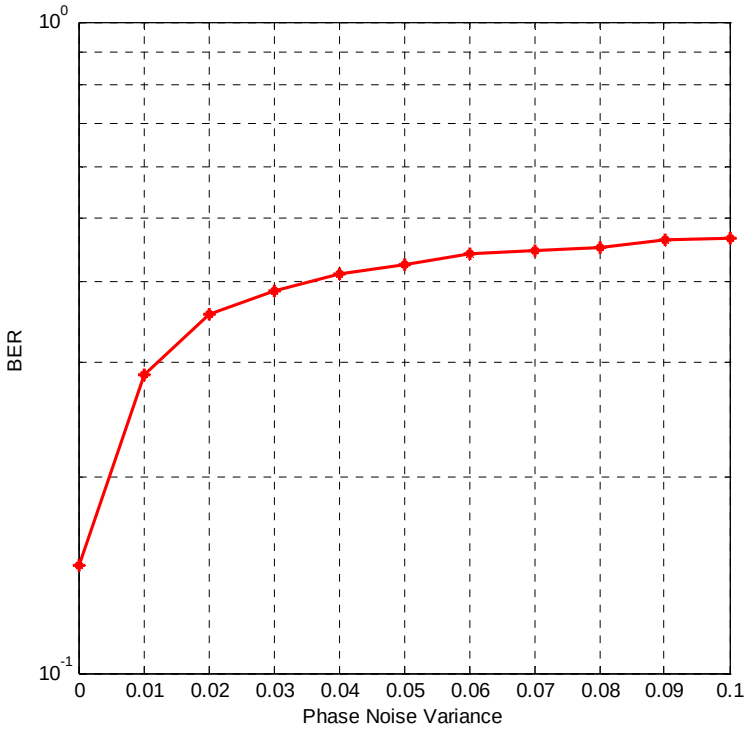

Figure 4.9: BER performance with phase noise in AWGN channels (SNR = 6 dB)

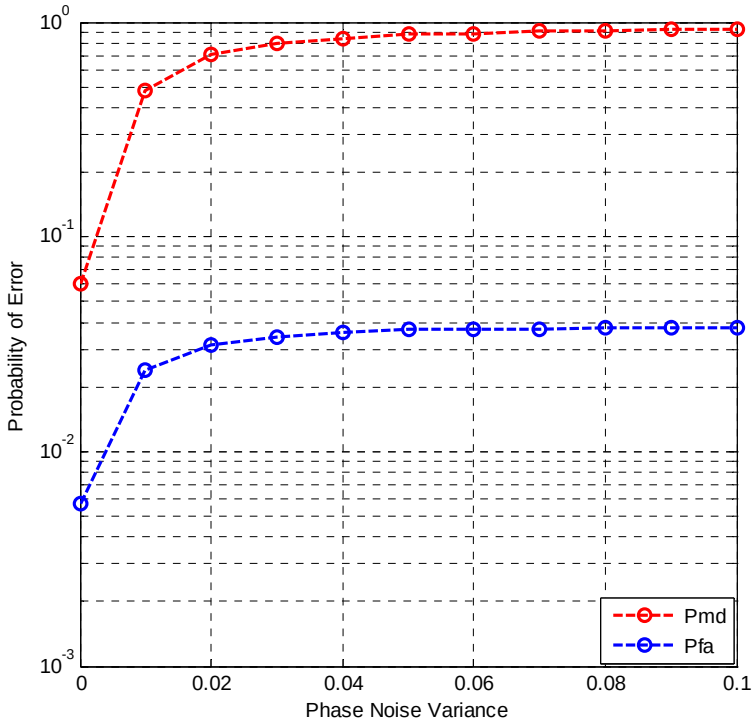

Figure 4.10: Error probabilities with phase noise in AWGN channels (SNR = 6 *dB*)

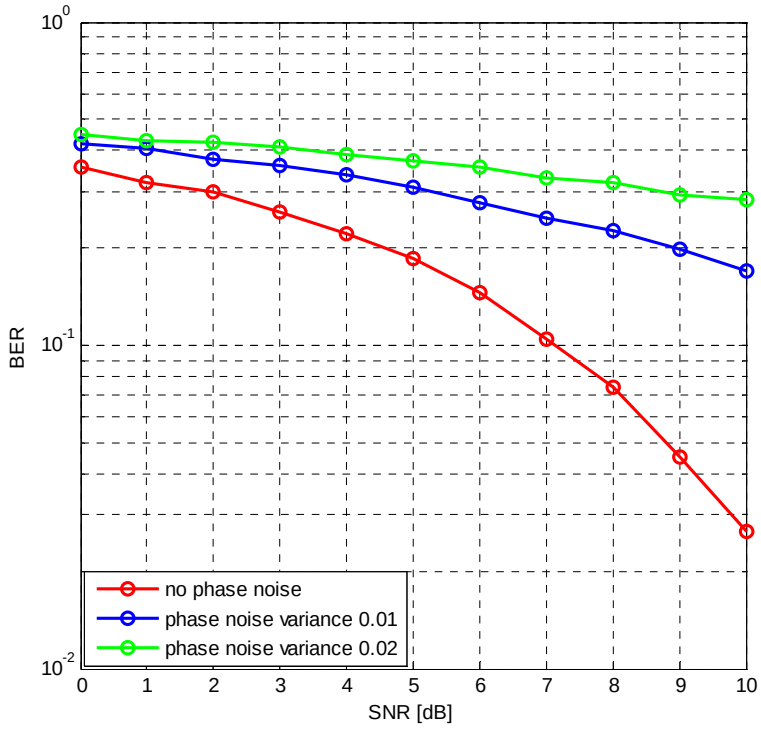

Figure 4.11: BER performance with different amounts of phase noise at different SNRs

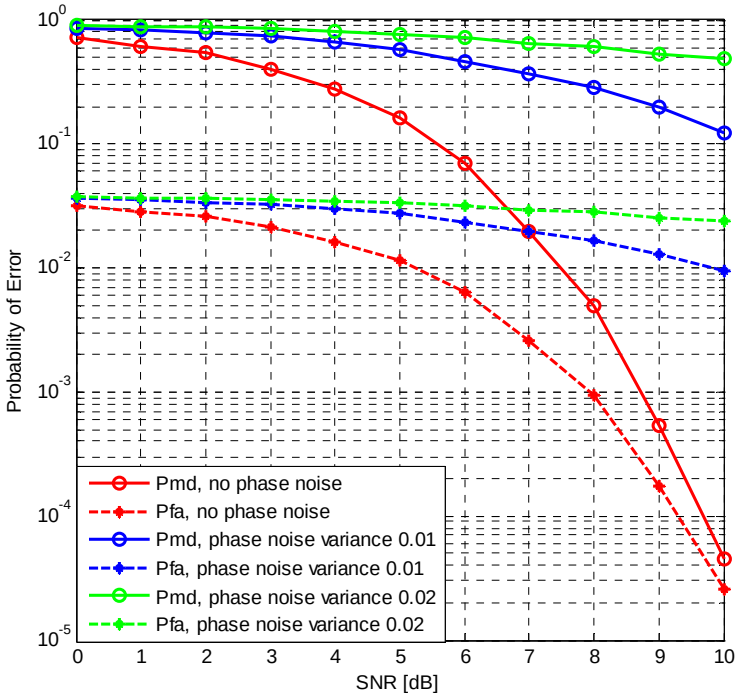

Figure 4.12: Error probabilities with different amounts of phase noise at different SNRs

4.3.2 Impact of carrier frequency offset

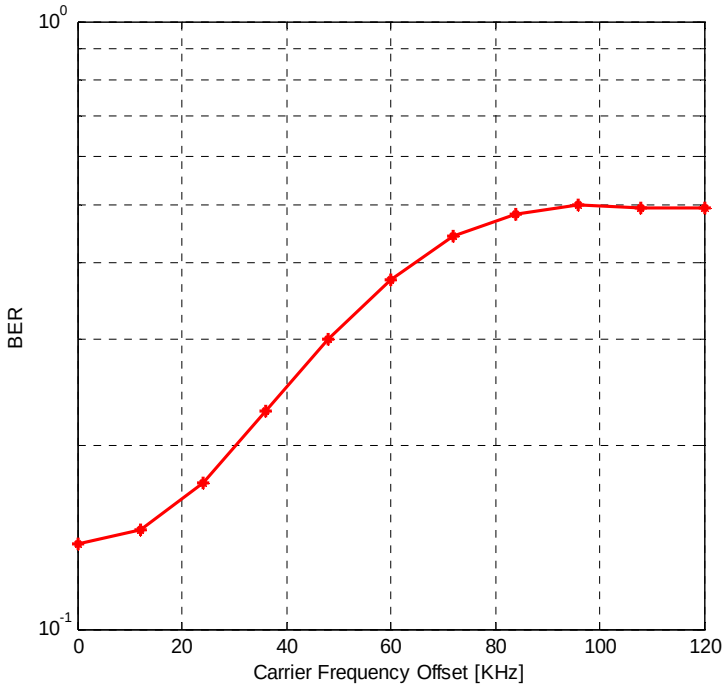

Figure 4.13: BER performance with carrier frequency offset in AWGN channels (SNR = 6 dB)

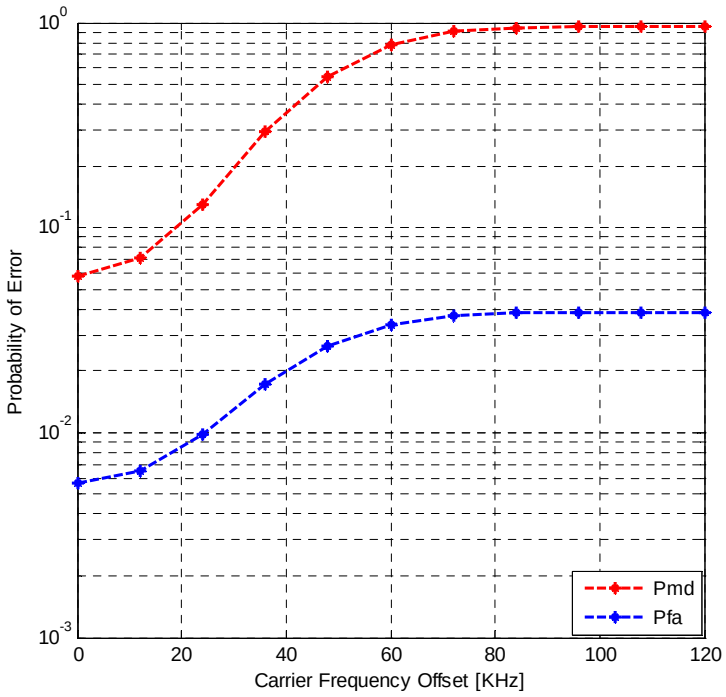

Figure 4.14: Error probabilities with carrier frequency offset in AWGN channels (SNR = d dB)

It can be seen from Figure 4.13 and 4.14 that the BER and P_{md} are nearly 50% and 100% respectively when the carrier frequency offset rises to 100 kHz. It is analyzed in Section 4.1.2 that in the presence of a carrier freuquency offset, the output signal suffers from a signal attenuation equal to:

$$\alpha = \frac{2\left(1-\cos\left(\Delta wT\right)\right)}{\left(\Delta wT\right)^2} = \frac{\sin^2 \pi\rho}{\pi^2\rho^2} \qquad (4.20)$$

where $\rho = \Delta f T$, with the carrier frequency offset Δf and the symbol time T.

Ideally, there is no frequency offset (i.e., $\Delta f = 0$) and $\rho = 0$. Then α becomes 1, which means that the output signal does not suffer from any attenuation. But when the carrier frequency offset Δf equals the inverse of the symbol time T (i.e., the data rate), $\rho = 1$. The signal attenuation factor α goes to zero. Therefore, no more energy is collected by the receiver matched to the incoming signal and the BER is close to 50% [29]. In the simulation, the data rate is 100 $kbps$. It explains why the BER goes up to 50% in Figure 4.13 when the carrier frequency offset reaches 100 kHz. It can also be interpretted by means of the cut-off frequency of an integrator. It is observed in Figure 2.2 that the cut-off frequency of an integrator is equal to the

data rate. As the carrier frequency offset goes up to 100 kHz, the desired signal is down-converted to the band around the cut-off frequency. So no signal energy can be acquired after the integrators, resulting in a BER of 50%.

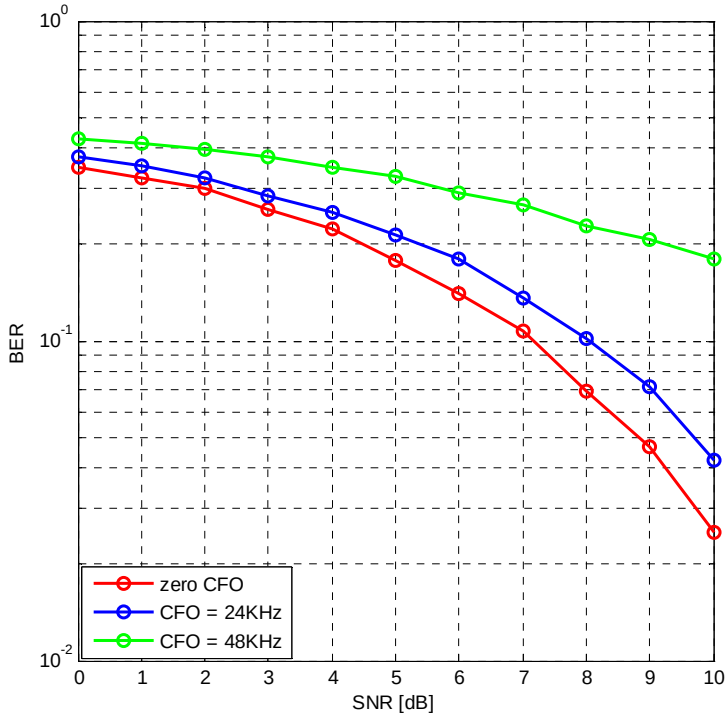

Figure 4.15: BER performance with different carrier frequency offsets at different SNRs

In Figure 4.15, for a BER of 0.2, the SNR degradation with a carrier frequency offset of 24 kHz is only 1 dB compared to the case without frequency offset, but the performance difference is much larger as the carrier frequency offset doubles. The effect of a carrier frequency offset of 48 kHz on the BER and error probabilities turns out to be the same as that of a phase noise variance of 0.01 described in Figure 4.11.

4.3.3 Impact of I/Q imbalance

The relationship between the BER performance and relative I/Q mismatch interference for different SNRs is plotted in Figure 4.17. It can be seen that the effect of I/Q mismatch on the receiver performance varies with the channel SNR. We observe from Figures 4.17 and 4.19 that the BER performance degradation with a higher SNR is more significant. For an SNR of 10 dB, the BER performance starts to degrade from the relative I/Q imbalance interference of -30 dB, but

we can only see the effect of I/Q mismatch on the BER performance from -20 dB for an SNR of 6 dB.

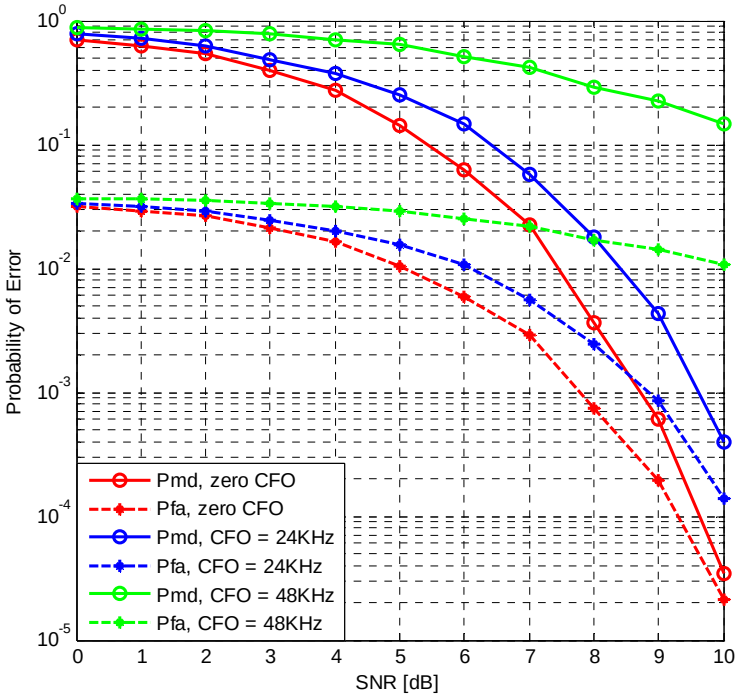

Figure 4.16: Error probabilities with different carrier frequency offsets at different SNRs

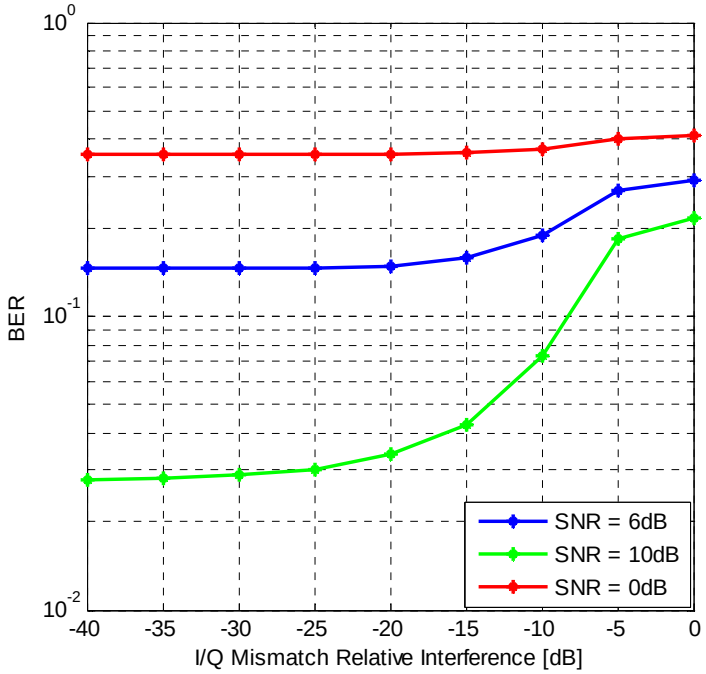

Figure 4.17: BER performance with I/Q mismatch in AWGN channels

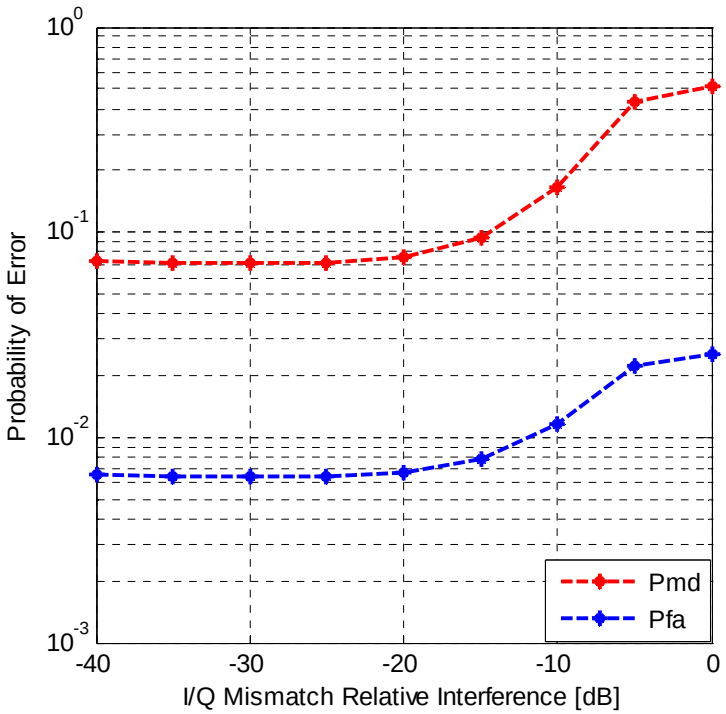

Figure 4.18: Error probabilities with I/Q mismatch in AWGN channels (SNR = 6 *dB*)

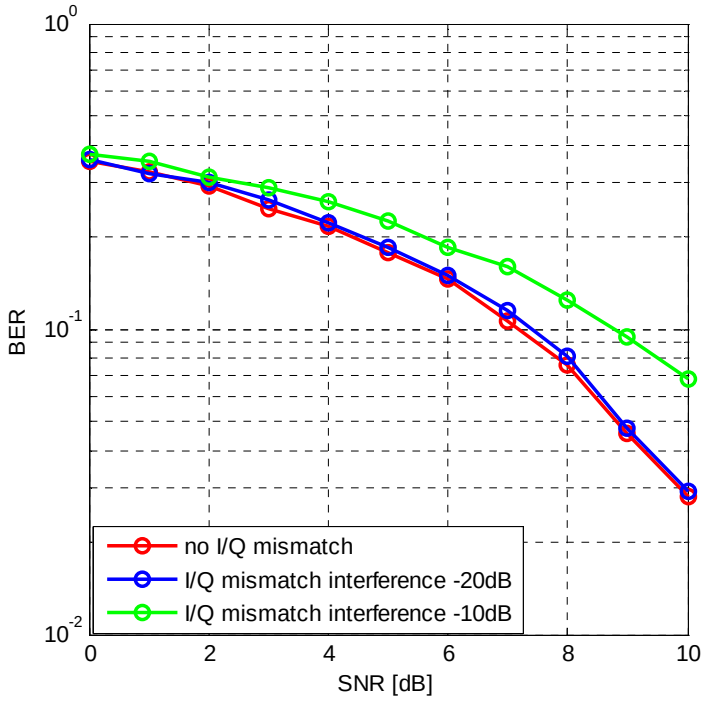

Figure 4.19: BER performance with different amounts of relative I/Q mismatch interference at different SNRs

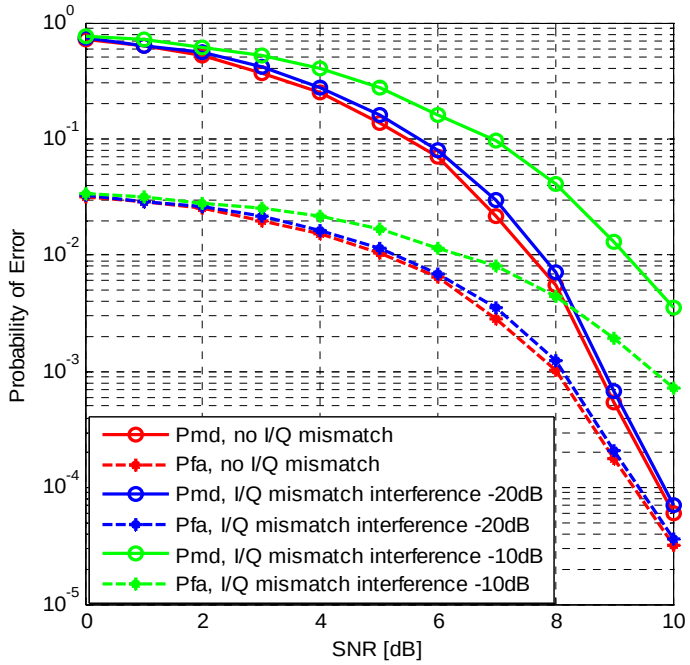

Figure 4.20: Error probabilities with different amounts of relative I/Q mismatch interference at different SNRs

4.3.4 Impact of ADC quantization noise

As I/Q imbalance, the effect of ADC quantization noise on the BER performance and error probabilities is varable with SNR. For a higher SNR, the influence of the number of bits in a digital output code on the detection performance is larger, as shown in Figures 4.21 and 4.22. It can be seen from Figures 4.23 and 4.24 that if the number of bits to represent an analog voltage level is raised to 3, the detection performance is close to the ideal case where the number of ADC quantization levels is infinite. Hence, a 3-bit ADC is an option for a good balance between the system complexity and detection performance.

In ADC quantization, the clipping level has to be a consideration as well. The received signal amplitude usually fluctuates and peaks occur in the signal that are significantly higher than the signal root-mean-squared (RMS) value. Since the signal amplitude is unknown in advance, the receiver has to adjust its gain to make the signal fit in the ADC dynamic range. If the signal is weakly amplified before the ADC, no clipping occurs but the ADC quantization noise is relatively high. On the other hand, if the signal is strongly amplified, the impact of the quantization noise becomes smaller, but the signal peaks can be clipped at full-scale, leading to severe signal distortion. In the simulations, the clipping level depends on the RMS level.

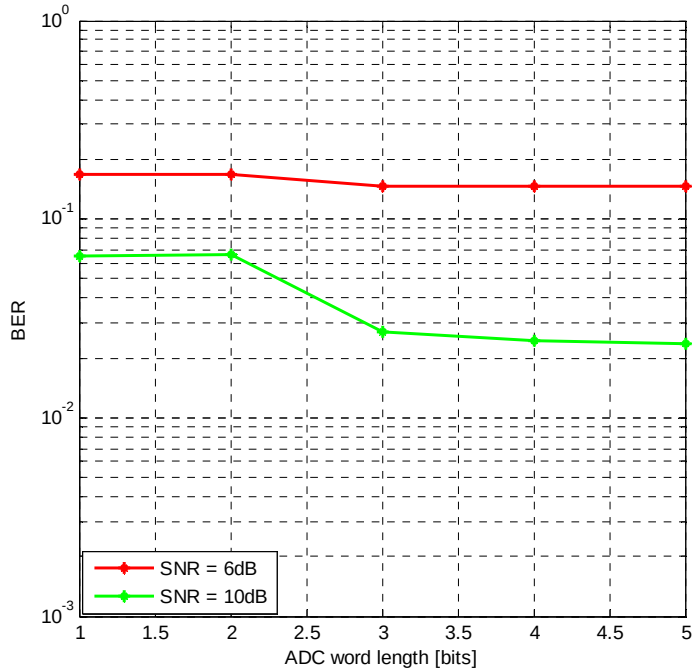

Figure 4.21: BER performance with ADC quantization noise in AWGN channels

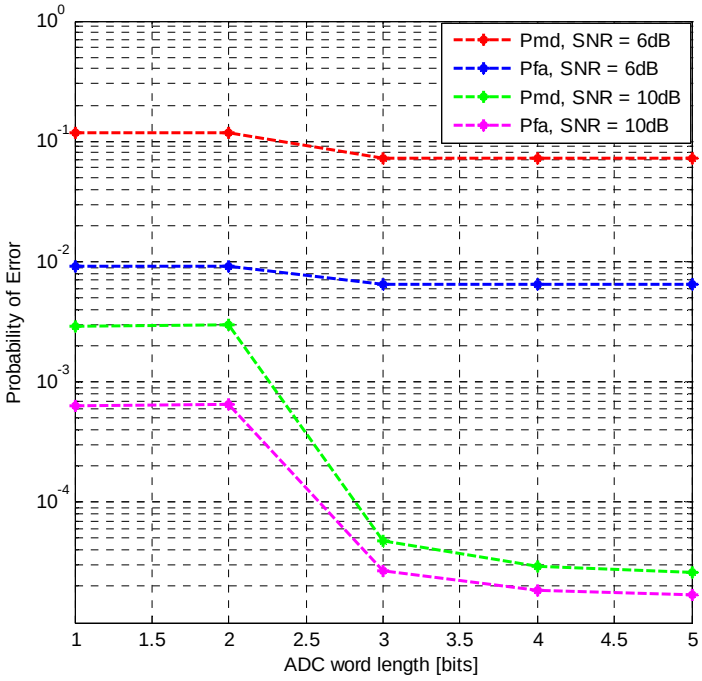

Figure 4.22: Error probabilities with ADC quantization noise in AWGN channels

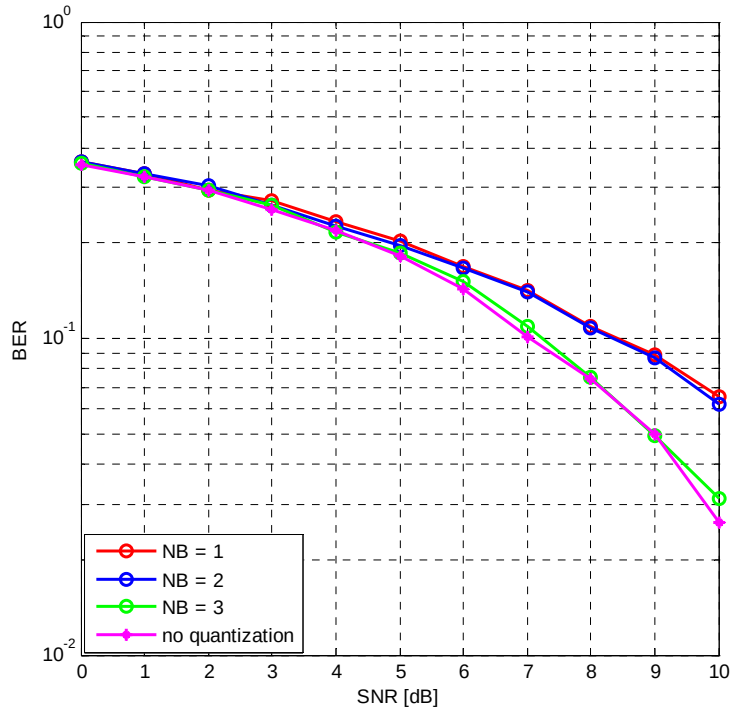

Figure 4.23: BER performance with different ADC word lengths at different SNRs

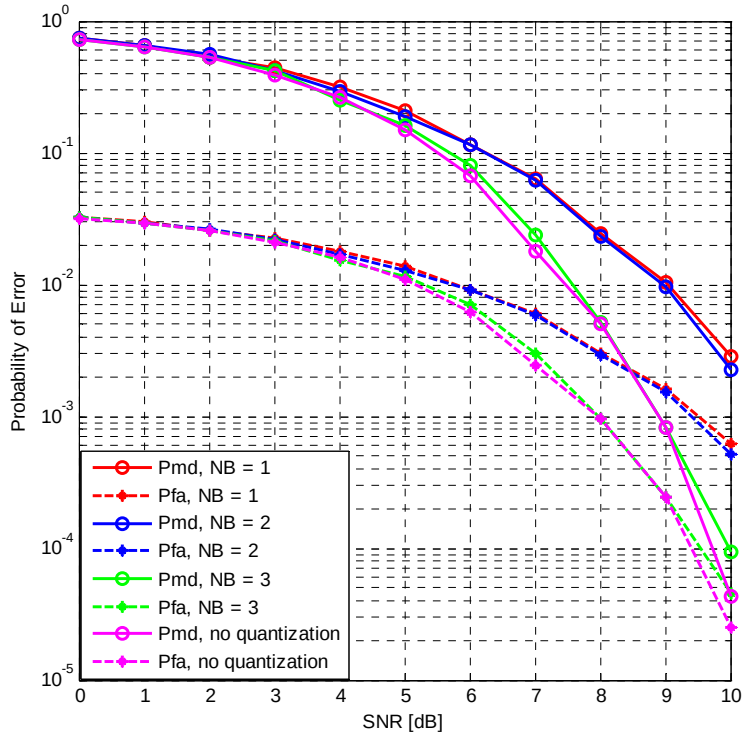

Figure 4.24: Error probabilities with different ADC word lengths at different SNRs

4.3.5 Impact of sampling clock offset

In the MC wakeup receiver, the output analog baseband signals are triangle waves due to the use of integrators. The optimal sampling points are at the peaks of the output signal, as shown in Figure 4.7. But due to sampling clock offsets, the sampling points are farther away from the peaks. Even worse, a complete sample will be shifted after a certain time. With a large accumulation of sampling time shifts at the n^{th} sample, the detection performance will be impaired, especially for a long packet. If the sub-address length in each carrier is too long, it is more likely that SCO has a severe influence on the detection performance. If the sampling clock frequency is shifted by 3%, the detection performance is close to the case without SCO in Figures 4.27 and 4.28. The reason is that the sampling points are still near the peak region even if they are not the optimal ones any more. Moreover, the number of bits in each sub-address is only 4 in the simulation, avoiding a huge accumulation of sampling time shifts. Thus a sampling clock offset of 3% leads to a small detection performance degradation.

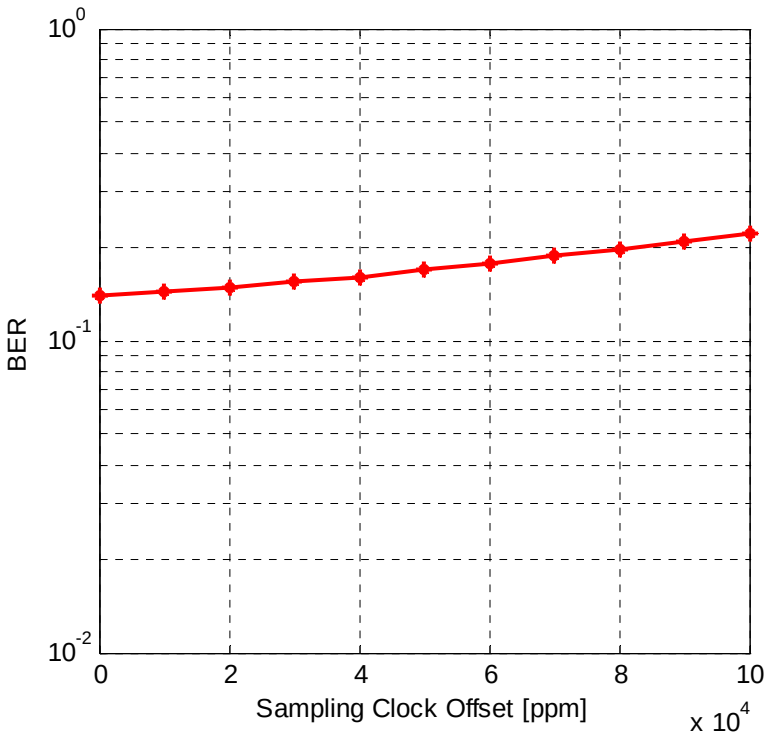

Figure 4.25: BER performance with sampling clock offset in AWGN channels (SNR = 6 dB)

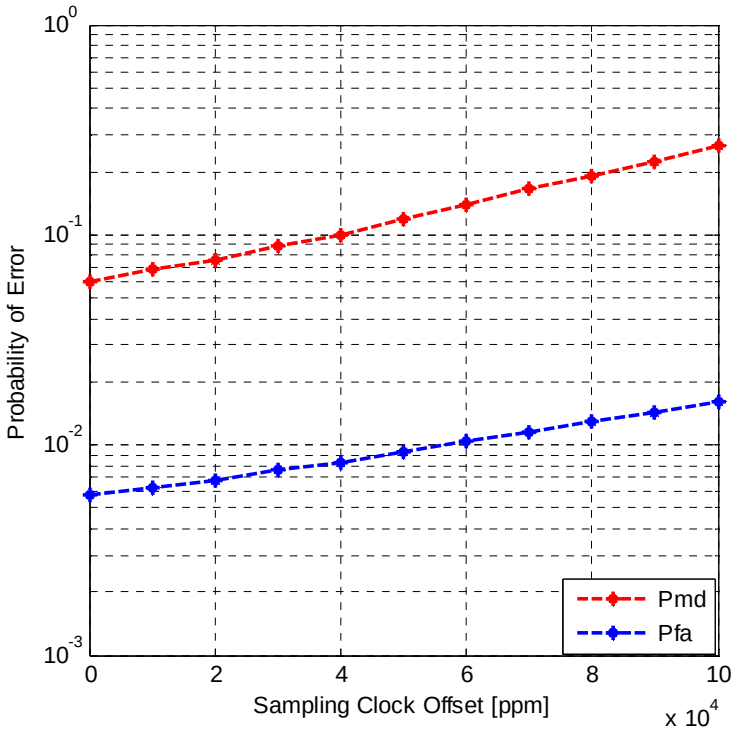

Figure 4.26: Error probabilities with sampling clock offset in AWGN channels (SNR = 6 *dB*)

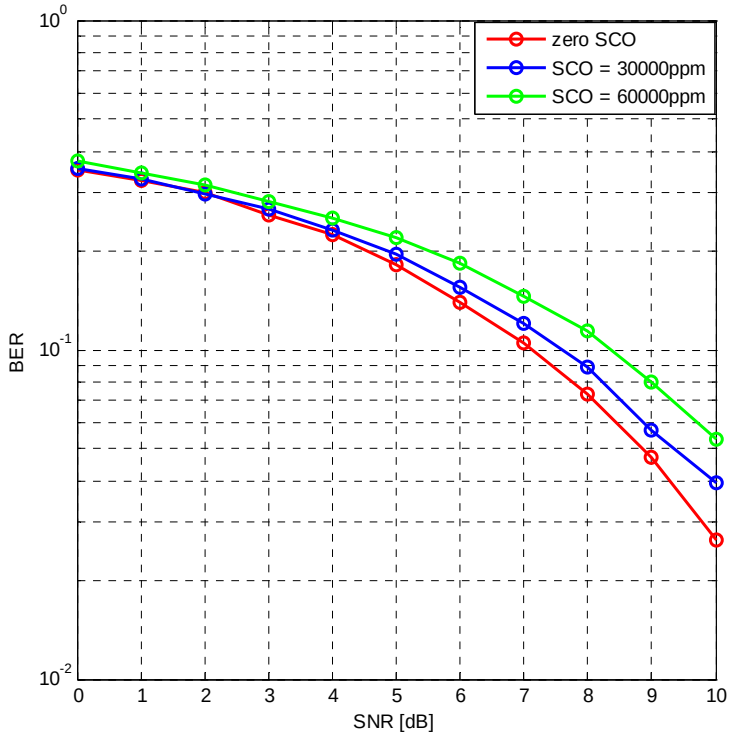

Figure 4.27: BER performance with different sampling clock offsets at different SNRs

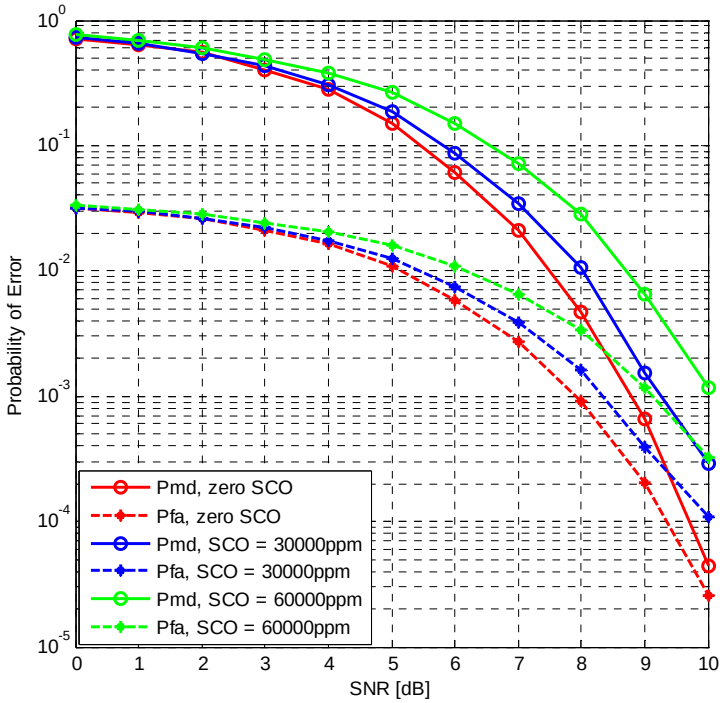

Figure 4.28: Error probabilities with different sampling clock offsets at different SNRs

4.4 Effect of non-idealities in Rayleigh fading channels

4.4.1 Rayleigh fading channel model

For communication systems, the AWGN channel is the most frequently assumed channel model, but it is quite simple and cannot sufficiently represent practical channels, as the signals in space experience other impairments besides noise. In reality, wakeup radio waves transmitted from antennas, travel through the space, undergoing absorption, reflection, diffraction and scattering. In order to simulate more realistic channels, fading channels are taken into consideration as well.

Due to the multipath effect, the received signal energy shows a time-varying behavior, which is called fading. This introduces a significant fluctuation in the signal amplitudes. Generally, the fading channels can be classified into Rayleigh fading channels and Rician fading channels based on the absence or presence of a direct path between the transmitter and receiver. The main difference of fading channels and AWGN channels exists in the fact that the fading amplitudes are either Rayleigh or Rician distributed.

In Rayleigh fading channels, the line-of-sight (LOS) path between the transmitter (Tx) and receiver (Rx) is completely obstructed. In other words, there is no dominant path between the Tx

and Rx, and the propagation of the signals is largely determined by the way of scattering. The amplitude fluctuation of the received signals follows a Rayleigh distribution.

In the simulation, Rayleigh fading channels are often modeled as Rayleigh flat fading channels. A received signal is said to undergo flat fading if the channel has a constant gain and a linear phase response over a bandwidth larger than the bandwidth of the transmitted signal [30]. The received signal has an amplitude fluctuation due to the variations of the channel gain over time. In flat fading, there is no inter-symbol interference (ISI).

The fading amplitude A_{d_i} at the i^{th} time instant is:

$$A_{d_i} = \sqrt{\frac{x_i^2 + y_i^2}{2}} \tag{4.21}$$

where x_i and y_i are samples of a zero-mean Gaussian random process with variance $\sigma_o^2 = 1$.

The power density function (PDF) of Rayleigh fading is:

$$f(A_d) = \frac{A_d}{\sigma_o^2} \exp\left[-\frac{A_d^2}{2\sigma_o^2}\right] \qquad A_d \geq 0 \tag{4.22}$$

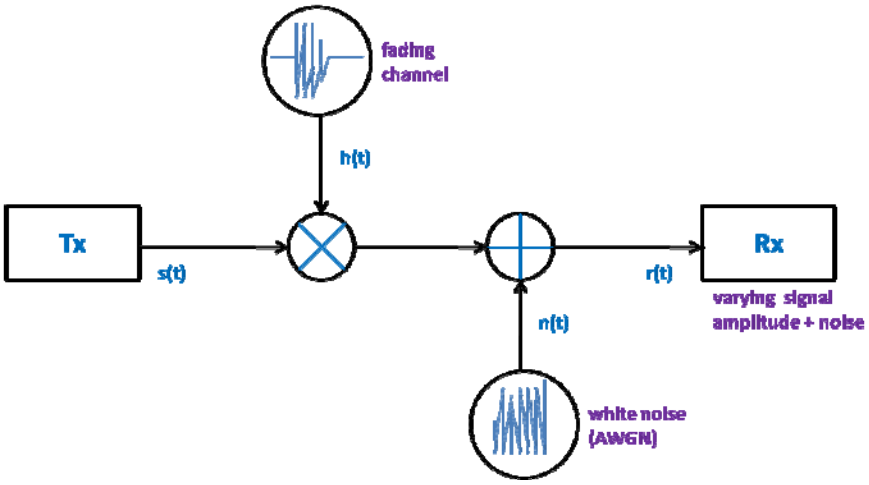

Figure 4.29: Rayleigh fading channel model

The received signal $r(t)$ can be mathematically expressed as:

$$r(t) = h(t) \cdot s(t) + n(t) \tag{4.23}$$

where $s(t)$ is the fading channel input and $n(t)$ is the additive white Gaussian noise. It is assumed that the channel between the transmitter and receiver is flat fading and the fading process $h(t)$ can be modeled as a zero-mean Gaussian process with unit variance [31].

4.4.2 Impact of phase noise

Due to the obstruction of a LOS path between the transmitter and receiver and the fluctuation of the received signal amplitude, the detection performance in Rayleigh fading channels is much worse than that in AWGN channels, as depicted in Figures 4.30 and 4.31. In Rayleigh fading channels, the BER is up to about 0.15, even if the SNR is 10 dB and no phase noise occurs.

With phase noise in the front-end, the receiver detection performance gets worse. To achieve a BER of 30%, an extra SNR of 4 dB is required for the case of a phase noise variance of 0.01, compared to the ideal case. As surveyed in Figure 4.30, the BER with phase noise has a linear-alike relationship with SNR.

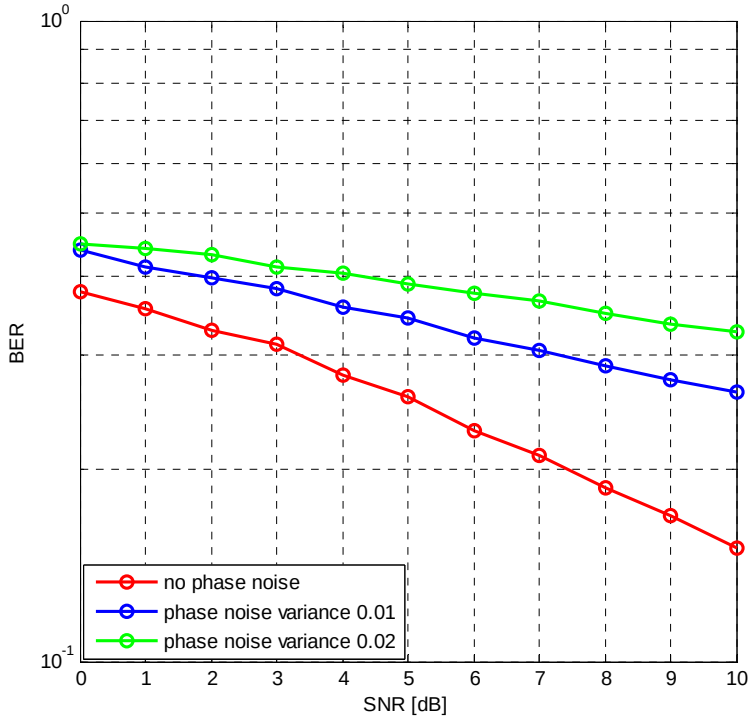

Figure 4.30: BER performance with different amounts of phase noise at different SNRs

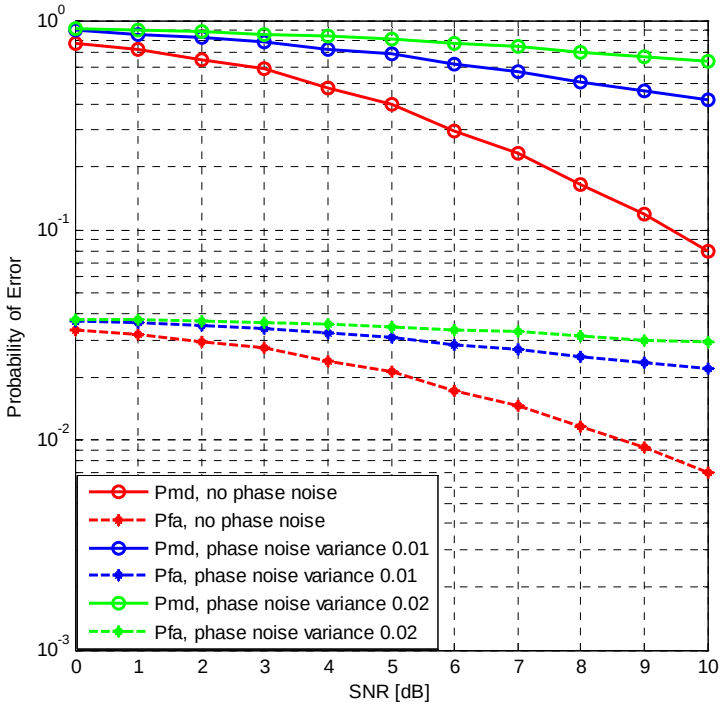

Figure 4.31: Error probabilities with different amounts of phase noise at different SNRs

4.4.3 Impact of carrier frequency offset

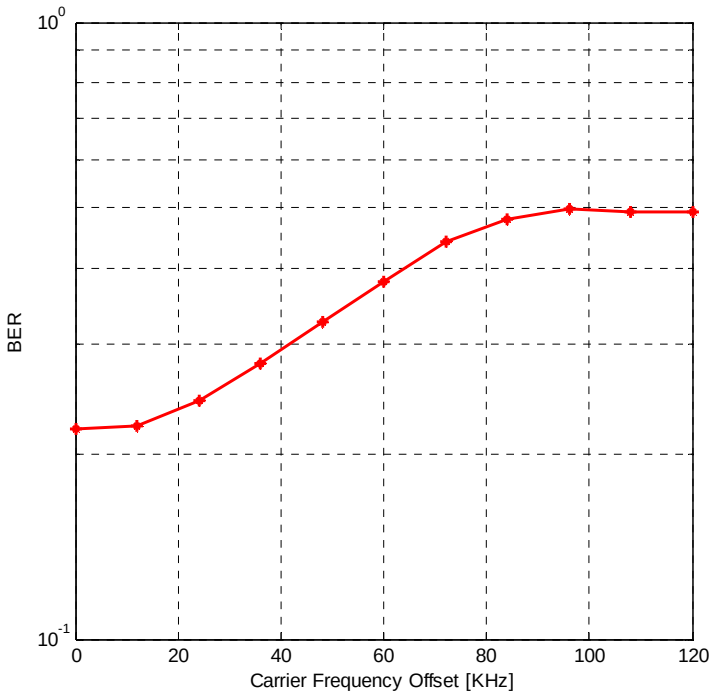

Figure 4.32: BER performance with frequency offset in Rayleigh fading channels (SNR = 6 dB)

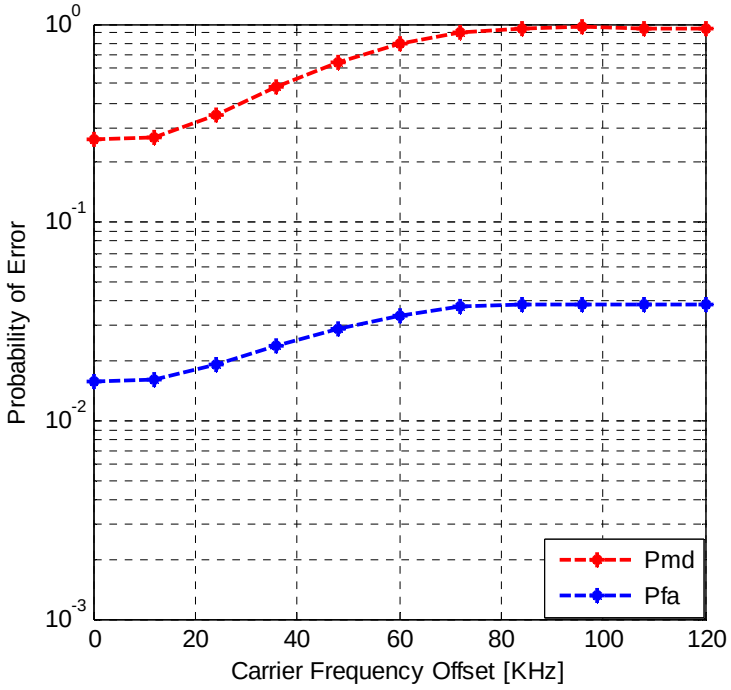

Figure 4.33: Error probabilities with frequency offset in Rayleigh fading channels (SNR = 6 *dB*)

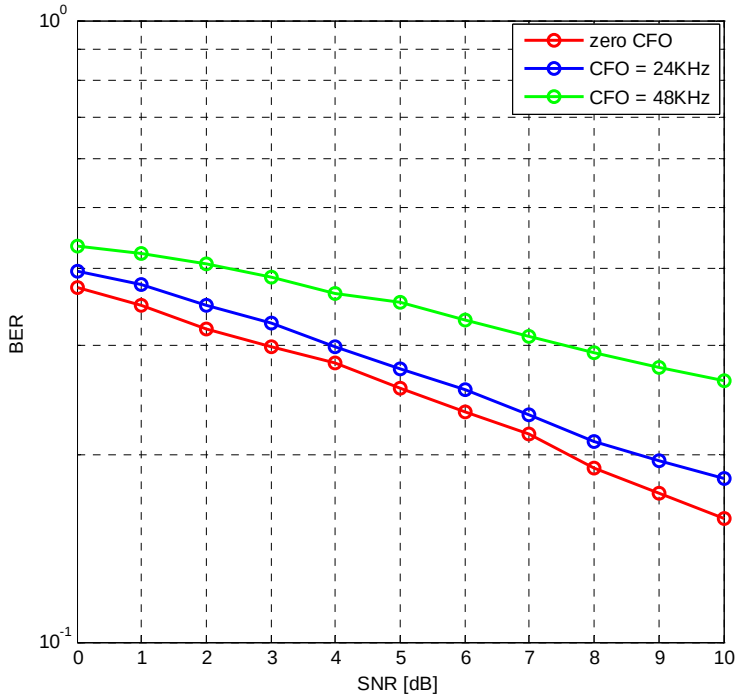

Figure 4.34: BER performance with different carrier frequency offsets at different SNRs

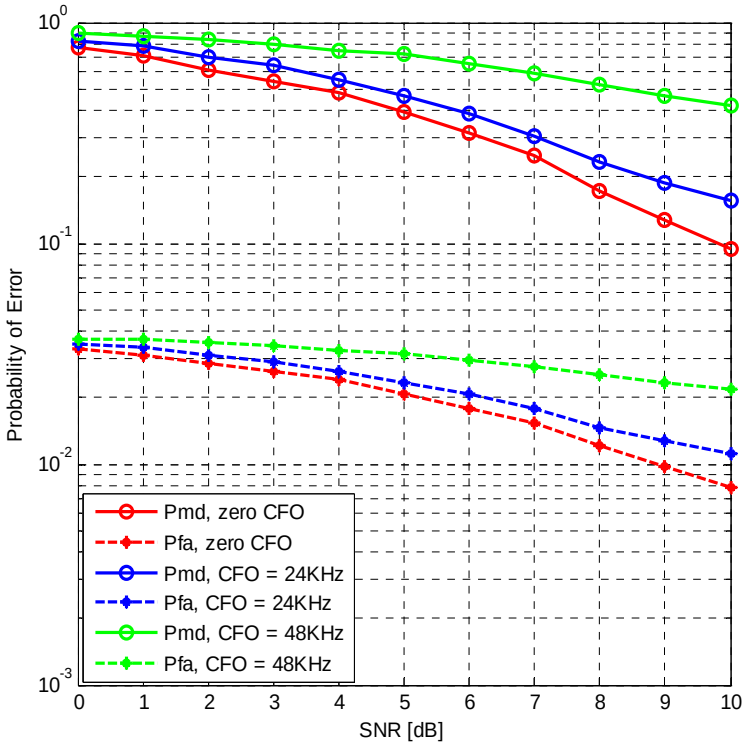

Figure 4.35: Error probabilities with different carrier frequency offsets at different SNRs

As analyzed in Section 4.3.2, the cut-off frequency of an integrator which is used as a low-pass filter equals the data rate. In the simulation, the wakeup packet in each frequency channel is transmitted at a rate of 100 $kbps$. As the carrier frequency offset goes up to 100 kHz, the BER is 50%, as displayed in Figure 4.32. We can see from Figures 4.32 and 4.33 that with a carrier frequency offset less than 20 kHz, the influence of the CFO on the detection performance is so small that it can be neglected. It can be concluded that a carrier frequency offset between 0 and 20 kHz is tolerable for the MC wakeup receiver in Rayleigh fading channels. From 20 kHz, the BER linearly increases with the carrier frequency offset.

4.4.4 Impact of I/Q mismatch

We can observe from Figures 4.36 and 4.37 that the I/Q imbalance still has a small effect on the receiver detection performance in Rayleigh fading channels. With a large relative I/Q mismatch interference of -20 dB, the BER, P_{md} and P_{fa} are still very close to the ideal cases.

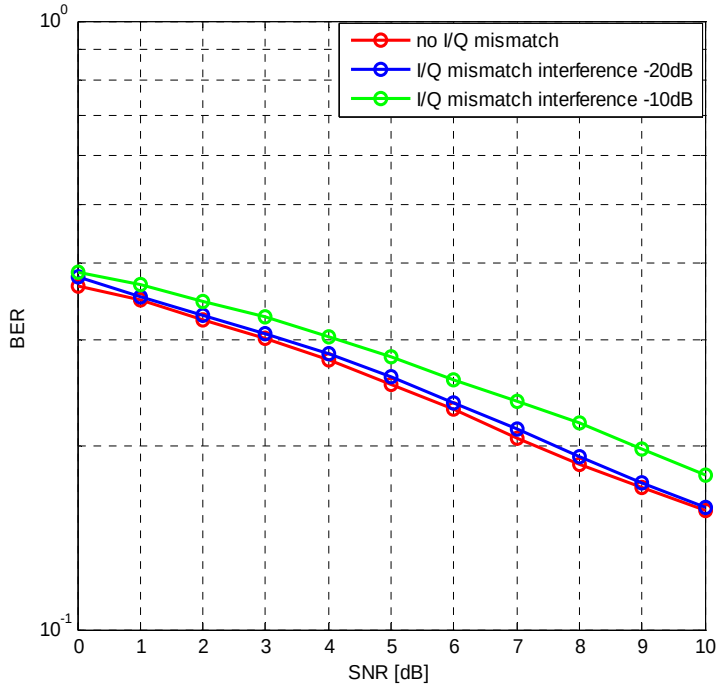

Figure 4.36: BER performance with different amounts of relative I/Q mismatch interference at different SNRs

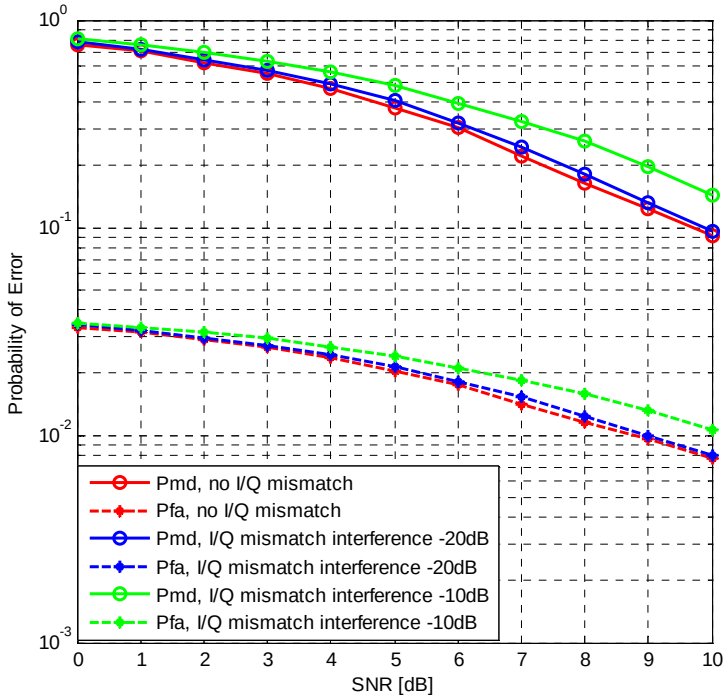

Figure 4.37: Error probabilities with different amounts of relative I/Q mismatch interference at different SNRs

4.4.5 Impact of ADC quantization noise

Figures 4.38 and 4.39 illustrate the benefit of more bits to represent an analog voltage level. The improvement of the detection performance with more bits in an output code is more significant for a higher SNR. At an SNR of 10 dB, the BER with a word length of 1 bit is around 0.25, but it can be decreased by 0.1 with a word length of 5 bits. A system performance degradation can be clearly observed in Figures 4.40 and 4.41, as a 1-bit ADC is used. With a 1-bit ADC, the optimal miss detection probability is only 40%. But it can significantly reduce to about 6% if the ADC word length goes to infinity (i.e., no ADC quantization noise exists). When the ADC word length is 3 bits, the detection performance is very close to the ideal case. In other words, the ADC quantization noise is negligible, in case an analog voltage level is expressed by a 3-bit output code.

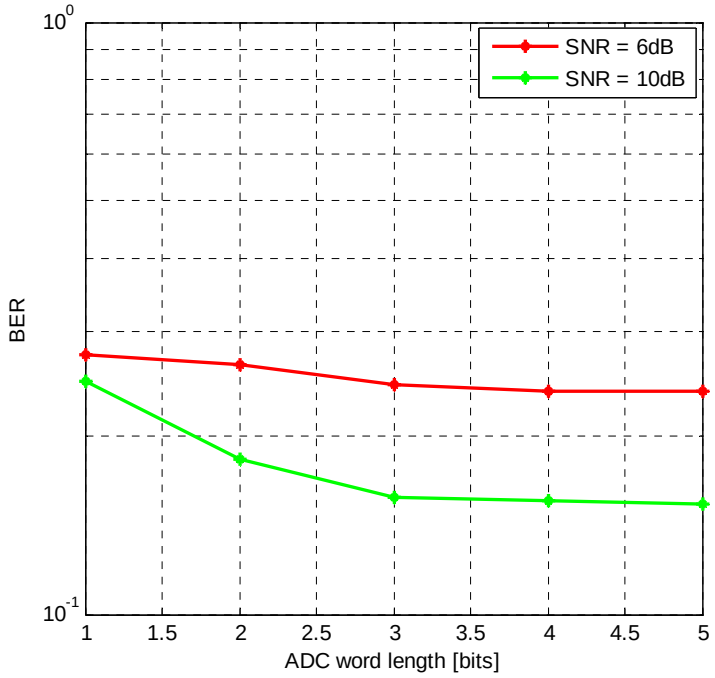

Figure 4.38: BER performance with ADC quantization noise in Rayleigh fading channels

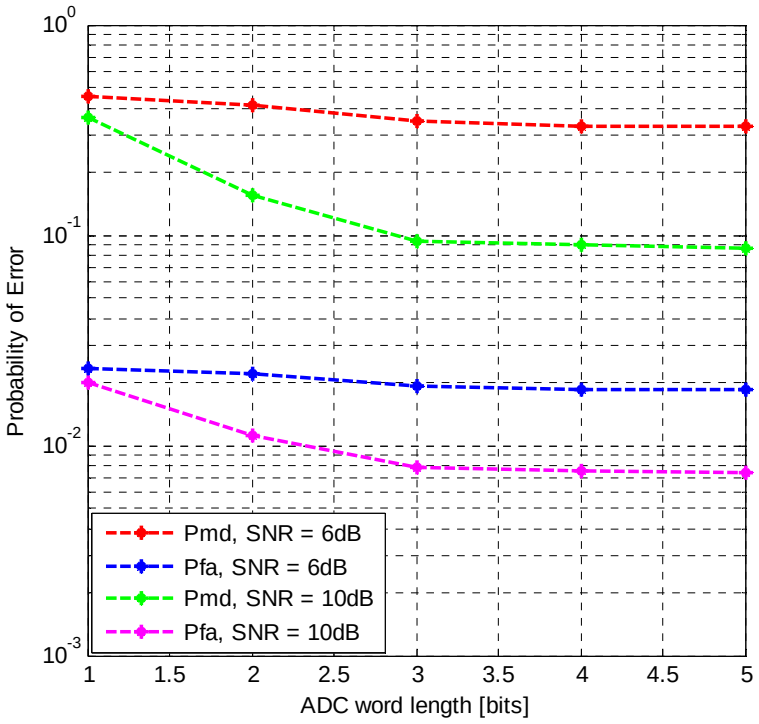

Figure 4.39: Error probabilities with ADC quantization noise in Rayleigh fading channels

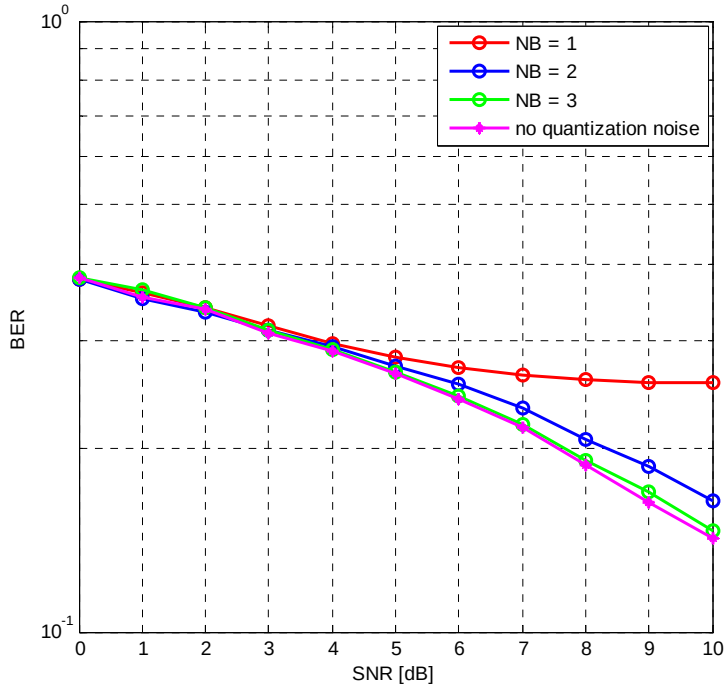

Figure 4.40: BER performance with different ADC word lengths at different SNRs

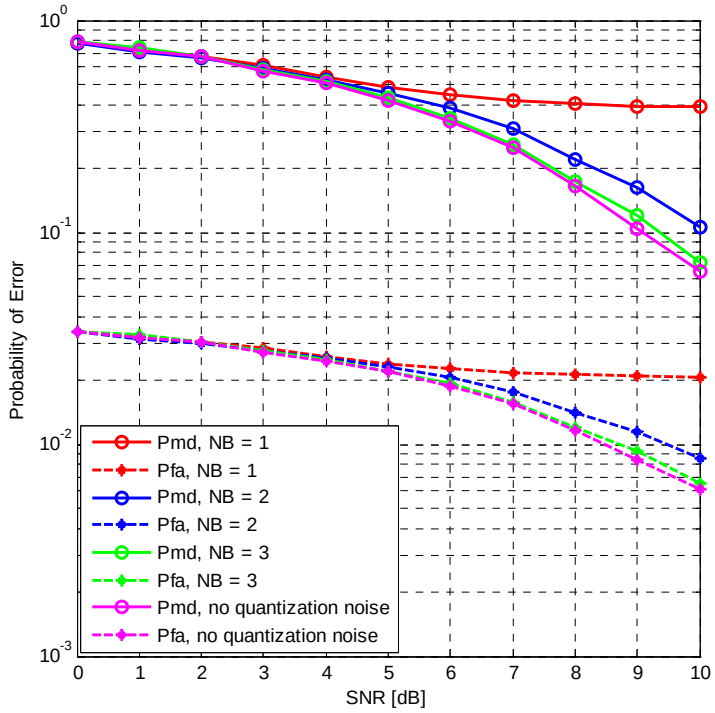

Figure 4.41: Error probabilities with different ADC word lengths at different SNRs

4.4.6 Impact of sampling clock offset

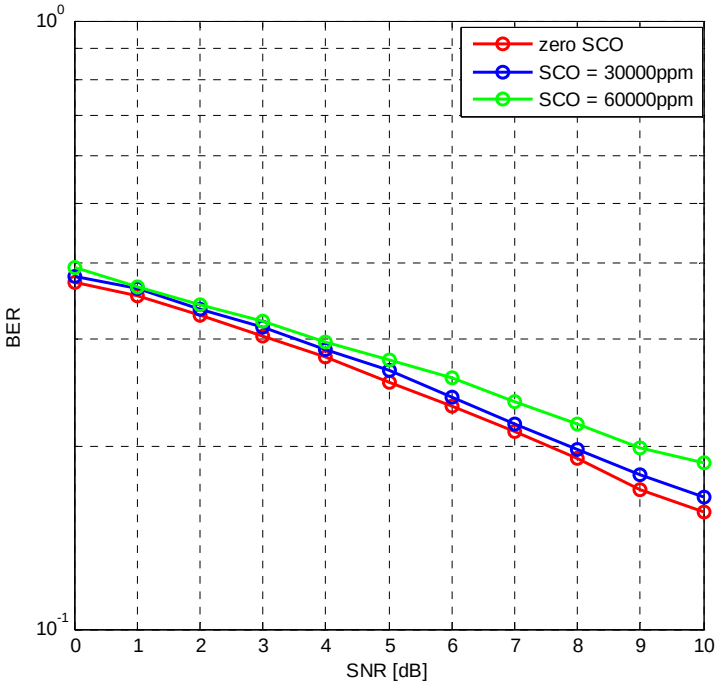

Figure 4.42: BER performance with different sampling clock offsets at different SNRs

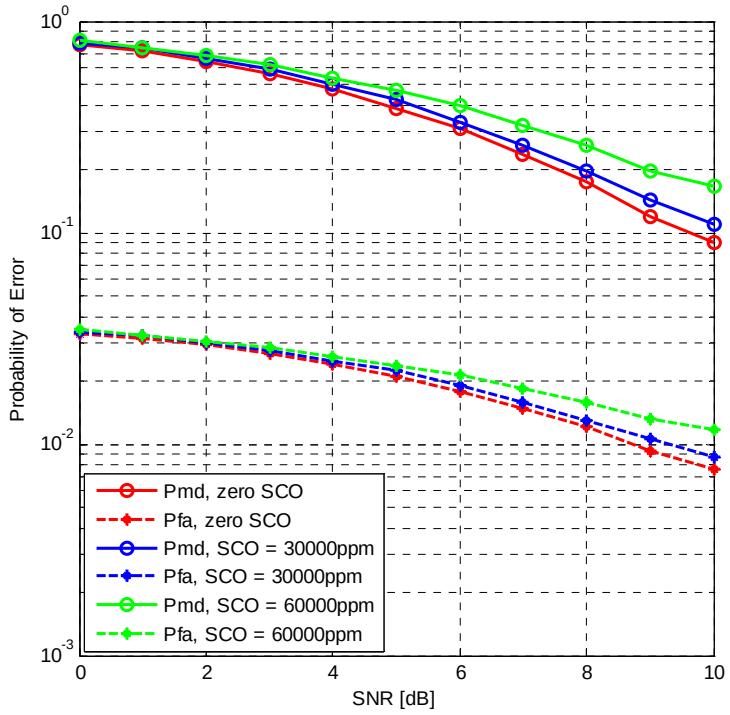

Figure 4.43: Error probabilities with different sampling clock offsets at different SNRs

Figures 4.42 and 4.43 indicate that the sampling clock offset does not cause a great degradation in the receiver detection performance in Rayleigh fading channels. As long as the packet synchronization is assured, the sampling points are still nearby the peaks of a triangle wave, even with a sampling clock offset of 30000 ppm.

4.5 Effect of non-idealities in Rician fading channels

4.5.1 Rician fading channel model

The fading channels are Rician-distributed if there is a dominant LOS path between the transmitter and receiver. The Rician fading channel scenario is shown in Figure 4.44.

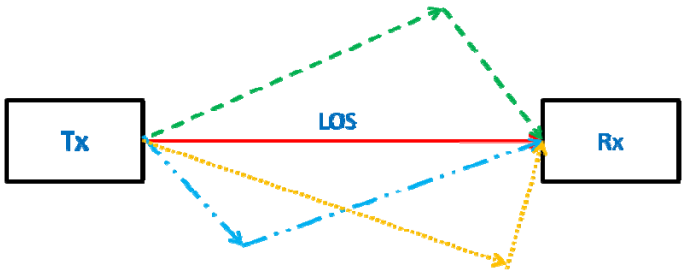

Figure 4.44: Rician fading channel scenario

The fading amplitude A_{d_i} at the i^{th} time instant can be expressed as:

$$A_{d_i} = \sqrt{\left(x_i + \beta\right)^2 + y_i^2} \tag{4.24}$$

where β represents the amplitude of the component along the LOS path, and x_i, y_i are samples of zero-mean stationary Gaussian random processes each with variance σ_o^2.

The Rician distribution is often characterized by the Rician factor K, which is defined as a ratio of the deterministic signal power from the LOS path to the diffuse signal power from indirect paths. The factor K reflects the contribution of the LOS path in the received signal power.

$$K = \beta^2 / 2\sigma_o^2 \tag{4.25}$$

The worst-case Rician fading channels associated with K = 0 are Rayleigh fading channels without LOS path between the transmitter and receiver. So Rayleigh fading is a special case of Rician fading. With the requirement that a Rician distribution is with unit mean-squared value [32] (i.e., $E\left\{r^2\right\} = 1$), the fading amplitude A_{d_i} becomes:

$$A_{d_i} = \sqrt{\frac{\left(x_i + \sqrt{2K}\right)^2 + y_i^2}{2\left(K+1\right)}} \tag{4.26}$$

where x_i and y_i are samples of zero-mean Gaussian random processes each with unit variance (i.e., $\sigma_o^2 = 1$).

The PDF of Rician fading is given as:

$$f\left(A_d\right) = \frac{A_d}{\sigma_o^2} \exp\left[-\frac{A_d^2 + \beta^2}{2\sigma_o^2}\right] \cdot I_o\left[\frac{A_d \beta}{\sigma_o^2}\right] \qquad A_d \geq 0 \tag{4.27}$$

where $I_o\left(\cdot\right)$ is the zero-order modified Bessel function of the first kind. If there is no LOS path between the transmitter and receiver, $\beta = 0$. The formula (4.27) reduces to:

$$f(A_d) = \frac{A_d}{\sigma_o^2} \exp\left[-\frac{A_d^2}{2\sigma_o^2}\right] \tag{4.28}$$

which is the PDF of Rayleigh fading and thus verifies that Rayleigh fading is a special case of Rician fading. In Figure 4.46, the PDFs of Rayleigh fading and Rician fading with different Rician factors are compared. Besides, the Rician fading channels turn out to be AWGN channels in which no fading exists, as the Rician factor K goes to infinity.

The Rician fading channels can be modeled in MATLAB with the code in Figure 4.45.

```
function r = rice_fading(Kdb, N, Mi)

K = 10^(Kdb/10);
const = 1/(2*(K+1));
x = randn(1,N);
y = randn(1,N);
r = sqrt(const*((x + sqrt(2*K)).^2 + y.^2));
rt = zeros(1,Mi*length(r));
ki = 1;
for i=1:length(r)
    rt(ki:i*Mi) = r(i);
    ki = ki+Mi;
end

r = rt;
```

Figure 4.45: Rician fading channel model in MATLAB

It can also be exploited that the contribution of the LOS path between the transmitter and receiver decides the channel quality. A Rayleigh fading channel is usually regarded as the worst-case channel among these three channels (i.e., AWGN, Rayleigh fading, and Rician fading channels), as the LOS path in this channel model is completely obstructed and the signal propagation is determined by scattering. In comparison, as discussed above, there is no fading in the AWGN channel, so its channel quality is better than fading channels. The channel quality of Rician fading channels depends on the Rician factor K, but it is always between AWGN channels and Rayleigh fading channels. The BER performance of the MC wakeup receiver without any impairment in these three different channel models is compared in Figure 4.47. In the simulation, the Rician factor K is $10\,dB$.

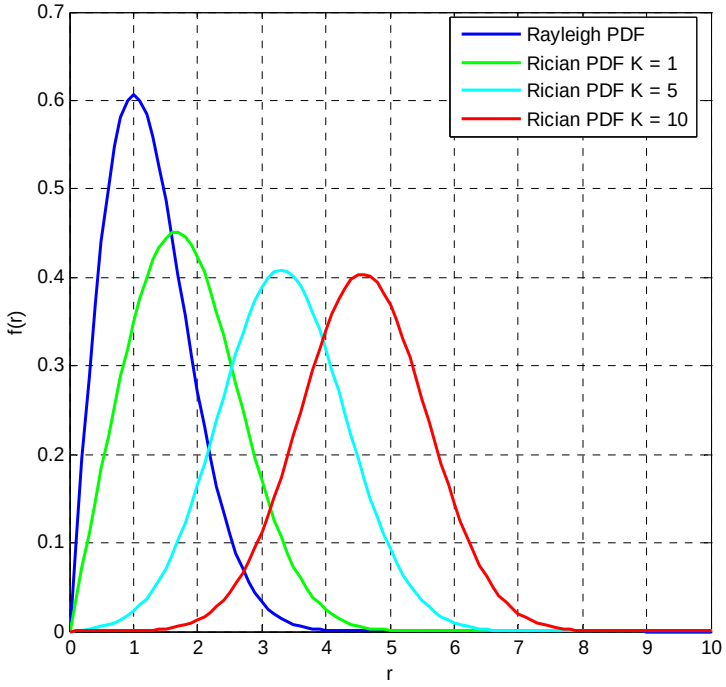

Figure 4.46: PDF of Rayleigh fading and Rician fading for $\sigma_o^2 = 1$

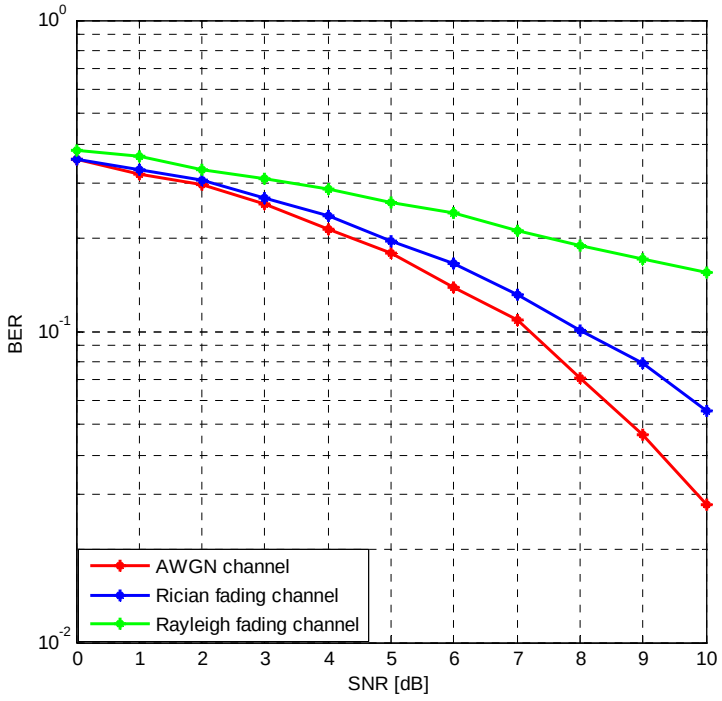

Figure 4.47: BER performance without any impairment for 3 different channel models

4.5.2 Impact of phase noise

It can be seen from Figure 4.48 that a SNR degradation of $5\,dB$ results from a phase noise variance of 0.01 for a BER of 20%. Figure 4.11 shows that in AWGN channels, the required SNR with a phase noise variance of 0.01 to achieve a BER of 0.2 is $9\,dB$, while it is only $4.5\,dB$ in the case without phase noise. Compared with AWGN channels, a larger extra SNR is required for a certain BER in Rician fading channels. Even with a phase noise variance of 0.01, the detection performance of the MC wakeup receiver is greatly impaired. For a lower BER, the performance difference introduced by phase noise is larger.

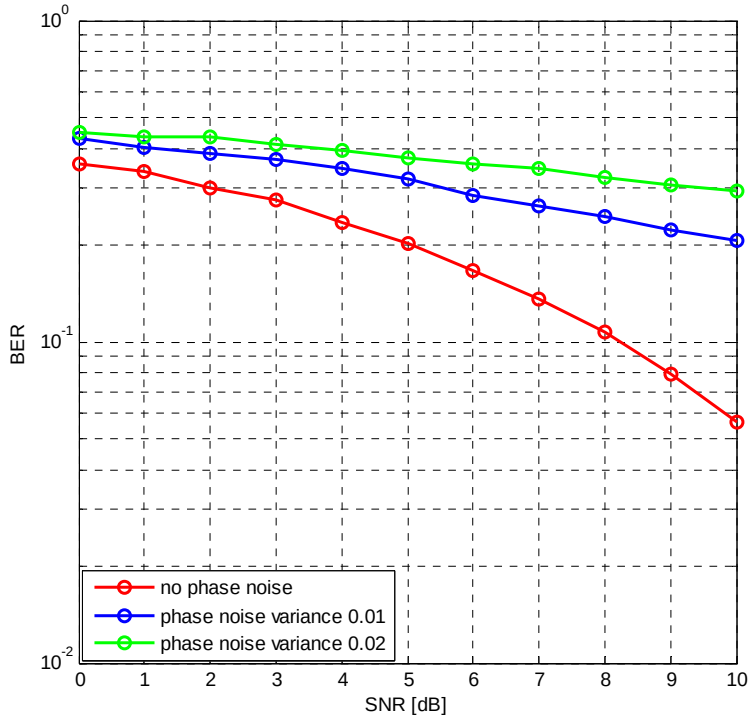

Figure 4.48: BER performance with different amounts of phase noise at different SNRs

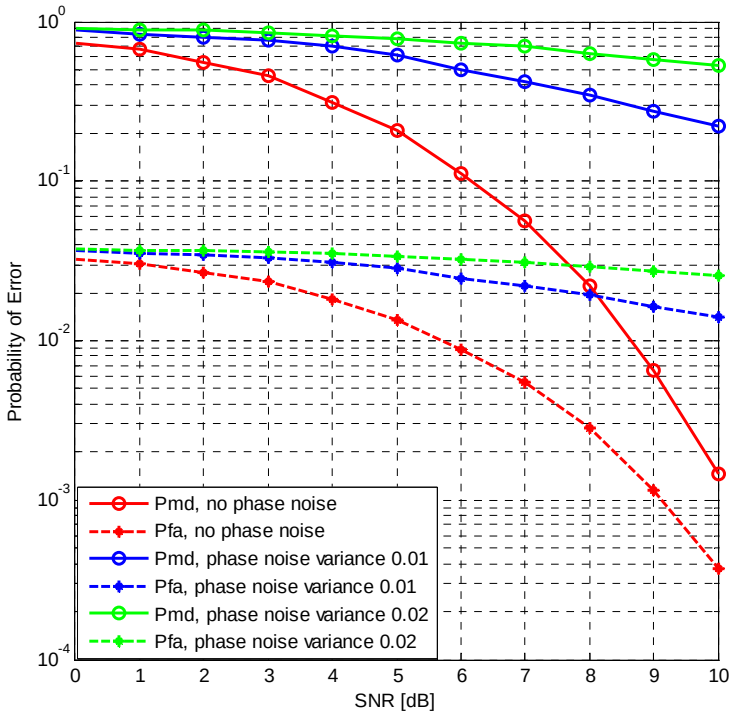

Figure 4.49: Error probabilities with different amounts of phase noise at different SNRs

5.4.3 Impact of carrier frequency offset

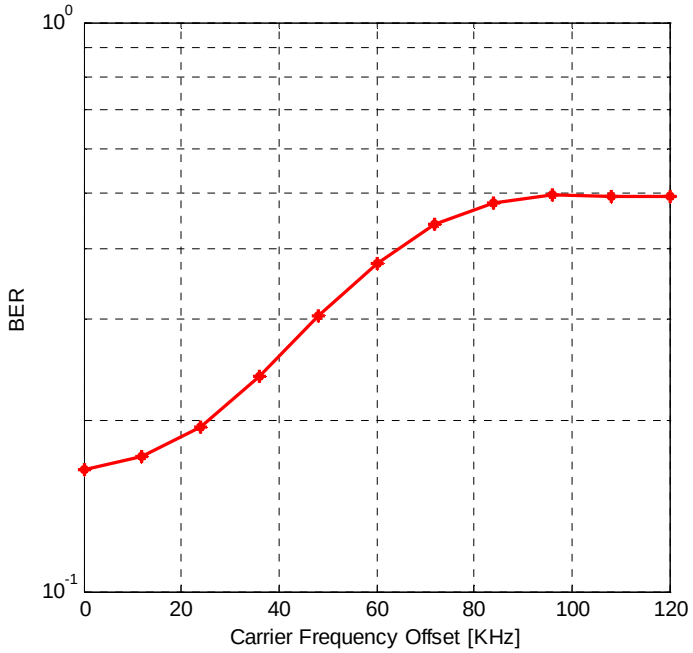

Figure 4.50: BER performance with carrier frequency offset in Rician fading channels (SNR = 6 dB)

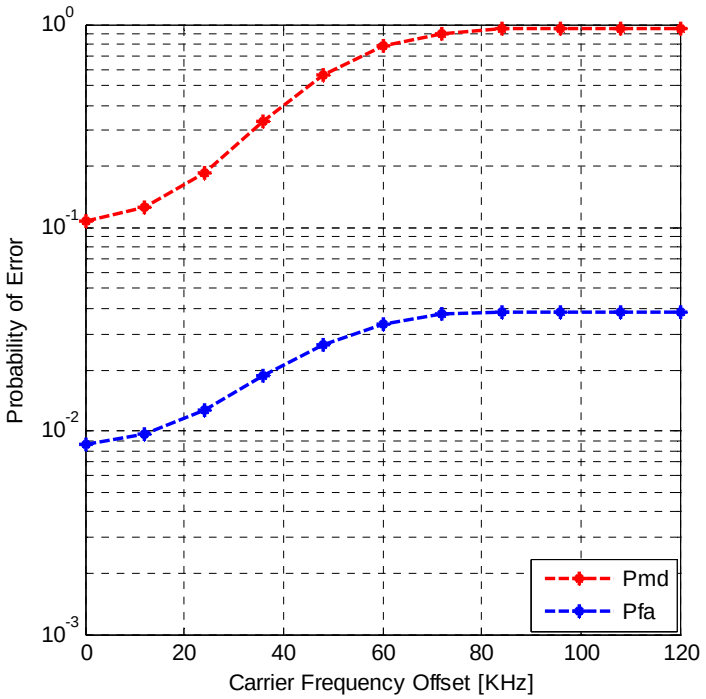

Figure 4.51: Error probabilities with carrier frequency offset in Rician fading channels (SNR = 6 dB)

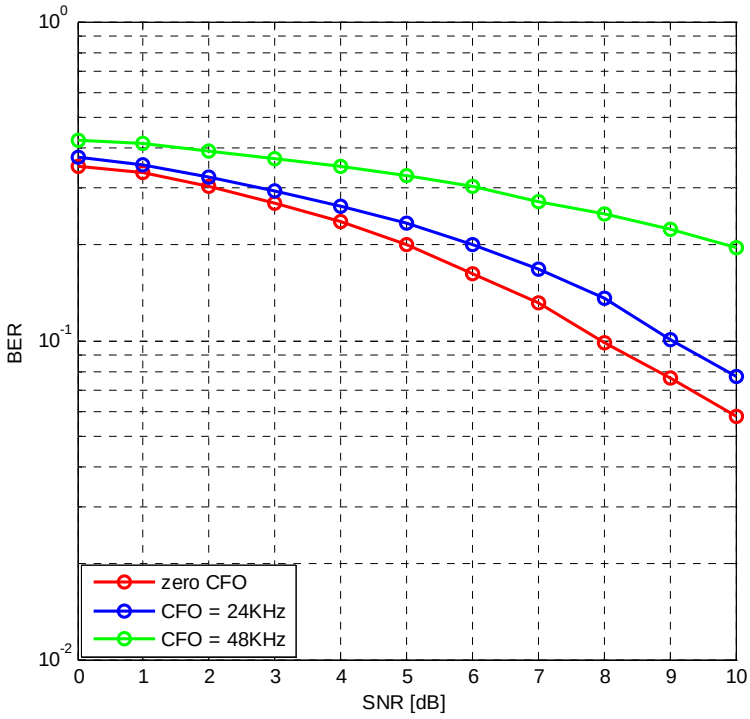

Figure 4.52: BER performance with different carrier frequency offsets at different SNRs

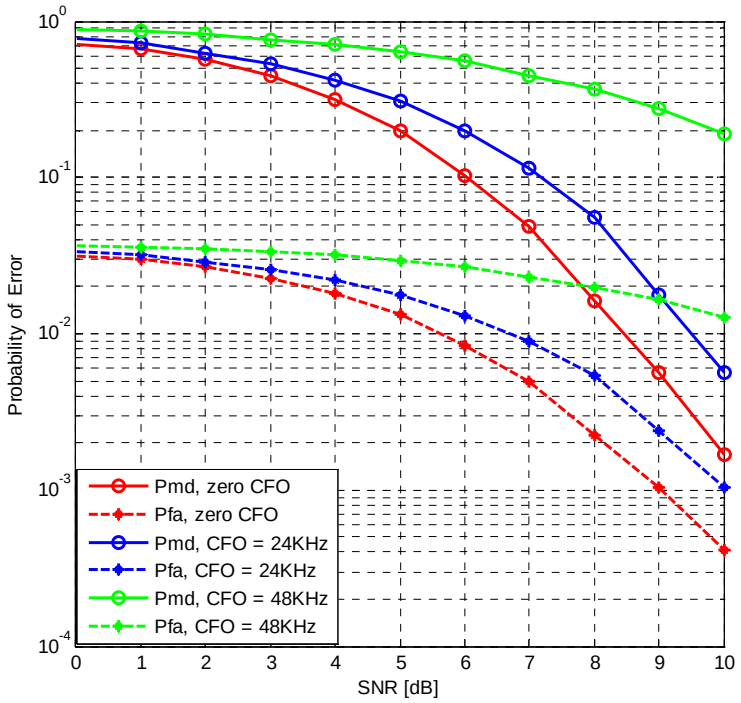

Figure 4.53: Error probabilities with different carrier frequency offsets at different SNRs

We can observe from Figure 4.52 that assuming a fixed BER, 1 dB more is needed for the SNR with a carrier frequency offset of 24 kHz compared to the ideal case. But the SNR degradation for a BER of 0.2 reaches 5 dB, as the carrier frequency offset swells to 48 kHz. As discussed in Section 4.3 and 4.4, the BER becomes 0.5, if the carrier frequency offset is 100 kHz or above. In terms of carrier frequency offset, the BER performance boundary is the same in Rician fading channels as in the two other channels. It is due to the property of the integrator. The cut-off frequency depends on the data rate, which is 100 $kbps$ in the simulation. The two error probabilities are also sensitive to the carrier frequency offset in the frond-end.

4.5.4 Impact of I/Q mismatch

In Rician fading channels, the effect of I/Q mismatch on the receiver detection performance is still small. For a BER of 0.2, an extra SNR of 1 dB is required with a relative I/Q imbalance interference of -10 dB. According to Figures 4.54 and 4.55, it is concluded that a relative I/Q mismatch interference of -20 dB below can be ignored due to the small degradation of the detection performance it introduces.

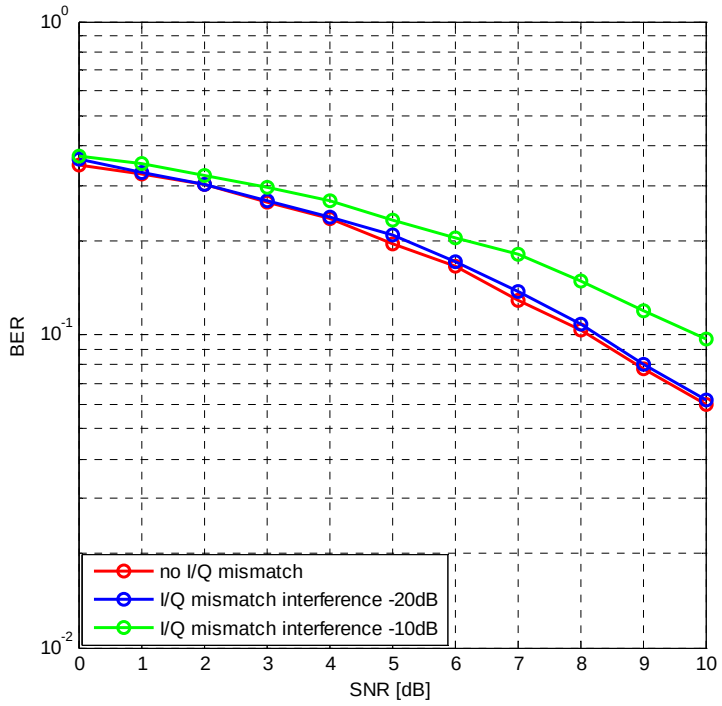

Figure 4.54: BER performance with different amounts of relative I/Q mismatch interference

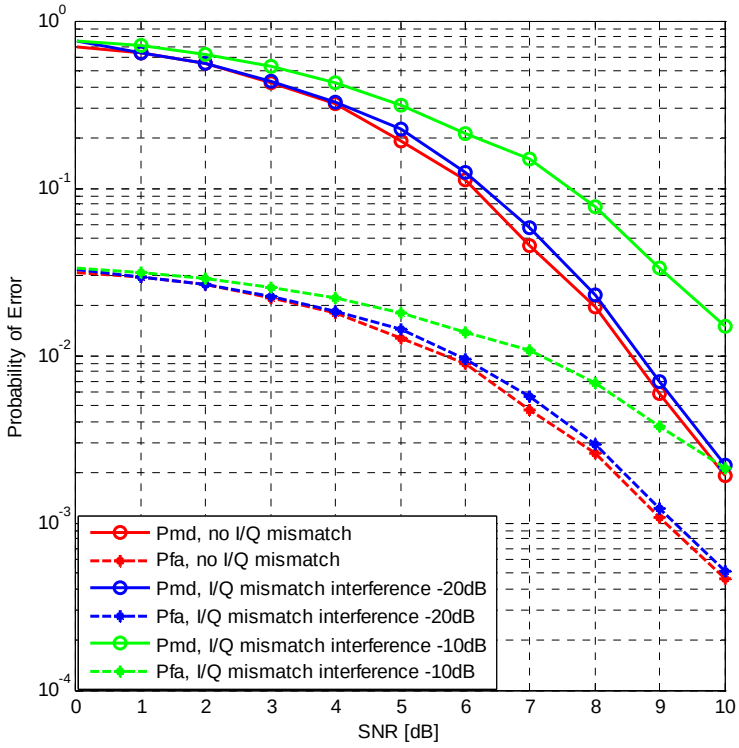

Figure 4.55: Error probabilities with different amounts of relative I/Q mismatch interference

4.5.5 Impact of ADC quantization noise

The performance improvement with a longer ADC word length in terms of BER, P_{md} and P_{fa} is demonstrated in Figures 4.56 and 4.57 below. As described in Figure 4.57, for an SNR of 10 dB, the miss detection probability can be improved from 0.04 to 0.001, if more than 3 bits are used to represent an analog value.

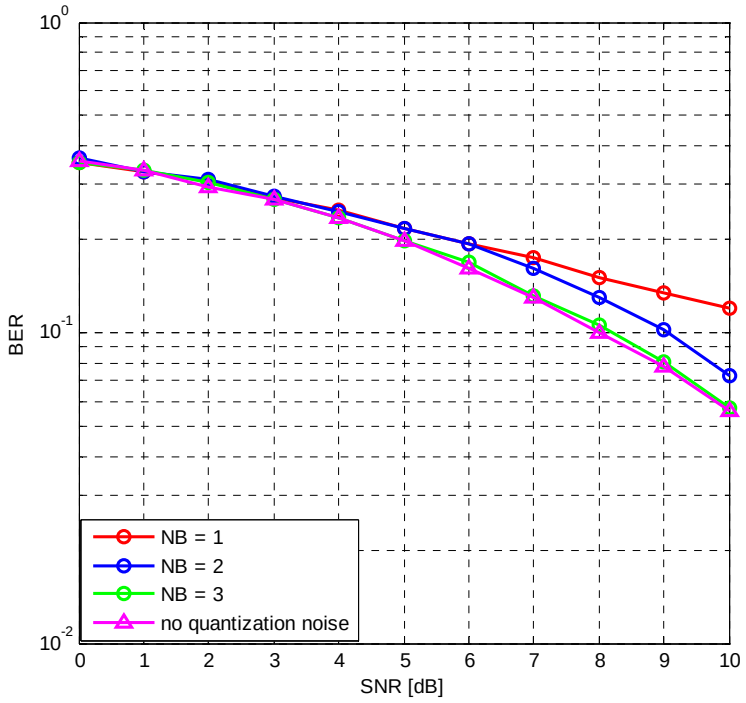

Figure 4.56: BER performance with different ADC word lengths at different SNRs

4.5.6 Impact of sampling clock offset

For a BER of 0.1, a sampling clock offset of 60000 ppm leads to a SNR degradation of 2 dB, compared to the case without sampling clock offsets. As in AWGN channels and Rayleigh fading channels, the impact of sampling clock offsets on the BER and error probabilities in Rician fading channels is not remarkable, compared to other impairments, such as phase noise and carrier frequency offset.

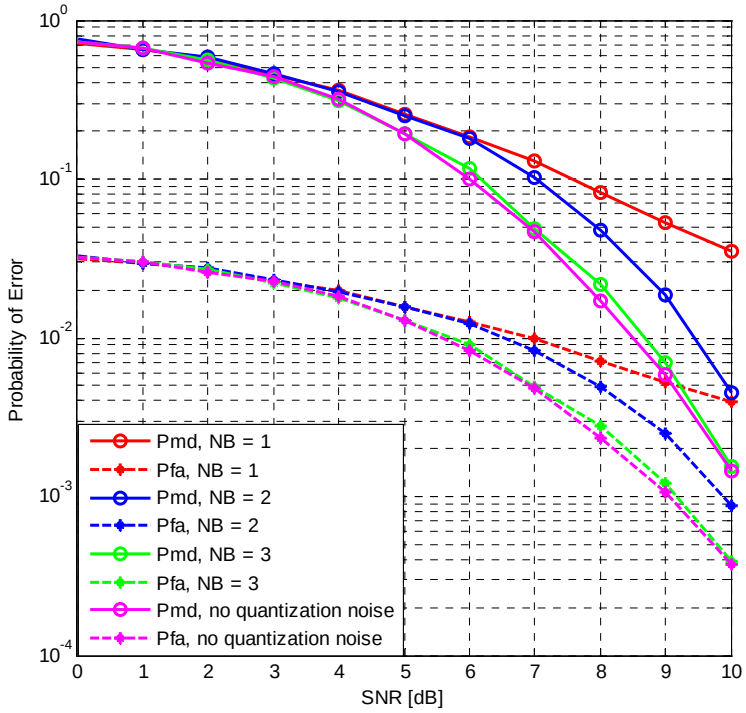

Figure 4.57: Error probabilities with different ADC word lengths at different SNRs

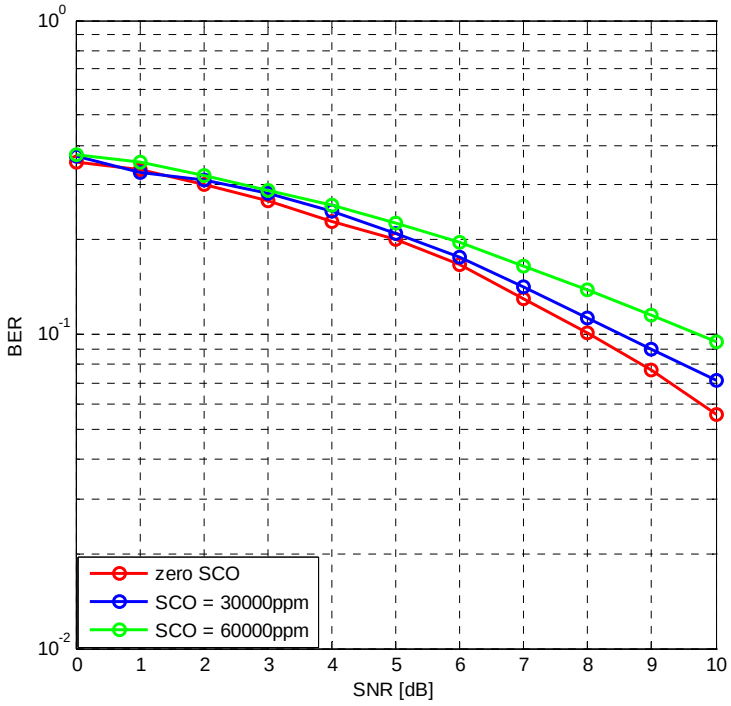

Figure 4.58: BER performance with different sampling clock offsets at different SNRs

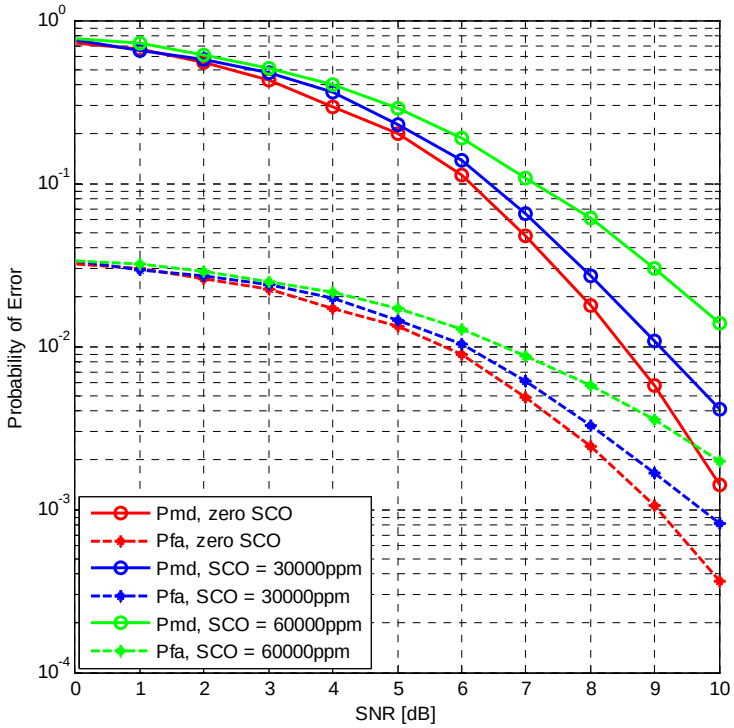

Figure 4.59: Error probabilities with different sampling clock offsets at different SNRs

4.6 Conclusions

The analysis of the effects of non-idealities on the detection performance of the MC wakeup receiver is conducted in this chapter. The non-idealities under consideration consist of phase noise, carrier frequency offset, I/Q imbalance, ADC quantization noise, as well as sampling clock offset. The performance boundaries with all these non-idealities are explored through simulation in MATLAB and Simulink. Three channel models are considered in our research, including AWGN channels, Rayleigh fading channels and Rician fading channels.

It is discovered from the simulation results that the phase noise and carrier frequency offset are the dominant impairments for the new MC wakeup receiver architecture of Figure 2.1. In comparison, the sampling clock offset has a small effect on the detection performance as long as the packet synchronization is assured. A significant detection performance improvement with more bits to represent an analog value can be observed in the simulation results. But it is at the cost of system complexity. Besides, the properties of fading channels lead to the fluctuations in the received signal amplitudes and degradation in the detection performance. The performance boundaries in fading channels indicate the worst cases in practice.

5 Further Discussions on Co-Channel Interference

In this chapter, the effects of co-channel interference (CCI) on the detection performance of the MC wakeup receiver are further studied. The worst detection performance in practice is explored, when all the frequency channels in use experience strong interference. In the last part of this chapter, we discuss the effect of the number of discarded channels on the address detection performance, when the channel selection mechanism is used to mitigate the interference.

5.1 Continuous wave interference

As discussed in Section 3.4.1, CW interference is also a single-tone interference. It can be mathematically expressed as:

$$s_i(t) = \sqrt{2P_i} \cdot \cos(2\pi f_o t + \phi_o) \tag{5.1}$$

where ϕ_o is a constant, representing the initial phase of a continous wave.

In our research, a 16-bit address is splitted into 4 sub-addresses and then 4 carriers are employed to carry the sub-address information. The data rate in each frequency channel is 100 *kbps* , and the channel spacing is 5MHz. All the other simulation parameters are as indicated in Table 4.2. The optimal case is that none of the 4 channels experiences strong CW interference. But if all the four carriers overlap with single-tone interference in spectrum as shown in Figure 5.1, the MC wakeup radio loses the benefit of frequency diversity. In practice, it is unlikely that all the carriers suffer from single-tone interference. For performance analysis, this case can be regarded as the worst case to explore the boundary of the detection performance.

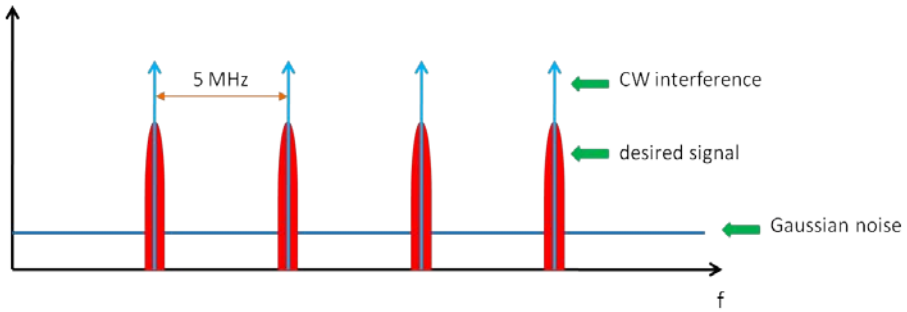

Figure 5.1: Worst case: all four carriers with co-channel CW interference

It can be seen from Figure 5.2 that the BER in the worst case is much higher than that with only one carrier suffering from CW interference. All the green lines in Figures 5.2 and 5.3 represent the performance boundaries with co-channel CW interference. It is noted that there is no channel selection mechanism in the simulation. In other words, even though a certain frequency channel undergoes a strong co-channel CW interference, it is still used for the address correlation detection.

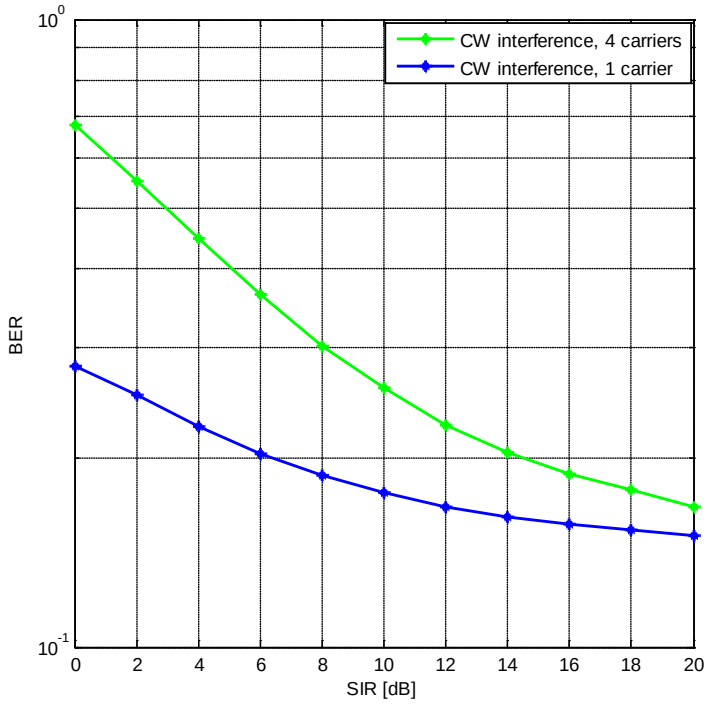

Figure 5.2: BER performance without any impairment in different CW interference cases (SNR = 6 dB)

We can observe from Figure 5.3 that below an SIR of 4 dB, no address gets detected as indicated by the large value of P_{md}. So, the MC wakeup receiver loses its importance if the SIRs of the channels are below 4 dB. In the region of 4 dB above, the two error probabilities P_{md} and P_{fa} gradually tend to the values as in AWGN channels without any interference. This phenomenon occurs at an SIR of more than 20 dB for an SNR of 6 dB when P_{md} and P_{fa} approach 6×10^{-2} and 6×10^{-3} respectively. The MC wakeup receiver still shows excellent performance in P_{fa} against P_{md} even if CCI exists in all the carriers in use. The reason is that the address sequence is an OVSF code and the distance between any two addrese sequences is 8 bits.

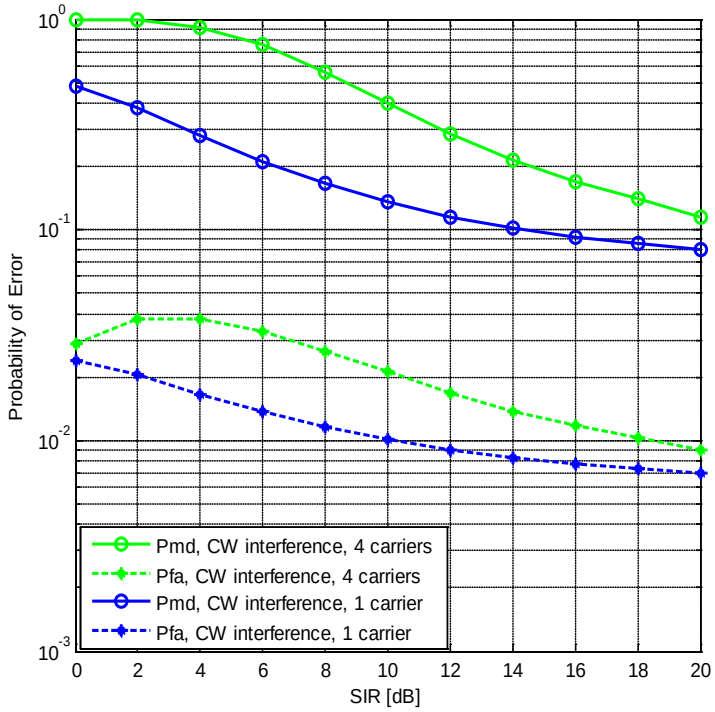

Figure 5.3: Error probabilities without any impairment in different CW interference cases (SNR = 6 dB)

5.2 Phase modulated interference

The expression for a PM interference signal provided in Section 3.4.2 is:

$$s_i(t) = A_i \cdot \cos(w_o t + \phi_o + \phi') \tag{5.2}$$

where ϕ' is a variable which denotes the phase that is used to carry the message. The rate of the phase change equals the data rate of the message signal. ϕ' for different phase modulations is illustrated in Figures 3.18 and 3.19.

Compared to CW interference, PM interference has a larger bandwidth and the bandwidth depends on the data rate of the message signal (i.e., the rate of the phase change in the PM interference signal). In the analysis of the effect of PM interference on the detection performance, the interference power P_i in the calculation of the SIR is defined as the power in the transmitted bandwidth of the desired signal, instead of the total power of that interferer at the full-scale band.

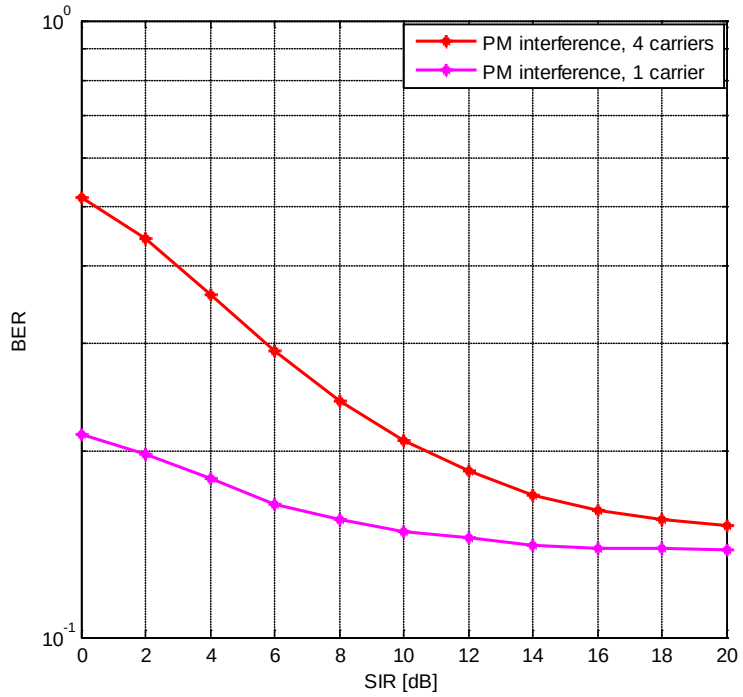

Figure 5.4: BER performance without any impairment in different PM interference cases (SNR = 6 dB)

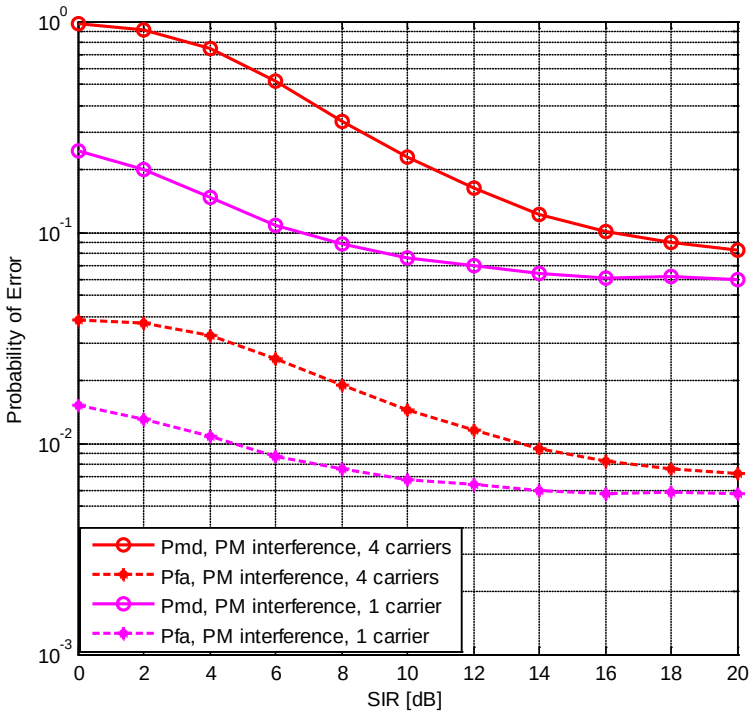

Figure 5.5: Error probabilities without any impairment in different PM interference cases (SNR = 6 dB)

In Section 3.4.2, it is concluded that the impact of CW interference on the receiver detection performance is more severe than that of PM interference. In Figures 5.4 and 5.5, all the red curves denote the boundaries of the BER and two error probabilities $\left(P_{md}, P_{fa}\right)$ in the presence of PM interference. All the boundary performances with PM interference in all the four carriers is still better than that with CW interference. If only one of the channels in use suffers from PM interference, the optimal BER, P_{md} and P_{fa} can be retrieved with an SIR of 14 dB or above. But in case of CW interference, the required SIR is more than 20 dB.

5.3 Discussions on the number of discarded channels

As presented in Chapter 2, channel selection mechanisms can be employed to improve the interference robustness and detection performance of the MC wakeup receiver, if some channels suffer from strong co-channel interference. These channels with strong interference are regarded as poor channels and then discarded. Only the sub-addresses in the remaining channels are used for the address detection. But the problem is what is the minimum number of carriers for a correct address retrieval. For example, in a 4-carrier wakeup radio, in case three channels experience significant interference and only one carrier is selected for the address detection, is it still possible to discover the transmitted address? The issue will be discussed and analysed in this section.

The analysis is based on the same simulation scenario as the previous ones. A unique 16-bit OVSF code is assigned to a MC wakeup receiver as the receiver address and the maximum number of available addresses is 15. The Hamming distance between any two OVSF codes A and B is 8 bits and the distribution of the different bits between A and B is presented in Table 5.1.

Table 5.1: Distribution of the different bits between any two OVSF codes

	f_1	f_2	f_3	f_4	p
Case 1	2	2	2	2	$\frac{11}{14}$
Case 2	0	0	4	4	$\frac{1}{14}$
Case 3	0	4	0	4	$\frac{1}{14}$
Case 4	0	4	4	0	$\frac{1}{14}$

In Table 5.1, f_1, f_2, f_3, and f_4 represent the different frequency channels in use, and *p* denotes the probability. For example, a 16-bit address A is assigned to a MC wakeup receiver. The transmited address is splitted into 4 sub-addresses and they are sent across 4 frequency channels. The transmitted address is one of the 15 possible codes and is unknown to the wakeup receiver. Miss detection probably occurs if the transmitted address is the same as the receiver address, while the difference between the two addresses may give rise to a false alarm. Only one among the 15 codes is the same as the receiver address A. The number of the different bits between A and other address codes is 8 and these different bits are distributed as shown in Table 5.1. In case 1, all these 8 bits are uniformly distributed in the 4 frequency channels. The number of the addresses with this situation is 11, out of all the 14 different addresses from A. Table 5.1 provides an insight into the property of an OVSF code set and the address allocation.

5.3.1 Without AWGN

For the discussions on the number of discarded channels, the simplest situation is first studied, i.e., no AWGN exists in the channels and those carriers that encounter strong co-channel interference are discarded. The probabilities of miss detection and false alarm are analyzed for different numbers of discarded channels respectively.

- One channel is removed:

The miss detection probability:
As mentioned above, the transmitted address is the same as the receiver address for the study in miss detection. With one carrier removed at the receiver, there are still 12 bits in the received address and they are the same as the corresponding bits in the local receiver address. According to the distribution of the different bits in Table 5.1, the wakeup receiver can discover itself as the target receiver and then responds to the wakeup signal. Therefore, $P_{md} = 0$.

The false alarm probability:
The transmitted address is different from the local receiver address. The different bits in between are distributed as in Table 5.1. If one channel is discareded, the number of different bits between the remaining 12 bits and the local receiver address may be 4, 6 or 8. Due to at least 4 different bits in between, the wakeup receiver decides it is not the intended receiver and then ignores the wakeup signal. In this case, $P_{fa} = 0$.

- Two channels are removed:

The miss detection probability:

It is seen from Table 5.1 that the received 8 bits are the same as the local receiver address, but it cannot guarantee that the wakeup signal will be accepted. For example, if the 3rd and 4th channel are removed, the remaining 8 same bits give rise to two possibilities, one of which is the case 2 as indicated in Table 5.1. Then the receiver has a miss detection probability of 0.5 in this condition. But in case the 1st and 2nd channel are discarded, the 8 same bits in the two other carriers indicate that the receiver is the target. So, $P_{md} = \frac{1}{6} \cdot \left(\frac{1}{2} \cdot 3 + 0 \cdot 3 \right) = \frac{1}{4}$.

The false alarm probability:

Similarly, the different bits between the local receiver address and the received address can be 0, 4, or 8. But only 0 different bits in between lead to a false alarm. $P_{fa} = \frac{11}{14} \cdot 0 + 3 \cdot \frac{1}{14} \cdot \frac{1}{6} \cdot \frac{1}{2} = \frac{1}{56}$.

- Three channels are removed:

The miss detection probability:

With three carriers removed at the receiver, the remaining 4 same bits can lead to several cases for miss detection. Provided that the selected channel is the first one as shown in Table 5.1, the miss detection probability is $\frac{3}{4}$. But it lessens to $\frac{1}{2}$ if other carrier is chosen. Hence, $P_{md} = \frac{1}{4} \cdot \left(\frac{3}{4} + 3 \cdot \frac{1}{2} \right) = \frac{9}{16}$.

The false alarm probability:

The possible number of different bits between the selected 4 bits and the corresponding bits in the local receiver address is 0, 2 and 4. $P_{fa} = \frac{11}{14} \cdot 0 + 3 \cdot \frac{1}{14} \cdot \left(\frac{1}{4} \cdot \frac{1}{4} + \frac{1}{4} \cdot \frac{1}{2} \right) = \frac{9}{224}$.

All the cases discussed above are summarized in Table 5.2. It can be observed that the two error probabilities $\left(P_{md}, P_{fa} \right)$ are zero in case of one carrier discarded. But they increase with more channels removed at the receiver, especially the probability of miss detection.

Table 5.2: Error probabilities with channel selection mechanism (without AWGN)

	# discarded carriers	P_{md}	P_{fa}
Without AWGN	1	0	0
	2	1/4	1/56
	3	9/16	9/224

5.3.2 With AWGN

The situation becomes more complicated if AWGN is taken into consideration besides co-channel interference. The reason is that AWGN introduces BER into the received address. The analysis method is the same as the one for the scenario without AWGN. But the expressions for the two error probabilities in the three different cases change.

- One channel is removed:

The miss detection probability:

The only case for a correct address detection is that all the remaining bits are the same as the corresponding bits in the local receiver address. As long as a bit is different, the wakeup signal will be abandoned. So, $P_{md} = 1 - \binom{12}{12}(1-P_e)^{12} P_e^0$.

The false alarm probability:

If all the same bits remain and different bits reverse due to the AWGN, the received address will be viewed the same as the local address and then a false alarm arises. All the possibilities for a false alarm are discussed individually and then combined.

6 bits different: $P'_{fa} = \binom{6}{6}(1-P_e)^6 P_e^0 \cdot \binom{6}{6} P_e^6 (1-P_e)^0$

4 bits different: $P''_{fa} = \binom{8}{8}(1-P_e)^8 P_e^0 \cdot \binom{4}{4} P_e^4 (1-P_e)^0$

8 bits different: $P'''_{fa} = \binom{4}{4}(1-P_e)^4 P_e^0 \cdot \binom{8}{8} P_e^8 (1-P_e)^0$

Therefore, $P_{fa} = \frac{11}{14} \cdot P'_{fa} + \frac{3}{14} \cdot \left(\frac{1}{2} \cdot P''_{fa} + \frac{1}{2} \cdot P'''_{fa} \right)$.

- Two channels are removed:

The miss detection probability:

As analyzed above, miss detection cannot be completely avoided, even if all the received 8 bits are the same as the corresponding ones in the local receiver address.

Then, $P_{md} = 1 - \binom{8}{8} (1 - P_e)^8 P_e^0 \cdot \left(1 - \frac{1}{4} \right)$

The false alarm probability:

Similar to the case of one carrier removed, the possibilities for a false alarm are as follows:

4 bits different: $P'_{fa} = \binom{4}{4} (1 - P_e)^4 P_e^0 \cdot \binom{4}{4} P_e^4 (1 - P_e)^0$

0 bits different: $P''_{fa} = \binom{8}{8} (1 - P_e)^8 P_e^0$

8 bits different: $P'''_{fa} = \binom{8}{8} P_e^8 (1 - P_e)^0$

The false alarm probability is given by: $P_{fa} = \frac{11}{14} \cdot \frac{3}{4} \cdot P'_{fa} + \frac{3}{14} \cdot \left(\frac{1}{12} \cdot P''_{fa} + \frac{2}{3} \cdot \frac{3}{4} \cdot P'_{fa} + \frac{1}{6} \cdot P'''_{fa} \right)$.

- Three channels are removed:

The miss detection probability:

$P_{md} = 1 - \binom{4}{4} (1 - P_e)^4 P_e^0 \cdot \left(1 - \frac{9}{16} \right)$

The false alarm probability:

2 bits different: $P'_{fa} = \binom{2}{2} (1 - P_e)^2 P_e^0 \cdot \binom{2}{2} P_e^2 (1 - P_e)^0$

0 bits different: $P''_{fa} = \binom{4}{4}(1-P_e)^4 P_e^0$

4 bits different: $P'''_{fa} = \binom{4}{4} P_e^4 (1-P_e)^0$

$$P_{fa} = \frac{11}{14}\cdot\frac{1}{4}\cdot\left(\frac{1}{4}+3\cdot\frac{1}{2}\right)\cdot P'_{fa} + \frac{3}{14}\cdot\left(\frac{1}{2}\cdot\frac{3}{8}\cdot P''_{fa} + \frac{1}{2}\cdot\frac{1}{2}\cdot P'''_{fa}\right)$$

The final expressions for P_{md} and P_{fa} in different cases are indicated in Table 5.3. In case there is no additive white Guassian noise (i.e., $P_e = 0$), the formulas in Table 5.3 reduce to those in Table 5.2.

Table 5.3: Error probabilities with channel selection mechanism (with AWGN)

	# discarded carriers	P_{md}	P_{fa}
AWGN	1	$1-(1-P_e)^{12}$	$\frac{3}{28}(1-P_e)^8 P_e^4 + \frac{11}{14}(1-P_e)^6 P_e^6 + \frac{3}{28}(1-P_e)^4 P_e^8$
	2	$1-\left(1-\frac{1}{4}\right)\cdot(1-P_e)^8$	$\frac{1}{56}(1-P_e)^8 + \frac{39}{56}(1-P_e)^4 P_e^4 + \frac{1}{28}P_e^8$
	3	$1-\left(1-\frac{9}{16}\right)\cdot(1-P_e)^4$	$\frac{9}{224}(1-P_e)^4 + \frac{11}{32}(1-P_e)^2 P_e^2 + \frac{3}{56}P_e^4$

Conclusions and Future Work 6

6.1 Conclusions

In this thesis, we first present an introduction and motivation for the wakeup radio. The focus of the research on wakeup radio nowadays exists in receiver power consumption and interference robustness. Since wakeup radio receivers operate in the lisence-free 2.4 GHz ISM band, a wakeup signal may be severely interfered by the noisy channel, which leads to performance degradation in terms of false alarm or miss detection. By making use of frequency diversity, a MC wakeup radio receiver is proposed as a solution to interference mitigation.

In chapter 2, this system architeture is explained and analyzed in detail. In a MC wakeup radio, the address code is reshaped into a matrix and the sub-addresses in columns are transmitted over different frequency channels. For the MC wakeup receiver, a channel selection mechanism is employed to combat the interference in channels. The channels with strong interference are discovered and removed to improve the receiver detection performance.

In chapter 3, two address detection schemes are presented, Hamming distance method and soft-bit correlation method. The detection performance with the latter scheme is dominant over that with the former one. But the soft-bit correlatiopn method demands a higher architecture complexity, leading to larger power consumption. The detection performance of the MC wakeup receiver in the presence of AWGN and interference is explored in this section as well. It is disclosed that CW interference has a more severe effect on the receiver performance than PM interference.

Besides the channel noise and interference, the non-idealities existing in the system itself also have a negative impact on the receiver detection performance. In chapter 4, the analysis of the influence of phase noise, carrier frequency offset, I/Q mismatch, ADC quantization noise and sampling clock offset on the MC wakeup receiver detection performance is conducted. In the simulations, different kinds of channels are considered, including AWGN, Rayleigh fading, as well as Rician fading channels. The conclusion is that carrier frequency offset and phase noise are the dominant impairments for the MC wakeup receiver among all the non-idealities under consideration.

In chapter 5, the worst case with co-channel continuous wave interference and phase modulated interference for the detection performance is further discussed. Based on the code properties, we carry out mathematical analysis on the channel selection mechanism for interference mitigation.

6.2 Suggestions for future work

6.2.1 Digital compensation

As analyzed before, the receiver detection performance is sensitive to carrier frequency offset. When the carrier frequency offset reaches $100\,kHz$, the BER is nearly 50%. This is largely resulted from the integrator, whose cut-off frequency depends on the data rate of the desired signal. In a wakeup radio, the data rate is low, leading to a high sensitivity to carrier frequency offset. In order to solve this problem, digital compensation can be conducted in the digital baseband. CFO must be estimated first so that it can be compensated for. Extra bits can be added in the wakeup packet preamble to assist with the CFO acquisition. Moreover, new algorithms can be designed to estimate CFO. A CFO tracking loop is usually employed for CFO compensation.

6.2.2 Power consumption

Due to the limited time and devices, the power consumption of the proposed MC wakeup receiver has not been tested yet. Based on some prior literature on receiver frond-end, the power consumption of this architecture can be estimated. Although digital compensation schemes can resist the negative effect of non-idealities on the detection performance, they are at the cost of system complexity and power consumption. In future work, power consumption should be taken into consideration, if extra circuits are added for non-ideality compensation. A decent tradeoff between power consumption and detection performance is always one of the goals in a wakeup radio receiver design.

Bibliography

[1] I. Demirkol, C. Ersoy and E. Onur, "Wake-up receiver for wireless sensor networks: benefits and challenges", *IEEE Wireless Communications*, vol. 16, pp. 88-96, Aug. 2009.

[2] J. Hui, Z. Ren and B. H. Krogh, "Sentry-based power management in wireless sensor network", *Proceedings of the 2nd International Conference on Information Processing in Sensor Network (IPSN'03)*, pp. 458-472, 2003.

[3] S. H. Min and J. J. Kim, "Ultra Low-power Wake-up Receiver", US Patent 20080108318, May 2008.

[4] A. Sikora and V. F. Groza, "Coexistence of IEEE802.15.4 with other Systems in the 2.4 GHz-ISM-Band", *Proceedings of the IEEE Instrumentation and Measurement Technology Conference (IMTC 2005)*, vol. 3, pp. 1786-1791, May 2005.

[5] Y. Zhou, G. Huang, S. K. Kim, S. Nam, and B. S. Kim, "A wideband OOK receiver for wireless capsule endoscope", *2009 European Microwave Conference (EuMC 2009)*, pp. 330-333, Oct. 2009.

[6] N. Pletcher, S. Gambini and J. Rabaey, "A 65uW, 1.9GHz RF to digital baseband wakeup receiver for wireless sensor nodes", *Proceedings of 2007 IEEE Custom Integrated Circuits Conference (CICC'07)*, pp. 539-542, Sept. 2007.

[7] P. Le-Huy and S. Roy, "Low-power 2.4GHz wake-up radio for wireless sensor networks", *2008 IEEE International Conference on Wireless and Mobile Computing (WIMOB'08)*, pp. 13-18, Oct. 2008.

[8] M. S. Durante, and S. Mahlknecht, "An ultra-low power wakeup receiver for wireless sensor nodes", *2009 the 3rd International Conference on Sensor Technologies and Applications (SENSORCOMM'09)*, pp. 167-170, 2009.

[9] Y. Zhang, S. Chen, et al., "A 3.72uW ultra-low power digital baseband for wake-up radios", *2011 International Symposium on VLSI Design, Automation and Test (VLSI-DAT)*, pp. 1-4, Apr. 2011.

[10] J. R. Long, W. Wu, et al., " Energy-efficient wireless front-end concepts for ultra low power radio", *2008 IEEE Custom Integrated Circuits Conference (CICC 2008)*, pp. 587-590, Sept. 2008.

[11] J. Vazifehdan and H. Shafiee, “Cooperative diversity in space-time coded wireless networks”, *the 9th International Conference on Communications Systems (ICCS 2004)*, pp. 215-219, Sept. 2004.

[12] P. Bradley, et al., “Low power multiple channel mixing architecture for detecting wake-up signals and related falsing protection algorithm”, US Patent 20090252042, Oct. 2009.

[13] “AS3931 3D Low Power Wakeup Receiver Datasheet”, AUSTRIAMICROSYSTEMS, Austria.

[14] “AS3932 3D Low Frequency Wakeup Receiver Datasheet”, AUSTRIAMICROSYSTEMS, Austria.

[15] “AS3933 3D Low Frequency Wakeup Receiver Datasheet”, AUSTRIAMICROSYSTEMS, Austria.

[16] V. K. Garg, *Wireless Communications and Networking*, San Francisco, CA: Morgan Kaufmann, 2007.

[17] D. Gong, Y. Yan and J. Lu, “Dynamic code assignment for OVSF code system”, *Proceedings of 2005 IEEE Global Telecommunications Conference (GLOBECOM ‘05)*, vol. 5, pp. 2865-2869, Dec. 2005.

[18] A. Mitra, “On pseudo-random and orthogonal binary spreading sequences”, *Journal of Information Technology*, vol. 4, pp. 137-144, 2008.

[19] D. Ash, “A comparison between OOK/ASK and FSK modulation techniques for radio links”, Technical report, RF Monolithic Inc., Dallas, United States, 1992.

[20] R. de Francisco and Y. Zhang, “An interference robust multi-carrier wake-up radio”, *2011 IEEE Wireless Communications and Networking Conference (WCNC)*, pp. 1265-1270, Mar. 2011.

[21] A. Annamalai and V. K. Bhargava, “Asymptotic error-rate behavior for non-coherent on-off keying in the presence of fading”, *IEEE Transactions on Communications*, vol. 47, pp. 1293-1296, Sept. 1999.

[22] J. M. Geist, “Asymptotic error rate behavior for non-coherent on-off keying”, *IEEE Transactions on Communications*, vol. 42, pp. 225, Feb./Mar./Apr. 1994.

[23] G. Zang, Y. Gao, and J. Mu, “Performance analysis of the cooperative DS/SS systems in single-tone interference over flat-Rayleigh fading channels”, *2010 International Conference on Communications, Circuits and Systems (ICCCAS)*, pp. 126-130, Jul. 2010.

[24] J. G. Proakis and M. Salehi, *Digital Communications*, 5th edition, McGraw-Hill, 2008.

[25] R. M. Cerda, "Impact of ultralow phase noise oscillators on system performance", *RF Design*, pp. 28-34, Jul. 2006.

[26] S. Bittner, S. Krone and G. Fettweis, Tutorial on Discrete Time Phase Noise Modeling for Phase Locked Loops. Available: http://www.vodafone-chair.com/staff/bittner/main_tutorial_phasenoise.pdf

[27] F. Horlin and A. Bourdoux, *Digital Compensation for Analog Front-Ends: A New Approach to Wireless Transceiver Design*, 1st edition, Great Britain: Wiley, 2008.

[28] Y. S. Cho, J. Kim, W. Y. Yang, and C. G. Kang, *MIMO-OFDM Wireless Communications with MATLAB*, Singapore: John Wiley & Sons, 2010.

[29] E. Lopelli, J. D. van der Tang and A. H. M. van Roermund, "FSK demodulator topologies for ultra-low power wireless transceivers", *ProRISC Workshop on Circuits, Systems and Signal Processing*, 2005.

[30] T. S. Rappaport, *Wireless Communications, Principles and Practice*, New Jersey: Prentice Hall, 1996.

[31] R. Iqbal, T. D. Abhayapala and T. A. Lamahewa, "Generalised clarke model for mobile-radio reception", *IET communications*, vol. 3, Iss. 4, pp. 644-654, Apr. 2009.

[32] N. Kostov, "Mobile radio channels modeling in MATLAB", *Journal of Radio Engineering*, vol. 12, pp. 12-16, Dec. 2003.